CHAPTER

Acoustic components

4

CHAPTER OUTLINE

4.1 INTRODUCTION

We have attempted to present the material in different parts of this text in three ways. First, in a form where acoustical phenomena can be visualized and thought of in terms, say as an example, of analogous electrical circuits. This form is found in the first three chapters. Second, where straight-forward mathematical analysis leads to results that are commonly encountered in engineering practice. This form is

Acoustics: Sound Fields and Transducers. DOI: 10.1016/B978-0-12-391421-7.00004-X

found in Chapter 7, where ready-made formulas and tables for loudspeaker systems are presented. Third, where advanced mathematical analysis is necessary to handle complex acoustical problems. This form is found in Chapter 14 where a program for speeding up the derivation of transfer functions is described. The advantage of mathematical analysis is that the formulas can be reused indefinitely.

In this chapter we will start with the acoustical and mechanical elements that are used to form electro-mechano-acoustic circuits which, in turn, are used to calculate the performance of loudspeakers, microphones, and acoustic filters. One obvious acoustical element is the air into which the sound is radiated. Others are air cavities, tubes, slots, and porous screens both behind and in front of actively vibrating diaphragms. These various elements have acoustic impedances associated with them, which can, in some frequency ranges, be represented as simple lumped elements. In other frequency ranges, distributed elements, analogous to electric lines, must be used in explaining the performance of the devices. This text does not pretend to advance the science of acoustic components to anything approaching a state of completion. Much research remains to be done. Non-linearities that occur at higher sound levels, such as shock waves and turbulence, are not covered here. It does attempt to interpret the available theories in such a way that the reader can construct and understand the performance of common acoustic devices.

PART X: ACOUSTIC ELEMENTS

4.2 ACOUSTIC MASS (INERTANCE)

A tube open at both ends and with rigid walls behaves as an acoustic mass if it is short enough so that the air in it moves as a whole without appreciable compression. In setting up the boundary condition, the assumption is made that the sound pressure at the open end opposite the source is nearly zero. This assumption would be true if it were not for the radiation impedance of the open end, which acts very much like a piston radiating into open air. However, this radiation impedance is small for a tube of small diameter and acts only to increase the apparent length of the tube slightly. Therefore, the radiation impedance will be added as a correction factor later.

Tube of medium diameter. In order to be able to neglect viscous losses inside the tube, the radius of the tube a in meters must not be too small. Also, in order to be able to neglect transverse resonances in the tube, the radius must not be too large. The equations which follow are valid for a radius in meters greater than about $0.05/\sqrt{f}$ and less than about $10/f$.

To demonstrate acoustic mass, take a tube of length ℓ'. Let us designate the boundary acoustic impedance at one end as $Z_A = 0$, i.e., $\tilde{p} = 0$. At the other end the acoustic impedance looking into the tube, using the solution of the one-dimensional wave Eq. (2.60), is

$$Z_A = j\frac{\rho_0 c}{\pi a^2}\tan k\ell' \tag{4.1}$$

where

ρ_0 is density of the gas in kg/m^3
c is speed of sound in m/s
a is radius of tube in m
k is wave-number $= \omega/c$ in m^{-1}.

For small values of $k\ell'$,

$$\tan k\ell' = k\ell' + \frac{(k\ell')^3}{3} \tag{4.2}$$

If $\ell' < 16$, the second term will be less than 5% as large as the first, so

$$Z_A = j\omega \frac{\rho_0 \ell'}{\pi a^2} = j\omega M_A \ \mathrm{N\cdot s/m^5} \tag{4.3}$$

$$M_A = \frac{\rho_0 \ell'}{\pi a^2} \text{ acoustic mass with units } \mathrm{kg/m^4} \tag{4.4}$$

End corrections. Most acoustic masses are tubes that terminate at one end or the other, or both, in open air or at the boundary of a large cavity. The air particles at the end of a tube do not instantaneously disperse from their organized status inside the tube so that their behavior at the end is equivalent to a short extension of the tube, i.e., an *end correction*. In what follows, we will simply give the end corrections, and later in the chapter will derive them.

End correction ℓ'' if the open end of the tube terminates in a wall—called an infinite baffle or flanged tube If $a < \lambda/25$ the end correction ℓ'' for this case is,

$$\ell'' = \frac{M_{A1}\pi a^2}{\rho_0} = \frac{8a}{3\pi} \approx 0.85a \text{ m} \tag{4.5}$$

The total mass M_A of Eq. (4.4) now becomes

$$M_A = \frac{\rho_0(\ell' + \ell'')}{\pi a^2} = \frac{\rho_0 \ell}{\pi a^2} \ \mathrm{kg/m^4} \tag{4.6}$$

If both ends terminate in a flange,

$$M_A = \frac{\rho_0(\ell' + 2\ell'')}{\pi a^2} = \frac{\rho_0 \ell}{\pi a^2} \ \mathrm{kg/m^4} \tag{4.7}$$

End correction ℓ'' if the open end of the tube terminates in open air—called an unflanged tube If $a < \lambda/25$ the end correction in this case is again like a mass but because the organized state of the gas particles drops off faster than in the flanged tube case, the size of M_{A1} is smaller. Hence,

$$\ell'' = \frac{M_{A1}\pi a^2}{\rho_0} = \frac{2a}{\pi} \approx 0.64a \text{ m} \tag{4.8}$$

Equations (4.6) and (4.7) are valid in either case, except ℓ'' must be properly chosen.

4.3 ACOUSTIC COMPLIANCES

In Eq. (2.72) we showed that a length of tube, rigidly closed on one end ($\ell = 0$), with a radius in meters greater than $0.05/\sqrt{f}$ (so that the sidewall friction can be neglected) and less than $10/f$ (so lateral standing waves are not present) has an input acoustic impedance at the open end equal to

$$Z_A = \frac{-j\rho_0 c}{\pi a^2} \cot k\ell' \tag{4.9}$$

where $Z_A = Z_s/(\pi a^2)$

ρ_0 is density of the gas in kg/m^3
c is speed of sound in m/s
a is radius of tube in m
k is wave-number $= \omega/c$ in m^{-1}
ℓ' is length of the tube in m.

For values of k that are not too large, the cotangent may be replaced by

$$\cot k\ell' = \frac{1}{k\ell'} - \frac{k\ell'}{3} \tag{4.10}$$

Thus

$$Z_A = -j\frac{1}{\omega(V/\rho_0 c^2)} + j\omega\frac{l'\rho_0}{3\pi a^2} \quad + \cdot \cdot \cdot \tag{4.11}$$

For $\ell' < \lambda/10$, Eq. (4.9) becomes

$$Z_A = -j\frac{1}{\omega C_A} \tag{4.12a}$$

The acoustic compliance obviously is:

$$C_A = \frac{V}{\rho_0 c^2} = \frac{V}{\gamma P_0} \text{ with units m}^5/\text{N} \tag{4.13}$$

Limitations on an acoustic compliance. An acoustic compliance obtained by compressing air in a closed volume can be represented by a two-terminal device, but one *terminal must always be at "ground potential."* That is to say, one terminal is outside of the enclosure *V,* which is at atmospheric pressure, i.e., a sound pressure of 0. *Therefore, it is never possible to insert an acoustic compliance between acoustic masses or acoustic resistances*.

Series acoustic compliance. To obtain a series acoustic compliance a diaphragm or stretched membrane must be used. Of course, diaphragms and stretched membranes resonate at various frequencies. The range where they act as compliances is restricted to that region well below the lowest frequency of resonance. A combination of a series acoustic compliance, an acoustic mass, and an acoustic resistance is shown in Fig. 4.1.

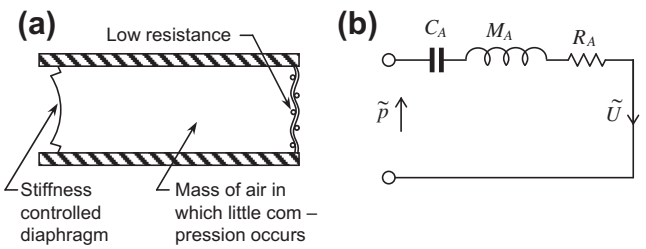

FIG. 4.1 (a) Example of a series acoustic compliance obtained with a stiffness-controlled diaphragm. (b) Analogous circuit.

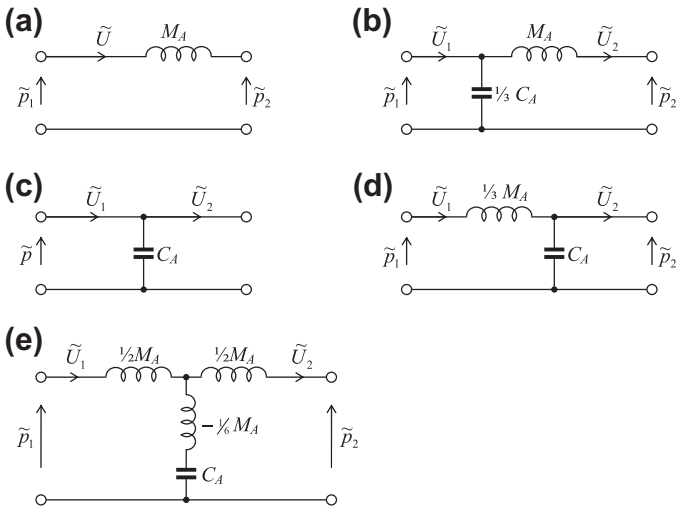

FIG. 4.2 Approximate analogous circuits for a short tube of medium diameter.

(a) and (b) Circuits used when $\tilde{p}_2/\tilde{U}_2$ is very small (open end). (c) and (d) Circuits used when $\tilde{p}_2/\tilde{U}_2$ is very large (closed end). (e) Circuit used for any value of $\tilde{p}_2/\tilde{U}_2$. Circuits (*a*) and (*c*) yield the impedance within about 5% for a tube length l' that is less than $\lambda/16$. Circuits (b), (d), and (e) yield the impedance within about 5% for $l' < \lambda/8$.

Analogous circuits for acoustic masses and compliances are shown in Fig. 4.2. The circuits in (a) and (c) are for cases where $\ell' < \lambda/16$ and involve C_A and M_A alone. When $\lambda/16 > \ell' > \lambda/8$ the second terms in Eqs. (4.2) and (4.10) cannot be neglected and this leads to the added elements $C_A/3$ in (b), $M_A/3$ in (d), and the more complicated symmetric circuit of (e).

If the tube is not round, we may replace a by $\sqrt{S/\pi}$, where S is the cross-sectional area of the tube.

Example 4.1. The old-fashioned jug of Fig. 4.3 is used in a country dance band as a musical instrument. You are asked to analyze its performance acoustically, If the inside dimensions of the jug

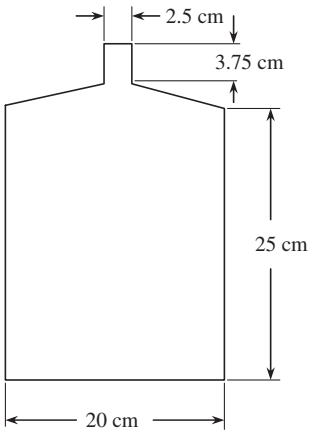

FIG. 4.3 Sketch of a musical jug.

are diameter = 20 cm and air-cavity height = 25 cm, give the analogous circuit, the element sizes, and the acoustic impedance for the air-cavity portion of the jug at 50, 100, and 300 Hz. Assume $T = 22°C$ and $P_0 = 10^5$ Pa. (*Note:* The neck portion will be discussed later in this part.)

Solution. The speed of sound at 22°C is about 345 m/s. Hence,

$\lambda_{50} = 6.9$ m
$\lambda_{100} = 3.45$ m
$\lambda_{300} = 1.15$ m

The length l of the jug is 0.25 m. Hence,

$$l = \frac{\lambda_{50}}{27.6} = \frac{\lambda_{100}}{13.8} = \frac{\lambda_{300}}{4.6} = 0.25 \text{ m}$$

At 50 Hz, where $l/\lambda = 1/28$, the cavity portion of the jug may be represented by an acoustic compliance:

$$C_A = \frac{V}{\gamma P_0} = \frac{7.85 \times 10^{-3}}{1.4 \times 10^5} = 5.61 \times 10^{-8} \text{ m}^5/\text{N}$$

$$Z_A = -j\frac{10^8}{314 \times 5.61} = -j5.7 \times 10^4 \text{ N}\cdot\text{s/m}^5$$

At 100 Hz, where $l/\lambda = 1/14$, the cavity portion of the jug may be represented by a series acoustic mass and acoustic compliance:

$$M_A = \frac{l\rho_0}{3\pi a^2} = \frac{0.25 \times 1.19}{3\pi(0.1)^2} = 3.2 \text{ kg/m}^4$$

$$C_A = 5.61 \times 10^{-8} \text{ m}^5/\text{N}$$

$$Z_A = j\left(628 \times 3.2 - \frac{10^8}{628 \times 5.61}\right) = -j2.6 \times 10^4$$

At 300 Hz, where $l/\lambda = 1/5$, the acoustic impedance of the cavity portion of the jug must be solved directly from Eq. (4.9):

$$Z_A = \frac{-j\rho_0 c}{\pi a^2}\cot kl$$

$$= \frac{-j(1.19 \times 345)}{\pi(0.1)^2}\cot\frac{2\pi \times 300 \times 0.25}{345}$$

$$Z_A = -j2.7 \times 10^3 \text{ N}\cdot\text{s/m}^5$$

Example 4.2. The jug of Example 4.1 has a neck with a diameter of 2.5 cm and a length of 3.75 cm (see Fig. 4.3). At what frequency will the jug resonate?

Solution. First, let us assume that the frequency of resonance is so low that the length of the neck l' is small compared with $\lambda/16$. Then, because the air in it is not constrained, it will be an acoustic mass:

$$M_A = \frac{\rho_0(l' + 0.85a + 0.61a)}{\pi a^2}$$

$$= 1.19\left(\frac{0.0375 + 1.46 \times 0.0125}{\pi(0.0125)^2}\right)$$

$$= 135 \text{ kg/m}^4$$

The volume velocity through the neck of the jug is the same as that entering the air cavity inside. Hence, the two elements are in series and will resonate at

$$f = \frac{1}{2\pi\sqrt{M_A C_A}} = \frac{10^4}{2\pi\sqrt{135 \times 5.61}}$$

$$= 58 \text{ Hz}$$

4.4 ACOUSTIC RESISTANCES

Any device in which the flow of gas occurs in phase with and directly proportional to the applied pressure may be represented as a pure acoustic resistance. In other words, there is no stored (reactive) energy associated with the flow. Four principal forms of acoustic resistance are commonly employed in acoustic devices: fine-meshed screens made of metal or cloth, small-bore tubes, narrow slits, and porous acoustical materials.

Screens are often used in acoustic transducers because of their low cost, ease of selection and control in manufacture, satisfactory stability, and relative freedom from inductive reactance. Slits are often used where an adjustable resistance is desired. This is accomplished by changing the width of the slit. Tubes have the disadvantage that unless their diameter is very small, which in turn results in a high resistance, there is usually appreciable inductive reactance associated with them. However, if a combination of resistance and inductance is desired, they are useful. Such combinations will be treated later in this part. Fibrous or porous acoustic materials, porous ceramics, and sintered metals are often used in industrial applications and are mixtures of mass and resistance. In all four forms of acoustic resistance, the frictional effects producing the resistance occur in the same manner.

In Fig. 4.4, we see the opposite sides 1 and 2 of a slit, or tube, or of one mesh of screen. An alternating pressure difference $(\tilde{p}_1 - \tilde{p}_2)$ causes a motion of the air molecules in the space between the sides 1 and 2. At 1 and 2 the air particles in contact with the sides must remain at rest. Halfway between the sides, the maximum amplitude of motion will occur. Frictional losses occur in a gas whenever adjacent layers of molecules move over each other with different velocities. Hence frictional losses occur in the example of Fig. 4.4 near each of the walls as marked by the letter (a). In any tube, slit, mesh, or interstice the losses become appreciable when the regions in which adjacent layers differ in velocity extend over the entire space.

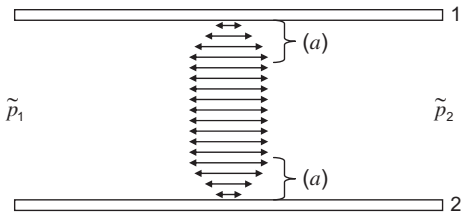

FIG. 4.4 Sketch showing the diminution of the amplitude of vibration of air particles in a sound wave near a surface.

The letters (*a*) show the regions in which viscous losses occur.

Screens. The specific acoustic resistances of a variety of dust screen sizes are shown in Table 4.1. The acoustic resistance is obtained by dividing the values of R_s in this table by the area of screen being considered.

Table 4.1 Specific acoustic resistances of dust screens

Type	R_S, rayls, N·s/m^3	Mesh opening, μm	No. holes/ cm^2	Open area, %	Thickness, μm	Weight, g/m^2
Acoustex 003	3	285	529	43%	255	110
Acoustex 006	6	105	4761	52%	63	25
Acoustex 010	10	120	3025	44%	105	51
Acoustex 020	20	68	8100	38%	62	32
Acoustex 032	32	38	22500	32%	48	25
Acoustex 047	47	38	19600	28%	48	31
Acoustex 075	75	25	32400	20%	52	33
Acoustex 090	90	41	8100	14%	125	86
Acoustex 145	145	27	19600	14%	70	52
Acoustex 160	160	21	36100	16%	58	45
Acoustex 260	260	18	40000	13%	60	48

Courtesy of Saati Spa—data based on existing product range

Care should be taken that a screen is tensioned before it is fitted. Otherwise it will not behave as a pure resistance, but more like a membrane with compliance. If it is too slack, its motion will be nonlinear. The acoustic resistances of screens are generally determined by test and not by calculations. **Tube of small diameter *[0.0005* $\sqrt{l}$ < radius a *(in meters)* < *0.002/* $\sqrt{f}$*].*** As derived in Par. 4.22, the acoustic impedance of a tube of very small diameter, neglecting the end corrections, is

$$Z_A = R_A + j\omega M_A \ \text{N}\cdot\text{s/m}^5 \tag{4.14}$$

where

$$R_A = \frac{8\mu l}{(1 + 4B_u)\pi a^4} \ \text{N}\cdot\text{s/m}^5 \tag{4.15}$$

$$M_A = \frac{4(1+3B_u)\rho_0\ l}{3(1+4B_u)\pi a^2}\ \text{kg/m}^4 \tag{4.16}$$

μ is viscosity coefficient. For air $\mu = 1.86 \times 10^{-5}$ N·s/m^2 at 20°C and 0.76 m Hg. This quantity varies with temperature, that is, $\mu \propto T^{0.7}$, where T is in °K.
l is length of tube in m.
a is radius of tube in m.
M_A is acoustic mass of air in tube in kg/m^4.
ρ is density of gas in kg/m^3.

and the boundary slip factor B_u is given by

$$B_u = (2\alpha_u^{-1} - 1)K_n \left(\simeq 0 \text{ for } a > 6\,\mu\text{m}\right), \tag{4.17}$$

where α_u is the accommodation coefficient, which is assumed to have a value of 0.9, and K_n is the (dimensionless) Knudsen number given by

$$K_n = \lambda_m / a, \tag{4.18}$$

where $\lambda_m = 60$ nm is the molecular mean free path length between collisions.

The mechanical impedance of a very small tube is found by multiplying Eq. (4.14) by $(\pi a^2)^2$, which yields

$$Z_M = 8\pi\mu\ l + j\frac{4}{3}M_M\omega \tag{4.19}$$

where $M_M = \rho_0 \pi a^2 l =$ mass of air in the tube in kilograms.

Narrow slit [1] [t (in meters) $< 0.003/\sqrt{f}$]. The acoustic impedance of a very narrow slit, neglecting end corrections, is

$$Z_A = \frac{12\mu\ l}{t^3 w} + j\frac{6\rho_0 l\omega}{5wt}\ \text{N·s/m}^5 \tag{4.20}$$

where

l is length of slit in m in direction in which the sound wave is traveling (see Fig. 4.5),
w is width of slit in m as viewed from the direction from which the wave is coming (see Fig. 4.5),
t is thickness of slit in m (see Fig. 4.5).

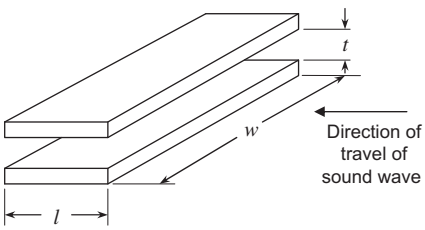

FIG. 4.5 Dimension of a narrow slit.

The mechanical impedance of a very narrow slit is given by multiplying Eq. (4.20) by t^2w^2:

$$Z_M = \frac{12\mu\, lw}{t} + j\frac{6}{5}M_M\omega \tag{4.21}$$

where $M_M = \rho_0 lwt$ = mass of air in the slit in kg.

Example 4.3. An acoustic resistance of 1 MN·s/m^5 is desired as the damping element in an earphone. Select a screen and the diameter of hole necessary to achieve this resistance.

Solution. As the resistance is needed for an earphone, it should be quite small. If we select an 020 mesh screen (see Table 4.1), the *specific* acoustic resistance is 20 rayls. For an acoustic resistance of 10^6 N·s/m^5, an area S is needed of

$$S = \frac{20}{10^6} = 20 \text{ mm}^2$$

The diameter d of the hole required for this area is

$$d = 2a = 2\sqrt{\frac{S}{\pi}} = 5.05 \text{ mm}$$

4.5 CAVITY WITH HOLES ON OPPOSITE SIDES—MIXED MASS-COMPLIANCE ELEMENT

A special case of an element that is frequently encountered in acoustical devices and that has often led to confusion in analysis is that shown in Fig. 4.6. Imagine this to be a doughnut-shaped element, each side of which has a hole of radius a bored in it. When a flow of air with a volume velocity $\tilde{U}_1$ enters opening 1, all the air particles in the vicinity of the opening will move with a volume velocity $\tilde{U}_1$. Part of this velocity goes to compress the air in the cylindrical space 3, and part of it appears as a movement of air that is not appreciably compressed. It was pointed out earlier that a portion of a gas that compresses without appreciable motion of the particles is to be treated as an acoustic compliance.

By inspection of Fig. 4.6 we see that the portion enclosed approximately by the dotted lines moves without appreciable compression and, hence, is an acoustic mass. That lying outside the dotted lines is

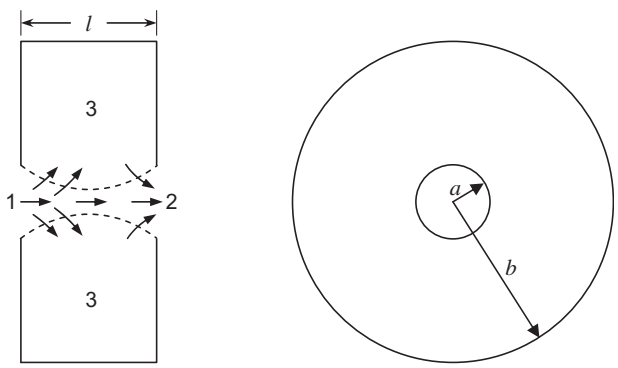

FIG. 4.6 Example of a mixed mass-compliance element made from a cavity with holes on opposite sides.

an acoustic compliance. The analogous circuit for this acoustic device is given in Fig. 4.7. The volume velocity $\tilde{U}_1$ entering opening 1 divides into two parts, one to compress the air ($\tilde{U}_3$) and the other ($\tilde{U}_2$) to leave opening 2. By judicious estimation we arrive at values for M_A. If the length l of the cylinder is fairly long and the volume 3 is large, M_A is merely the end correction l'' of Eq. (4.5). If the volume 3 is small, then M_A becomes nearly the acoustic mass of a tube of radius a and length $l/2$. The acoustic compliance is determined by the volume of air lying outside of the estimated dotted lines of Fig. 4.6.

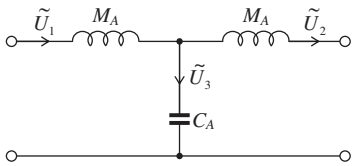

FIG. 4.7 Analogous circuit for the device of Fig. 4.6.

4.6 INTERMEDIATE-SIZED TUBE—MIXED MASS-RESISTANCE ELEMENT [a (in meters) > 0.01/ $\sqrt{f}$ and a < 10/f] [2]

The acoustic impedance for a tube with a radius a (in meters) that is less than 0.002/ $\sqrt{f}$ was given by Eqs. (4.14) and (4.16). Here we shall give the acoustic impedance for a tube whose radius (in meters) is greater than 0.01/ $\sqrt{f}$ but still less than 10/f. For a tube whose radius lies between 0.002/ $\sqrt{f}$ and 0.01/ $\sqrt{f}$ interpolation must be used. The acoustic impedance of the intermediate-sized tube is equal to

$$Z_A = R_A + j\omega M_A \tag{4.22}$$

where

$$R_A = \frac{\sqrt{2\omega\rho_0\mu}}{\pi a^2}\left(\frac{l'}{a} + (2)\right) \text{ N·s/m}^5 \tag{4.23}$$

$$M_A = \frac{\rho_0(l' + (2)l'')}{\pi a^2} \text{ kg/m}^2 \tag{4.24}$$

a is radius of tube in m.
ρ_0 is density of air in kg/m^3.
μ is viscosity coefficient. For air $\mu = 1.86 \times 10^{-5}$ N·s/m^2 at 20°C and 0.76 m Hg. This quantity varies with temperature, that is, $\mu \propto T^{0.7}$, where T is in °K.
l' is actual length of the tube.
l'' is end correction for the tube. It is given by Eq. (4.5) if the tube is flanged or Eq. (4.8) if the tube is unflanged. The numbers (2) in parentheses in Eqs. (4.23) and (4.24) must be used if both ends of the tube are being considered. If only one end is being considered, replace the number (2) with the number 1.
ω is angular frequency in rad/s.

4.7 PERFORATED SHEET—MIXED MASS-RESISTANCE ELEMENT [a (in meters) > 0.01/ $\sqrt{f}$ and $a < 10/f$] [2]

Many times, in acoustics, perforated sheets are used as mixed acoustical elements. We shall assume a perforated sheet with the dimensions shown in Fig. 4.8 and holes whose centers are spaced more than one diameter apart. For this case the acoustic impedance for each area b^2, that is, each hole, is given by

$$Z_A = R_A + j\omega M_A$$

where

$$R_A = \frac{\sqrt{2\omega\rho_0\mu}}{\pi a^2}\left\{\frac{t}{a} + 2\left(1 - \frac{A_h}{A_b}\right)\right\} \text{ kg}\cdot\text{s/m}^5 \tag{4.25}$$

$$M_A = \frac{\rho_0}{\pi a^2}\left\{t + 1.7a\left(1 - \frac{2.1a}{b}\right)\right\} \text{ kg/m}^4 \tag{4.26}$$

$A_h = \pi a^2$ is area of hole in m^2,
$A_b = b^2$ is area of a square around each hole in m^2,
t is thickness of the sheet in m.

If there are n holes, the acoustic impedance is approximately equal to $1/n$ times that for one hole.

Definition of Q. If this mass-resistance element is used with a compliance to form a resonant circuit, we are often interested in the ratio of the angular frequency of resonance ω_0 to the angular bandwidth ω (rad/s) measured at the half-power points. This ratio is called the "Q" of the circuit and is a measure of the sharpness of the resonance curve.

The "Q_A" of a perforated sheet when used with a compliance of such size as to produce resonance at angular frequency ω_0 is

$$Q_A = \frac{\omega_0 M_A}{R_A} = \sqrt{\frac{\omega_0\rho_0}{2\mu}}\, a\, \frac{t + 1.7a(1 - (a/b))}{t + 2a(1 - (\pi a^2/b^2))} \tag{4.27}$$

The Q_A is independent of the number of holes in the perforated sheet. We repeat that these formulas are limited to cases where the centers of the holes are spaced more than a diameter apart.

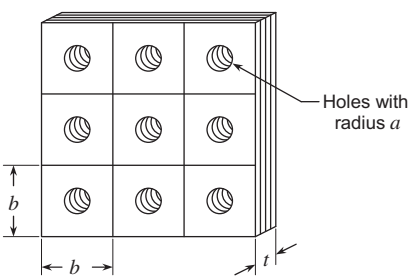

FIG. 4.8 Thin perforated sheet with holes of radius *a*, and length *l*, spaced a distance *b* on centers.

4.8 ACOUSTIC TRANSFORMERS

As for the other acoustical elements, there is no configuration of materials that will act as a "lumped" transformer over a wide frequency range. Also, what may appear to be an acoustic transformer when impedances are written as mechanical impedances may not appear to be one when written as acoustic impedances, and vice versa. As an example of this situation, let us investigate the case of a simple discontinuity in a pipe carrying an acoustic wave.

Junction of two pipes of different areas. A junction of two pipes of different areas is equivalent to a discontinuity in the area of a single pipe (see Fig. 4.9a).

If we assume that the diameter of the larger pipe is less than $\lambda/16$, then we may write the following two equations relating the pressure and volume velocities at the junction:

$$\tilde{p}_1 = \tilde{p}_2 \tag{4.28}$$

$$\tilde{U}_1 = \tilde{U}_2 \tag{4.29}$$

Equation (4.28) says that the sound pressure on both sides of the junction is the same. Equation (4.29) says that the volume of air leaving one pipe in an interval of time equals that entering the other pipe in the same interval of time. The transformation ratio for acoustic impedances is unity so that no transformer is needed.

For the case of a circuit using lumped *mechanical* elements the discontinuity appears to be a transformer with a turns ratio of S_1: S_2 because, from Eq. (4.28),

$$\frac{\tilde{f}_1}{S_1} = \frac{\tilde{f}_2}{S_2} \tag{4.30}$$

and, from Eq. (4.29),

$$\tilde{u}_1 S_1 = \tilde{u}_2 S_2 \tag{4.31}$$

where $\tilde{f}_1$ and $\tilde{f}_2$ are the forces on the two sides of the junction and $\tilde{u}_1$ and $\tilde{u}_2$ are the average particle velocities over the areas S_1 and S_2. We have

$$\tilde{f}_1 = \frac{S_1}{S_2}\tilde{f}_2 \tag{4.32}$$

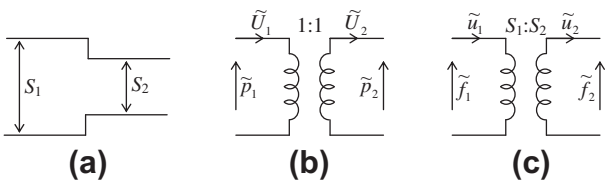

FIG. 4.9 (a) Simple discontinuity between two pipes. (b) Acoustic-impedance transducer representation of (a); because the transformation ratio is unity, no transformer is required. (c) Mechanical impedance transducer representation of (a).

and

$$\tilde{u}_2 = \frac{S_1}{S_2}\tilde{u}_1 \tag{4.33}$$

so that

$$Z_{M1} = \frac{\tilde{f}_1}{\tilde{u}_1} = \left(\frac{S_1}{S_2}\right)^2 \frac{\tilde{f}_2}{\tilde{u}_2} = \left(\frac{S_1}{S_2}\right)^2 Z_{M2} \tag{4.34}$$

A transformer is needed in this case and is drawn as shown in Fig. 4.9c.

It must be noted that a reflected wave will be sent back toward the source by the simple discontinuity. We saw in Part IV that, in order that there be no reflected wave, the specific acoustic impedance in the second tube $(\tilde{p}_2/\tilde{u}_2)$ must equal that in the first tube $(\tilde{p}_1/\tilde{u}_1)$. This is possible only if $S_1 = S_2$, that is, if there is no discontinuity.

To find the magnitude and phase of the reflected wave in the first tube resulting from the discontinuity, we shall use material from Part IV. Assume that the discontinuity exists at $x = 0$. The specific acoustic impedance in the first tube is

$$Z_{S1} = \frac{\tilde{p}_1}{\tilde{u}_1} \tag{4.35}$$

If the second tube is infinitely long, the specific acoustic impedance for it at the junction will be

$$Z_{S2} = \frac{\tilde{p}_2}{\tilde{u}_2} = \rho_0 c \tag{4.36}$$

[see Eq. (2.89)]. The impedance Z_{S1} at the junction is, from Eqs. (4.28) and (4.33),

$$Z_{S1} = \frac{\tilde{p}_1}{\frac{S_2\tilde{u}_2}{S_1}} = \frac{\tilde{p}_2}{\frac{S_2\tilde{u}_2}{S_1}} \tag{4.37}$$

From Eqs. (4.36) and (4.37),

$$Z_{S1} = \frac{S_1}{S_2}\rho_0 c \tag{4.38}$$

Using Eqs. (2.46) and (2.87), setting $x = 0$, we may solve for the reflected wave $\tilde{p}_-$ in terms of the incident wave $\tilde{p}_+$.

$$\tilde{p}_1 = \tilde{p}_+ - \tilde{p}_- \tag{4.39}$$

$$\tilde{u}_1 = \frac{1}{\rho_0 c}(\tilde{p}_+ - \tilde{p}_-) \tag{4.40}$$

$$\frac{\tilde{p}_1}{\tilde{u}_1} = \frac{S_1}{S_2}\rho_0 c = \rho_0 c \frac{\tilde{p}_+ + \tilde{p}_-}{\tilde{p}_+ - \tilde{p}_-} \tag{4.41}$$

$$\tilde{p}_- = \frac{S_1 - S_2}{S_1 + S_2}\tilde{p}_+ \tag{4.42}$$

The sound pressure $\tilde{p}_T$ of the transmitted wave in the second tube at the junction point must equal the sound pressure in the first tube at that point,

$$\tilde{p}_T = \tilde{p}_+ + \tilde{p}_- \tag{4.43}$$

so that

$$\tilde{p}_T = \frac{2S_1}{S_1 + S_2}\tilde{p}_+ \tag{4.44}$$

If S_1 equals S_2, there is no reflected wave $\tilde{p}_-$ and then $\tilde{p}_+ = \tilde{p}_T$.

Note also that if S_2 becomes vanishingly small, this case corresponds to the case of a rigid termination at the junction. For this case,

$$\tilde{p}_- = \tilde{p}_+ \tag{4.45}$$

and

$$\tilde{p}_+ + \tilde{p}_- = 2\tilde{p}_+ \tag{4.46}$$

This equation illustrates the often-mentioned case of *pressure doubling*. That is to say, when a plane sound wave reflects from a plane rigid surface, the sound pressure at the surface is double that of the incident wave.

Two pipes of different areas joined by an exponential connector [3]. An exponential connector may be used to join two pipes of different areas. Such a connector (see Fig. 4.10) acts as a simple discontinuity when its length is short compared with a wavelength and as a transformer for *acoustic* impedances when its length is greater than a half wavelength.

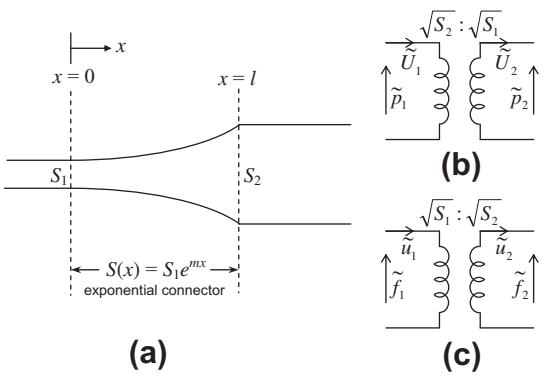

FIG. 4.10 (a) Exponential connector between two pipes. (b) high-frequency representation of (a) using acoustic-impedance transducer. (c) high-frequency representation of (a) using mechanical-impedance transducer.

If the second tube is infinitely long, then at $x = l$ (see Fig. 4.10),

$$\frac{\tilde{p}_2}{\tilde{u}_2} = \rho_0 c \tag{4.47}$$

If the cross-sectional area of the exponential connector is given by

$$S(x) = S_1 e^{mx} \tag{4.48}$$

and the length of the connector is l, then the specific acoustic impedance at $x = 0$ is

$$Z_{S1} = \frac{\tilde{p}_1}{\tilde{u}_1} = \rho_0 c \frac{\cos(bl + \theta) + j \sin(bl)}{\cos(bl - \theta) + j \sin(bl)} \tag{4.49}$$

where

$$b = 1/2 \sqrt{(4\omega^2/c^2) - m^2} \text{ in m}^{-1}$$

m is flare constant in m^{-1} [see Eq. (4.48)]
$\theta = \tan^{-1}(m/2b)$
c is speed of sound in m/s
l is length of the exponential connector in m
ρ_0 is density of air in kg/m^3.

At low frequencies (b imaginary and λ/l large),

$$\frac{\tilde{p}_1}{\tilde{U}_1} = \frac{\tilde{p}_2}{\tilde{U}_2} \qquad \text{or} \qquad Z_{A1} = Z_{A2} \tag{4.50}$$

At high frequencies (b real and $l/\lambda > 1$),

$$\frac{\tilde{p}_1}{\tilde{u}_1} = \frac{\tilde{p}_2}{\tilde{u}_2} \tag{4.51}$$

or

$$Z_{A1} = \frac{S_2}{S_1} Z_{A2} \tag{4.52}$$

At intermediate frequencies the transformer introduces a phase shift, and the transformation ratio varies between the limits set by the two equations above.

The transformation ratio for acoustic impedance at high frequencies is seen from Eq. (4.52) to be $\sqrt{S_2/S_1}$ (see Fig. 4.10b). That is to say,

$$Z_{A1} = \left(\sqrt{\frac{S_2}{S_1}}\right)^2 Z_{A2} \tag{4.53}$$

For mechanical impedance at high frequencies the transformation ratio is seen from Eq. (4.52) to be $\sqrt{S_1/S_2}$ (see Fig. 4.10c). That is to say,

$$Z_{M1} = \left(\sqrt{\frac{S_1}{S_2}}\right)^2 Z_{M2}$$

Example 4.4. It is desired to resonate the cavity in front of the diaphragm of a call loudspeaker, such as that found in a cellphone, to 3 kHz using an array of laser drilled sound outlet holes. The cavity has a volume of 0.4 cm^3 and a wall thickness of 1 mm. Determine the size and number of holes needed, assuming a $Q_A = 1.5$ and a ratio of hole diameter to on-center spacing of 0.5.

Solution. From Eq. (4.27) we see that, approximately,

$$Q_A \approx \frac{a\sqrt{1.18\omega_0}}{\sqrt{2 \times 1.86 \times 10^{-5}}}$$

$$a = \frac{1.5 \times 0.00397 \times \sqrt{2}}{\sqrt{6.28 \times 3000}} = 61.3\ \mu\text{m}$$

The diameter of the hole is 123 μm.

The reactance of the cavity at resonance equals

$$X_B = \frac{1}{\omega_0 C_A} = \frac{\gamma P_0}{18840 \times\ V} = \frac{1.4 \times 10^{11}}{18840 \times 0.4} = 18.6 \times 10^6\ \text{N}\cdot\text{s/m}^5$$

The desired acoustic mass of the holes is

$$M_A = \frac{X_B}{\omega_0} = \frac{18.6 \times 10^6}{18840} = 985\ \text{kg/m}^4$$

If there are n holes, the acoustic mass for each hole equals

$$nM_A = n(985)\ \text{kg/m}^4$$

From Eq. (4.26),

$$n(985) = \frac{1.18}{\pi(61.3^2 \times 10^{12})}(0.001 + (1.7 \times 18.6 \times 10^{-6})(0.75))$$

$$n = \frac{(1.18)(1.024 \times 10^{-3})}{\pi(985)(3.76 \times 10^{-9})} \approx 104\ \text{holes}$$

Example 4.5. Design a single-section T low-pass wave filter, as shown in Fig. 4.6 and Fig. 4.7, with a cutoff frequency of 100 Hz and Q value of $1/\sqrt{2}$ for critical damping. The filter is driven by a piston at the entrance on the left and terminated with an impedance of $R_0 = 10^3\ \text{N}\cdot\text{s/m}^5$ at the exit on the right.

Solution. Because the filter is driven by a piston with a defined velocity, it can be regarded as having a source impedance that is very large in comparison with the acoustic mass on the left of Fig. 4.7. We can therefore ignore that element. The filter is thus reduced to a second-order type with a cutoff frequency of

$$f_0 = \frac{1}{2\pi\sqrt{M_A C_A}}$$

The design Q is equal to

$$Q = \frac{1}{R_0}\sqrt{\frac{M_A}{C_A}}$$

From these two equations we can solve for C_A and M_A.

$$M_A = \frac{1}{4\pi^2 f_0^2 C_A}$$

$$= \frac{R_0 Q}{2\pi f_0}$$

So

$$C_A = \frac{1}{2\pi f_0 R_0 Q}$$

$$= \frac{\sqrt{2}}{2\pi \times 100 \times 10^3} = 2.25 \times 10^{-6}\ \text{m}^5/\text{N}$$

$$M_A = \frac{10^3}{2\pi \times 100 \times \sqrt{2}} = 1.125\ \text{kg/m}^4$$

From Sec. 4.6 and Eq. (4.24), with l' equal to zero, we get the size of the hole in the device of Fig. 4.6.

$$M_A = \frac{\rho_0(0.85a)}{\pi a^2}$$

$$\frac{(1.18)(0.85)}{\pi a} = 1.125$$

$$a = 28.4\ \text{cm}$$

The diameter of the hole is 0.57 m. The volume of the cavity is

$$V = C_A \gamma P_0 = 1.4 \times 2.25 \times 10^{-6} \times 10^5$$
$$= 0.315\ \text{m}^3$$

The elements for the T section are thereby determined.

PART XI: ELEMENTARY REFLECTION AND RADIATION OF SOUND

In order fully to specify a source of sound, we need to know, in addition to other properties, its directivity characteristics at all frequencies of interest. Some sources are non-directional, that is to say, they radiate sound equally in all directions and as such are called spherical radiators. Others may be highly directional, either because their size is naturally large compared to a wavelength or because of special design. In particular, we shall examine how the shape of the radiator influences its directivity.

The most elementary radiator of sound is a spherical source whose radius is small compared to one-sixth of a wavelength. Such a radiator is called a *simple source* or a *point source*. Its properties are specified by the magnitude of the velocity of its surface and by its phase relative to some reference. More complicated sources such as plane or curved radiators may be treated analytically by applying boundary conditions or as a combination of simple sources, each with its own surface velocity and phase, and these will be covered in Chapters 12 and 13.

A particularly important consideration in the design of loudspeakers and horns is their directivity characteristics. This chapter serves as an important basis for later chapters dealing with loudspeakers, baffles, and horns.

The basic concepts governing radiation of sound must be grasped thoroughly at the outset. It is then possible to reason from those concepts in deducing the performance of any particular equipment or in planning new systems. Examples of measured radiation patterns for common loudspeakers are given here as evidence of the applicability of the basic concepts.

The *directivity pattern* of a transducer used for the emission or for reception of sound is a description, usually presented graphically, of the response of the transducer as a function of the direction of the transmitted or incident sound waves in a specified plane and at a specified frequency.

The *beam width* of a directivity pattern is used in this text as the angular distance between the two points on either side of the principal axis where the sound pressure level is down 6 dB from its value at $\theta = 0$.

Before considering specific sound sources, we will first study some fundamental properties of sound waves using the example of reflection from a plane.

4.9 REFLECTION OF A PLANE WAVE FROM A PLANE

Reflections from a plane are *specular*, meaning that they are well defined due to the regular geometry of the reflecting surface, as opposed to *diffuse*, as in the case of an irregular reflecting object. In the latter case, the sound waves are reflected in many different directions. However, although a sphere reflects sound over a wide angle, as we shall see in Sections 12.3 and 12.4, the reflection is specular because the reflecting surface is regular. Refer to Fig. 4.11. A plane wave with amplitude $\tilde{p}_I$ is incident upon a plane at $x = 0$, the surface of which has a specific acoustic impedance Z_s. Depending on the value of Z_s, a portion of the incident wave is reflected with amplitude $\tilde{p}_R$. The angle θ_I between the

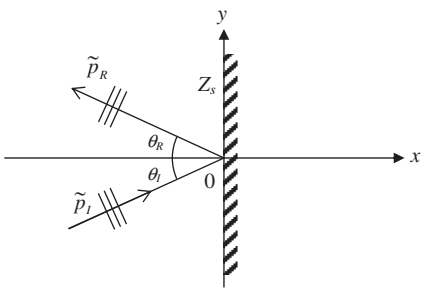

FIG. 4.11 Reflection of a plane wave from a plane at $x = 0$.

incident wave and the normal to the plane, formed by the x axis, is the *angle of incidence*. Similarly, the angle θ_R between the reflected wave and the normal to the plane is the *angle of reflection*. In this instance, we assume neither wave has any component in the z direction (away from the page).

Substituting $k_x = k\cos\theta$, $k_y = k\sin\theta$, and $k_z = 0$ in the wave equation solution of Eq. (2.119) (which satisfies $k^2 = k_x^2 + k_y^2 + k_z^2$), we obtain the following expression for the pressure field in the negative x region of Fig. 4.11:

$$\tilde{p}(x,y) = \tilde{p}_I e^{-jkx\cos\theta_I} e^{-jky\sin\theta_I} + \tilde{p}_R e^{jkx\cos\theta_R} e^{jky\sin\theta_R}. \tag{4.54}$$

where the particle velocity in the x direction is given by

$$\begin{aligned}\tilde{u}_x(x,y) &= \frac{1}{-jk\rho_0 c}\frac{\partial}{\partial x}\tilde{p}(x,y) \\ &= \frac{1}{\rho_0 c}\left(\tilde{p}_I e^{-jkx\cos\theta_I} e^{-jky\sin\theta_I}\cos\theta_I - \tilde{p}_R e^{jkx\cos\theta_R} e^{jky\sin\theta_R}\cos\theta_R\right).\end{aligned} \tag{4.55}$$

Let us now consider the boundary condition for two values of Z_S. When $Z_s = \infty$, the surface is totally rigid and the normal particle velocity at $x = 0$ is zero. This is often referred to as a *Neumann* boundary condition. Hence

$$\tilde{u}_x(0,y) = \frac{1}{\rho_0 c}\left(\tilde{p}_I e^{-jky\sin\theta_I}\cos\theta_I - \tilde{p}_R e^{jky\sin\theta_R}\cos\theta_R\right) = 0, \tag{4.56}$$

which is satisfied if

$$\theta_R = -\theta_I \tag{4.57}$$

and

$$\tilde{p}_R = \tilde{p}_I. \tag{4.58}$$

The latter would appear to be a reasonable assumption considering that no losses occur during a reflection from a perfectly rigid boundary. When $Z_s = 0$, the surface is totally flexible or *resilient* and the surface pressure is zero. This is often referred to as a *Dirichlet* boundary condition and is somewhat akin to the boundary condition at the mouth of an open pipe if we assume that the radiation load is negligible. It is also often referred to as a "pressure release" boundary condition. In this case

$$\tilde{p}(0,y) = \tilde{p}_I e^{-jky\sin\theta_I} + \tilde{p}_R e^{jky\sin\theta_R} = 0, \tag{4.59}$$

which is satisfied if

$$\theta_R = -\theta_I \tag{4.60}$$

and

$$\tilde{p}_R = -\tilde{p}_I. \tag{4.61}$$

Again the latter would appear to be a reasonable assumption considering that no losses occur during a reflection from a perfectly resilient boundary. Eq. (4.60) is known as the *law of reflection*. Generally,

the law of reflection can be shown to hold for all boundary impedance values. The impedance at the plane is simply the ratio of the pressure to particle velocity:

$$Z_s = \frac{\tilde{p}(0,y)}{\tilde{u}_x(0,y)}\Big|_{\theta_R=-\theta_I} = \frac{(\tilde{p}_I + \tilde{p}_R)\rho_0 c}{(\tilde{p}_I - \tilde{p}_R)\cos\theta_I}. \tag{4.62}$$

Rearranging for $\tilde{p}_R$ gives

$$\tilde{p}_R = -\frac{1 - (Z_s \cos\theta_I)/\rho_0 c}{1 + (Z_s \cos\theta_I)/\rho_0 c}\tilde{p}_I. \tag{4.63}$$

What this equation tells us is that if we let $Z_s = \rho_0 c$, only normal incident waves (*i.e.* $\theta_I = 0$) are totally absorbed. If $\theta_I \neq 0$, there will be a reflected wave. In other words: *A $\rho_0 c$ boundary condition is not an open window.* This has quite far reaching implications in acoustics. For example, when waves from a sound source in an anechoic chamber reach the walls, they are rarely perfectly normal. Hence absorbent "wedges" are typically used in order to produce multiple or diffuse reflections so that after a certain number of reflections, the reverberant sound field is reduced to an acceptable level. Also, when modeling sound sources using the finite element method, it is usually necessary to create a virtual anechoic chamber filled with air elements. A sphere coated with $\rho_0 c$ elements should produce acceptable results provided that the sphere is large enough for the waves that reach its inner surface to be spherically-diverging far-field ones. Otherwise, if the field immediately adjacent to the inner surface is the complex near-field, then reflections are guaranteed. We shall study the differences between the near-field and far-field pressure due to various sound sources further on in this text.

4.10 RADIATION FROM A PULSATING SPHERE

The pulsating sphere may be one of the most difficult sound sources to realize in practice, but it is the easiest three-dimensional source to analyze. Due to rotational symmetry, it can be treated as a one-dimensional problem with just a single radial ordinate *r*. Many practical sources behave in a similar way at low frequencies where they become virtually omnidirectional, as we shall see. Also, ultrasonic hydrosounders are often in the form of a sphere coated with a piezoelectric transducer. Essentially, the pulsating sphere is a sphere whose radius oscillates harmonically. In the limiting case, it will lead us to the point source, which forms a fundamental building block in acoustics.

Pressure field. Since the sphere is radiating into free space, where there are no reflections, we take the outward going part of the solution to the spherical wave equation (2.25) given by Eq. (2.107), where $\tilde{p}_+$ is an unknown coefficient to be determined from the boundary conditions. Let us now impose a boundary condition at the surface of the sphere whereby the particle velocity normal to the surface, given by Eq. (2.108), is equal to the uniform surface velocity $\tilde{u}_0$ so that $\tilde{u}(R) = \tilde{u}_0$, where R is the radius, which gives

$$\tilde{A}_+ = -\frac{jkR^2\rho_0 c e^{jkR}}{1 + jkR}\tilde{u}_0. \tag{4.64}$$

Inserting this into Eq. (2.107) and substituting $\tilde{U}_0 = 4\pi R^2 \tilde{u}_0$, where $\tilde{U}_0$ is the total volume velocity, yields

$$\tilde{p}(r) = -jk\rho_0 c\tilde{U}_0 \frac{e^{-jk(r-R)}}{4\pi r} D, \tag{4.65}$$

where D is called a directivity function, but here it has no angular dependency and is merely a frequency response function given by

$$D = \frac{1}{1+jkR}. \tag{4.66}$$

which is plotted in Fig. 4.12. Likewise from Eq. (2.108) for the velocity we have

$$\begin{aligned} \tilde{u}(r) &= \frac{1}{-jk\rho_0 c}\frac{\partial}{\partial r}\tilde{p}(r) \\ &= -(1+jkr)\tilde{U}_0 \frac{e^{-jk(r-R)}}{4\pi r^2} D. \end{aligned} \tag{4.67}$$

Radiation impedance. The specific radiation impedance is found by dividing the pressure at $r = R$ from Eq. (4.65) by the surface velocity $\tilde{u}_0$ as follows:

$$Z_s = \frac{\tilde{p}(R)}{\tilde{u}_0} = \frac{jkR}{1+jkR}\rho_0 c, \tag{4.68}$$

or

$$Z_s = \boldsymbol{R}_s + jX_s = \frac{k^2R^2 + jkR}{k^2R^2 + 1}\rho_0 c. \tag{4.69}$$

It turns out that this is the same as the impedance from Eq. (2.109) for a freely propagating spherical wave at a distance R from the origin. It is also the first time derivative of D from Eq. (4.66), above, multiplied by $\rho_0 R$. The real and imaginary parts, $\boldsymbol{R}_s$ and X_s are plotted in Fig. 4.13.

It is seen from Fig. 4.13 that for $kR < 0.3$, that is, when the diameter is less than one-tenth of the wavelength, the radiation impedance is mainly that of a *mass* reactance because the resistive component is negligible compared with the reactance component. This mass loading may be thought of as a layer of air on the outside of the sphere, the thickness of which equals 0.587 of the radius of the sphere. At all frequencies, the loading shown in Fig. 4.13 may be represented by the equivalent circuit inset.

We also observe from Fig. 4.12 that for $kR < 0.3$, the radiated sound pressure is proportional to the volume *acceleration* $(j\omega\tilde{U}_0)$ so that the radiated intensity, which is proportional to the square of the radiated pressure (see Eq. (1.12)), is held constant. This is due to the fact that the decreasing velocity (which is the time integral of the acceleration) is compensated for by the rising radiation resistance, which is proportional to the square of the velocity:

$$I = \left|\frac{\tilde{p}(r)}{\sqrt{2}}\right|^2 \frac{1}{\rho_0 c} = \left|\frac{\tilde{u}_0}{\sqrt{2}}\right|^2 \frac{\boldsymbol{R}_s}{4\pi r^2} \tag{4.70}$$

The relationship between radiation impedance and far-field pressure forms the basis of a useful theorem developed in Sec. 13.13. For $kR > 3$, the pressure is proportional to the volume *velocity* $\tilde{U}_0$ because the radiation impedance is mainly resistive.

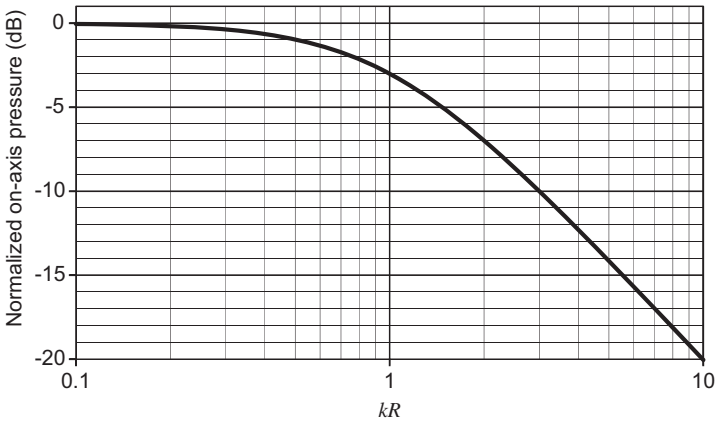

FIG. 4.12 Plot of 20 $\log_{10}(|D|)$ for a pulsating sphere with constant radial acceleration.

Frequency is plotted on a normalized scale, where $kR = 2\pi R/\lambda = 2\pi fR/c$.

Equations (4.65) and (4.67) are significant because they reveal the difference between the responses of a microphone sensitive to pressure and a microphone sensitive to particle velocity as the microphones are brought close to a small spherical source of sound at low frequencies. As r is made smaller, the output of the pressure-responsive microphone will double for each halving of the distance between the microphone and the center of the spherical source. Expressed in decibels, the output increases 6 dB for each halving of distance. For the velocity-responsive microphone, the output variation is not so simple.

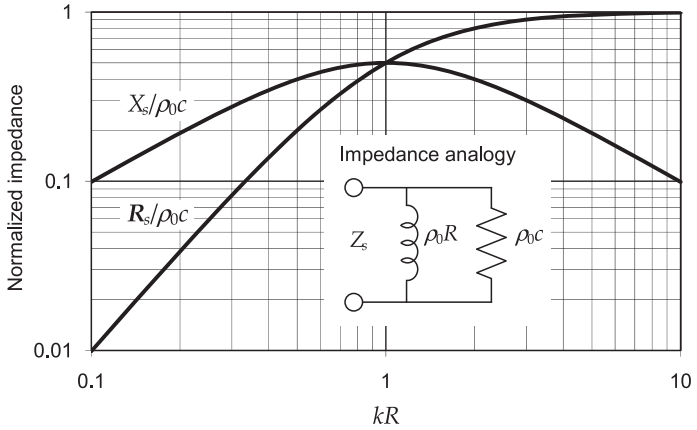

FIG. 4.13 Real and imaginary parts of the normalized specific radiation impedance $Z_s/\rho_0 c$ of the air load on a pulsating sphere of radius R located in free space.

Frequency is plotted on a normalized scale where $kR = 2\pi fR/c = 2\pi R/\lambda$. Note also that the ordinate is equal to $Z_M/\rho_0 cS$, where Z_M is the mechanical impedance; and to $Z_A S/\rho_0 c$, where Z_A is the acoustic impedance. The quantity S is the area for which the impedance is being determined, which in this case is $S = 4\pi R^2$ and $\rho_0 c$ is the characteristic impedance of the medium.

Only at sufficiently large distances ($k^2r^2 >> 1$) does the output increase 6 dB for each halving of distance. For shorter distances the second term inside the parentheses on the right-hand side of Eq. (4.67) becomes large, and the magnitude of $\tilde{u}$ increases at a rate exceeding +6 dB for each halving of distance. For very short distances ($k^2r^2 << 1$), the rate of increase of $\tilde{u}$ approaches a limit of +12 dB for each halving of distance. It is for this reason that the voice of a vocalist sounds "bassy" when he or she sings very near to a velocity-sensitive microphone which was designed to have its best response when located a large distance from the source of sound. This is commonly known as the proximity effect.

Another significant thing is to be learned from Eq. (4.69). At low frequencies it is very difficult to radiate sound energy from a small loudspeaker. A small loudspeaker may be likened to a pulsating balloon of some small radius R. The specific acoustic impedance Z_s of the air presented to each square centimeter of the balloon is given by Eq. (4.69) and Fig. 4.13. At low frequencies, the impedance becomes nearly purely reactive, and the resistance becomes very, very small. Hence, the power radiated by a small loudspeaker becomes very small. At high frequencies, $kR > 2$, the impedance Z_s becomes nearly purely resistive and has its maximum value of $\rho_0 c$, so that the power radiated for a given value of $\tilde{U}_0$ reaches its maximum.

4.11 RADIATION FROM A MONOPOLE POINT SOURCE (SIMPLE SOURCE)

Pressure and particle velocity. The pressure and particle velocity in the sound field of a monopole point source are obtained by setting $R \rightarrow 0$ in Eqs. (4.65) and (4.67) respectively:

$$\tilde{p}(r) = -jk\rho_0 c\tilde{U}_0 \frac{e^{-jkr}}{4\pi r}, \tag{4.71}$$

$$\tilde{u}(r) = -(1 + jkr)\tilde{U}_0 \frac{e^{-jkr}}{4\pi r^2}, \tag{4.72}$$

where

$\tilde{U}_0$ is volume velocity in m^3/s of the very small source and is equal to $(4\pi a^2)\tilde{u}_0$.
$\tilde{p}$ is sound pressure in Pa at a distance r from the simple source.

Strength of a point source [3]. The magnitude of the total air flow at the surface of a simple source in m^3/s is given by $\tilde{U}_0$ and is called the *strength of a point source*.

Intensity at distance r. At a distance r from the center of a simple source the intensity is given by

$$I = \left|\frac{\tilde{p}(r)}{\sqrt{2}}\right|^2 \frac{1}{\rho_0 c} = \left|\frac{\tilde{U}_0}{\sqrt{2}}\right|^2 \frac{f^2\rho_0}{4r^2 c} \text{ W/m}^2. \tag{4.73}$$

When the dimensions of a source are *much smaller* than a wavelength, the radiation from it will be much the same no matter what shape the radiator has, as long as all parts of the radiator vibrate substantially in phase. The intensity at any distance is directly proportional to the square of the volume velocity and the frequency. We will show in Sec. 12.2 how the point source itself can form a very useful building block for solving problems in acoustics

4.12 COMBINATION OF POINT SOURCES IN PHASE

The basic principles governing the directivity patterns from loudspeakers can be learned by studying combinations of simple sources. This approach is very similar to the consideration of Huygens wavelets in optics, which will be discussed more in Sec. 12.1. Basically, our problem is to add, vectorially, at the desired point in space, the sound pressures arriving at that point from all the simple sources. Let us see how this method of analysis is applied.

Two point sources in phase. The geometric situation is shown in Fig. 4.14. It is assumed that the distance r from the two point sources to the point P at which the pressure p is being measured is large compared with the separation b between the two sources.

The spherical sound wave arriving at the point p from source 1 will have traveled a distance $r - \Delta r$ where

$$\Delta r = \frac{1}{2} b \sin\theta \tag{4.74}$$

and from Eq. (4.71) the sound pressure will be

$$\tilde{p}_1(r,\theta) = \frac{\tilde{A}_+}{r - \Delta r} e^{-jk(r-\Delta r)}, \tag{4.75}$$

where

$$\tilde{A}_+ = -jk\rho_0 c\tilde{U}_0/(4\pi).$$

The wave from source 2 will have traveled a distance $r + \Delta r$, so that

$$\tilde{p}_2(r,\theta) = \frac{\tilde{A}_+}{r + \Delta r} e^{-jk(r+\Delta r)}. \tag{4.76}$$

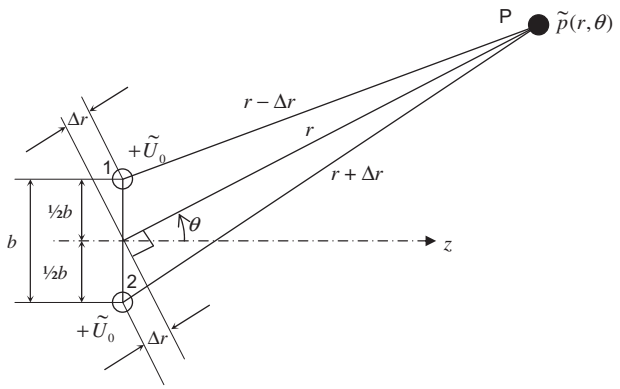

FIG. 4.14 Two point (simple) sources vibrating in phase located a distance *b* apart and at distance *r* and angle θ with respect to the observation point *P*.

The sum of $p = p_1 + p_2$, assuming $r >> b$, gives

$$\tilde{p}(r,\theta) = \frac{\tilde{A}_+}{r} e^{-jkr}(e^{jk\Delta r} + e^{-jk\Delta r}). \tag{4.77}$$

Multiplication of the numerator and the denominator of Eq. (4.77) by

$$\exp(jk\Delta r) - \exp(-jk\Delta r)$$

and replacement of the exponentials by sines, yields

$$\tilde{p}(r,\theta) = \frac{2\tilde{A}_+}{r} e^{-jkr} D(\theta), \tag{4.78}$$

where the directivity function $D(\theta)$ is given by

$$D(\theta) = \frac{\sin 2k\Delta r}{2\sin k\Delta r} = \cos k\Delta r, \tag{4.79}$$

where we have used $\sin 2x = 2 \sin x \cos x$. Substituting Eq. (4.74) and $k = 2\pi/\lambda$ in Eq. (4.79) gives

$$D(\theta) = \frac{\sin\left((2\pi\, b/\lambda)\sin\theta\right)}{2\sin\left((\pi\, b/\lambda)\sin\theta\right)} = \cos\left((\pi\, b/\lambda)\sin\theta\right). \tag{4.80}$$

Referring to Fig. 4.14, we see that if b is very small compared with a wavelength, the two sources essentially coalesce and the pressure at a distance r at any angle θ is double that for one source acting alone. The directivity pattern will be that of Fig. 4.25 for a pulsating sphere, i.e., omnidirectional.

As b gets larger, however, the pressures arriving from the two sources will be different in phase and the directivity pattern will not be a circle. In other words, the sources will radiate sound in some directions better than in others. Maxima will occur when

$$m\lambda = b\sin\theta, \qquad m = 0,\ 1,\ \cdots \tag{4.81}$$

and nulls will occur when

$$\left(m + \frac{1}{2}\right)\lambda = b\sin\theta, \qquad m = 0,\ 1,\ \cdots. \tag{4.82}$$

As a specific example, let $b = \lambda/2$. For $\theta = 0$ or 180° it is clear that the pressure arriving at a point P will be double that from either source. However, for $\theta = \pm\ 90^\circ$ the time of travel between the two simple sources is just right so that the radiation from one source completely cancels the radiation from the other. Hence, the pressure at all points along the $\pm\ 90^\circ$ axis is zero. Remember, we have limited our discussion to $r >> b$.

Directivity patterns, expressed in decibels relative to the pressure at $\theta = 0$, are given in Fig. 4.15 for the two in-phase sources with $b = \lambda/4;\ \lambda/2;\ \lambda;\ 3\lambda/2;$ and 2λ.

A very important observation can be made from the directivity patterns for this simple type of radiator that applies to all types of radiation. The longer the extent of the radiator (i.e., here, the greater b is), the sharper will be the principal lobe along the $\theta = 0$ axis at any given frequency and the greater

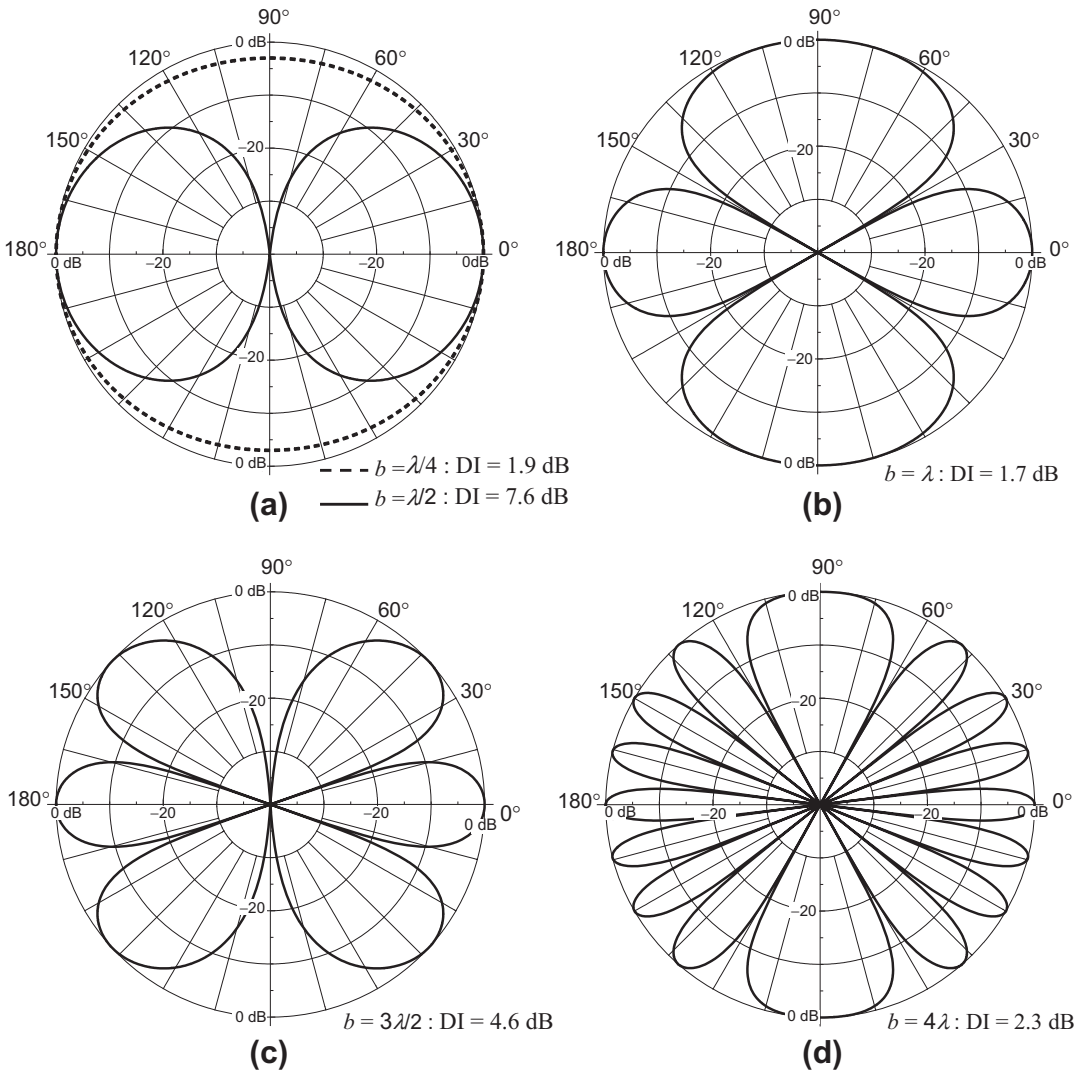

FIG. 4.15 Far-field directivity patterns for the two in-phase point sources of Fig. 4.14.

Symmetry of the directivity patterns occurs about the axis passing through the two sources. Hence, only a single plane is necessary to describe the directivity characteristics at any particular frequency. The directivity index (DI) is given at $\theta = 0°$. (The directivity index is discussed in Sec. 4.16.)

the number of side lobes. As we shall see in the next paragraph, it is possible to suppress the side lobes, that is to say, those other than the principal lobes at 0 and 180°, by simply increasing the number of elements.

Linear array of point sources. The geometric situation for this type of radiating array is shown in Fig. 4.16. The sound pressure produced at a point P by N identical in-phase point sources, lying in

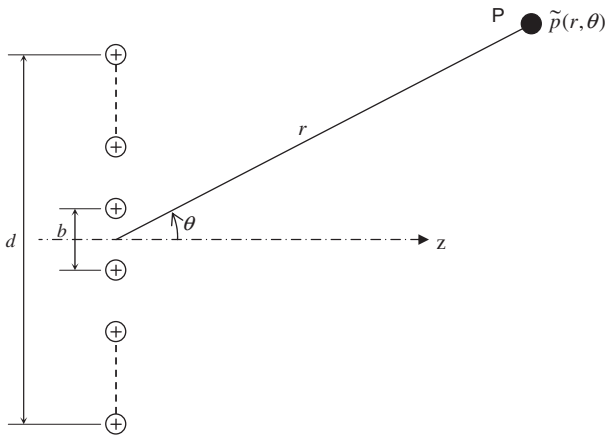

FIG. 4.16 A linear array of *N* simple sources, vibrating in phase, located a distance *b* apart.

The center of the array is at distance r and angle θ with respect to the observation point P.

a straight line, the sources a distance b apart and with the extent $d = (N-1)b$ small compared with the distance r, is

$$\tilde{p}(r,\theta) = N\frac{\tilde{A}_+}{r}e^{-jkr}D(\theta), \tag{4.83}$$

where

$$D(\theta) = \frac{1}{N}\sum_{n=\frac{1-N}{2}}^{\frac{N-1}{2}} e^{-jnkb\sin\theta} = \frac{1}{N}\sum_{n=\frac{1-N}{2}}^{\frac{N-1}{2}} \cos(nkb\sin\theta). \tag{4.84}$$

Using the identity of Eq. (51) from Appendix II, this simplifies to

$$D(\theta) = \frac{\sin\left((N\pi\, b/\lambda)\sin\,\theta\right)}{N\sin\left((\pi\, b/\lambda)\sin\,\theta\right)}. \tag{4.85}$$

From Fig. 4.17(*d*), we see that when the wavelength is smaller than the pitch b of the point sources, we have global maxima with an amplitude of 0 dB and local maxima of smaller amplitude in between. The ratio between the amplitudes of the global maxima and the smallest local maxima approaches N as N increases. In this case, where $N = 4$, the ratio is 3.7 or 11.3 dB. Global maxima will occur when

$$m\lambda = b\sin\,\theta, \qquad m = 0,\ 1,\ \cdots \tag{4.86}$$

and nulls will occur when

$$m\lambda = Nb\sin\,\theta, \qquad \begin{cases} m = \ 1,\ 2,\ \cdots \\ m \neq 0,\ N,\ 2N,\ \cdots \end{cases}. \tag{4.87}$$

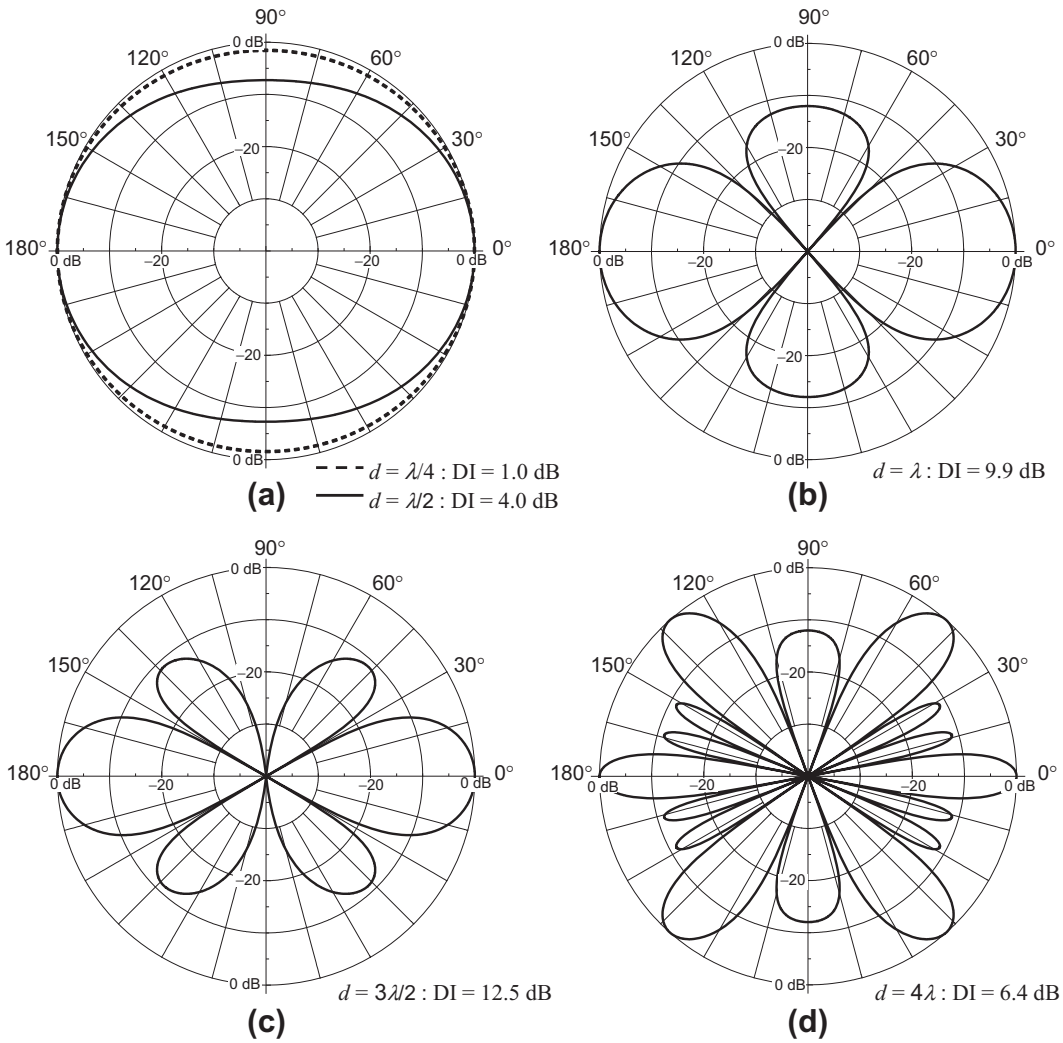

FIG. 4.17 Far-field directivity patterns for a linear array of four simple in-phase sources evenly spaced over a length *d*. The directivity index (DI) is given at $\theta = 0^\circ$.

Hence the global maxima are determined by the pitch of the individual point sources and the nulls are determined by the total length of the array. The global maxima correspond to the sampling wave-number (or spatial sampling frequency) k_S of the array, that is the wave-number at which the point sources are one wavelength apart, so that $k_S = 2\pi/b$. In this case, $d = 3b$ so that $\lambda_S = d/3$. Below this wavelength, the maxima of the directivity function no longer decay with increasing angle, but begin to rise again after a specific angle given by $\lambda = 2b \sin\theta$. This phenomenon is known as *spatial aliasing* and is particularly important for microphone arrays.

As a special case, let us assume that the number of points becomes very large and that the separation b becomes very small. Then, as before,

$$d = (N-1)b \approx Nb \tag{4.88}$$

which we insert into Eq. (4.85) and, noting that the denominator term $N\sin(\pi\, d/(N\lambda)\sin\,\theta) \rightarrow (\pi\, d/\lambda)\sin\,\theta$ as $N \rightarrow \infty$, we obtain the following directivity function for a linear line array

$$D(\theta) = \frac{\sin\left((\pi\, d/\lambda)\sin\,\theta\right)}{(\pi\, d/\lambda)\sin\,\theta}. \tag{4.89}$$

As before, it is assumed that the extent of the array d is small compared with the distance r. Nulls will occur when

$$m\lambda = d\sin\,\theta, \qquad m = 1,\ 2,\ \cdots. \tag{4.90}$$

Now that there are no spaces between the point sources, which have coalesced into a line source, the global maxima have vanished and we are left with local maxima that decay with increasing angle θ.

Plots of Eq. (4.85) for $N = 4$ and $d = \lambda/4$, $\lambda/2$, λ, $3\lambda/2$, and 2λ are shown in Fig. 4.17. Similar plots for $N \rightarrow \infty$ and $b \rightarrow 0$, that is, Eq. (4.89), are given in Fig. 4.18.

The principal difference among Fig. 4.15, Fig. 4.17, and Fig. 4.18 for a given ratio of array length to wavelength is in the suppression of the "side lobes." That is, sound is radiated well in the $\theta = 0^\circ$ and $\theta = 180^\circ$ directions for all three arrays. However, as the array becomes longer and the number of elements becomes greater, the radiation becomes less in other directions than at $\theta = 0^\circ$ and $\theta = 180^\circ$.

4.13 STEERED BEAM-FORMING ARRAY OF POINT SOURCES

We saw in the previous paragraph that at high frequencies a linear array of point sources becomes highly directional. There are many applications in acoustics where we wish to concentrate sound in a particular direction, or in the case of microphones, receive sound from a particular direction while blocking unwanted sounds from elsewhere. This can be achieved by applying appropriate time delays or advances to the point sources as shown in Fig. 4.19 in order to "steer" the beam in the desired direction at an angle α to the z axis. The other difference between Fig. 4.19 and the previous Fig. 4.16 is that we have rotated the reference z axis by 90° so that it is now the axis of rotational symmetry. This is important for when we come to optimize the array.

Although in this example delays *and* advances are applied to the sources in the positive and negative z positions respectively, we would in practice only use delays so that the source with the largest advance would have zero delay and the delay would increase progressively towards the source with the largest delay, which would have its delay doubled. However, the symmetrical arrangement

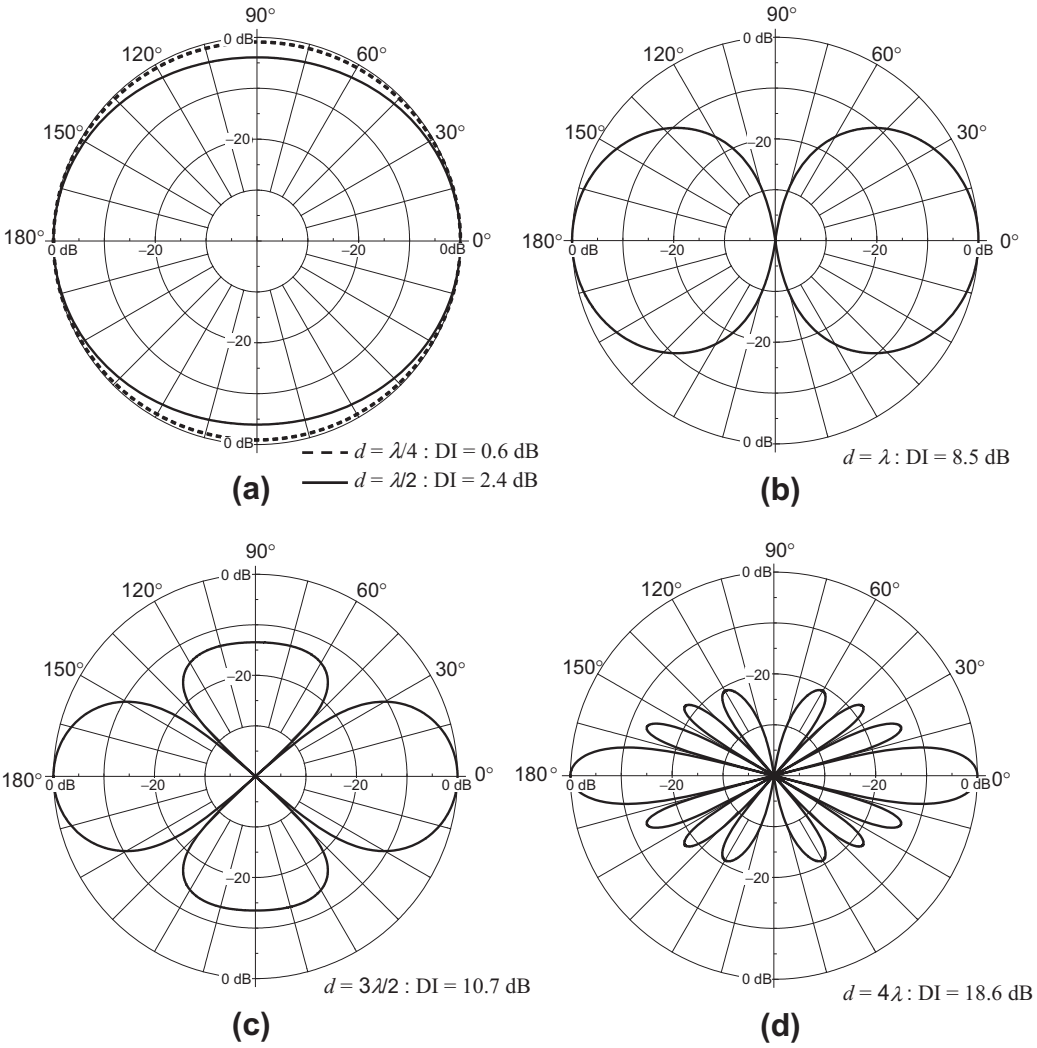

FIG. 4.18 Far-field directivity patterns for a linear line array radiating uniformly along its length *d*. The directivity index (DI) is given at $\theta = 0^\circ$.

shown in Fig. 4.19 simplifies the analysis somewhat. In the first instance, let us assume that all the sources have equal strengths. Then we can write

$$D(\theta) = \frac{1}{N} \sum_{n=\frac{1-N}{2}}^{\frac{N-1}{2}} e^{-jnkb(\cos\theta - \cos\alpha)}. \tag{4.91}$$

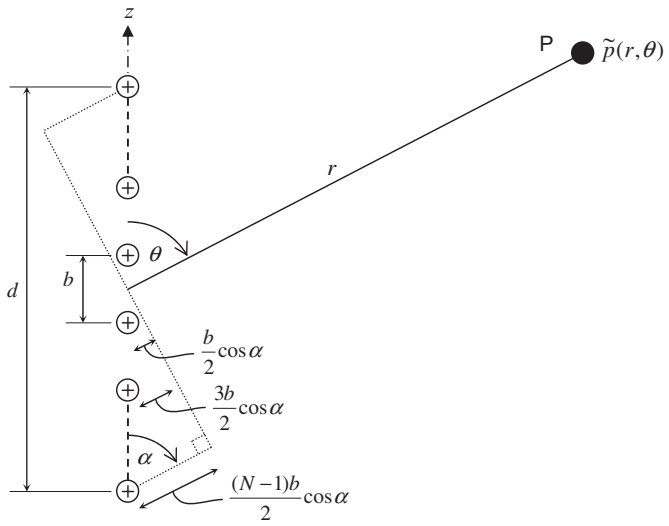

FIG. 4.19 A steered beam-forming array of *N* simple sources, located a distance *b* apart and vibrating with different phases.

The time advance applied to each source at a negative distance z from the center is given by the distance shown divided by the speed of sound c. Each source at a positive distance z from the center (not marked) has a time delay equal to the time advance of its opposite source the same negative distance z from the center. The center of the array is at distance r and angle θ with respect to the observation point P.

For simplicity, let us assume an even number of sources N so that the contribution from each side is equal and the sinusoidal parts of the exponents cancel each other

$$D(\theta) = \frac{2}{N}\sum_{n=1}^{N/2}\cos((n-1/2)kb(\cos\theta - \cos\alpha)), \tag{4.92}$$

which leads to

$$D(\theta) = \frac{\sin((N\pi\, b/\lambda)(\cos\theta - \cos\alpha))}{N\sin((\pi\, b/\lambda)(\cos\theta - \cos\alpha))}. \tag{4.93}$$

which is plotted for $d = \lambda/2$ and $d = 5\lambda$ in Fig. 4.20a and Fig. 4.20b respectively. We see that when the wavelength is greater than the length d of the array, the directivity degenerates to virtually omnidirectional. However, we can add different weightings A_n to the sources and optimize them using a technique known as the *least-mean-squares* method:

$$D(\theta) = \frac{2}{N}\sum_{n=1}^{N/2}A_n\cos((n-1/2)kb(\cos\theta - \cos\alpha)). \tag{4.94}$$

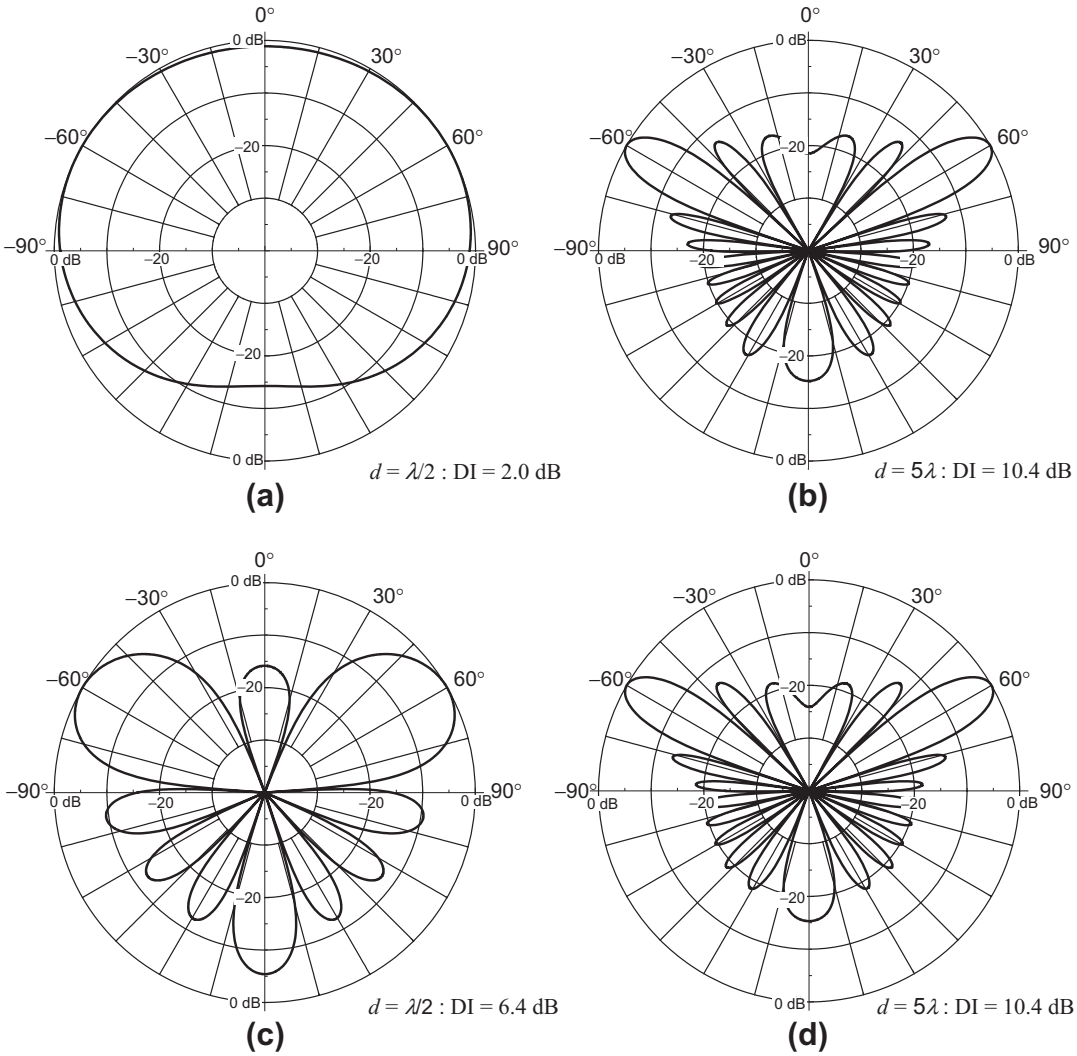

FIG. 4.20 Far-field directivity patterns for a beam-forming array of ten simple sources evenly spaced over a length *d*, where the steering angle $\alpha = 60°$.

The directivity index (DI) is given at $\theta = \alpha$. In (a) and (b) are shown directivity patterns for ten sources of equal strength but with different time delays/advances according to Fig. 4.19. In (c) and (d) are shown directivity patterns for ten sources with the same time delays/advances as (a) and (b) but with strengths optimized using the least-mean-squares method.

First of all, we define a target or reference directivity function $D_{ref}(\theta)$ to which we wish to find the best "fit". The ideal directivity function is simply an infinite impulse at the angle α which can be written using the Dirac delta function:

$$D_{ref}(\theta) = \delta(\theta - \alpha). \tag{4.95}$$

Of course, we may choose any function we like for $D_{ref}(\theta)$ depending on what directivity pattern we are aiming for. Let us define an error function $E(A_n)$ as

$$E(A_n) = \int_{-\pi}^{\pi} \left| D(\theta) - D_{ref}(\theta) \right|^2 \sin\theta \, d\theta. \tag{4.96}$$

In order to minimize the error, we differentiate it with respect to A_n and set the result to zero:

$$\begin{aligned} \frac{\partial}{\partial A_n} E(A_n) = 2 \int_{-\pi}^{\pi} & \cos((m - 1/2)kb(\cos\theta - \cos\alpha)) \\ & \times \left(D(\theta) - D_{ref}(\theta)\right) \sin\theta \, d\theta = 0, \qquad m = 1, 2, \cdots N, \end{aligned} \tag{4.97}$$

which can be expressed in the following short form:

$$\sum_{n=1}^{N/2} A_n I_{mn} = J_m, \qquad m = 1, 2, \cdots N, \tag{4.98}$$

where

$$I_{mn} = \frac{2}{N} \int_{-\pi}^{\pi} \cos((m - 1/2)kb(\cos\theta - \cos\alpha)) \cos((n - 1/2)kb(\cos\theta - \cos\alpha)) \sin\theta \, d\theta. \tag{4.99}$$

The solution to the integral I_{mn} has two parts

$$I_{mn} = K_{mn} + L_{mn}, \tag{4.100}$$

where

$$K_{mn} = \begin{cases} \dfrac{\sin((m-n)kb(1+\cos\alpha)) + \sin((m-n)kb(1-\cos\alpha))}{N(m-n)kb}, & m \neq n \\ \dfrac{2}{N}, & m = n, \end{cases} \tag{4.101}$$

$$L_{mn} = \frac{\sin((m+n-1)kb(1+\cos\alpha)) + \sin((m+n-1)kb(1-\cos\alpha))}{N(m+n-1)kb}, \tag{4.102}$$

and

$$J_m = \int_{-\pi}^{\pi} D_{ref}(\theta)\cos\left((m - 1/2)kb(\cos\theta - \cos\alpha)\right)\sin\theta\, d\theta = \sin\alpha. \tag{4.103}$$

where we have used the property of the Dirac delta function from Eq. (154) of Appendix II. Equation (4.98) is a set of simultaneous equations which we now write in matrix form

$$\mathbf{M}\cdot\mathbf{a} = \mathbf{b} \Rightarrow \mathbf{a} = \mathbf{M}^{-1}\cdot\mathbf{b} \tag{4.104}$$

where

$$\mathbf{M}(m,n) = I_{mn} = K_{mn} + L_{mn} \tag{4.105}$$

$$\mathbf{a}(n) = A_n \tag{4.106}$$

$$\mathbf{b}(m) = J_m = \sin\alpha \tag{4.107}$$

Directivity patterns are plotted from Eq. (4.94) for $d = \lambda/2$ and $d = 5\lambda$ in Fig. 4.20c and Fig. 4.20d respectively using coefficients A_n calculated from Eqs. (4.101), (4.102), and (4.104). We see that for small wavelengths ($\lambda = d/5$) there is very little difference between the directivity pattern of the sources of equal strengths in (b) and that of the optimized sources in (d). However, there is a significant difference when the wavelength is larger than d ($\lambda = 2d$) as can be seen from (a) and (c). Beam-forming arrays often have source strengths which progressively decrease towards the outer edges in order to reduce the side lobes. These are known as "shaded arrays"[4] and the technique is similar to windowing as used in Fourier transforms. Of course, delays can also be used in arrays in order to prevent high-frequency beaming so that the directivity pattern is as wide as possible regardless of wavelength. [5]

4.14 DIPOLE POINT SOURCE (DOUBLET)

A dipole point source is a pair of monopole point sources, separated a very small distance apart and vibrating in opposing phase. The geometric situation is shown in Fig. 4.21. The average distance r to the observation point P is assumed to be large compared with the separation b between the two sources.

It can be clearly seen that the sound pressure at $\theta = 90^\circ$ and $\theta = 270^\circ$ will be zero, because the contribution at those points will be equal from the two sources and 180° out of phase. The pressures at $\theta = 0^\circ$ and $\theta = 180^\circ$ will depend upon the ratio of b to the wavelength λ. For example, if $b = \lambda$, we shall have zero sound pressure at those angles just as we did for $b = \lambda/2$ in the case of two in-phase sources. In the present case, we have a maximum pressure at $\theta = 0^\circ$ and $\theta = 180^\circ$ for $b = \lambda/2$.

The usual case of interest, however, is the one for

$$b << \lambda \tag{4.108}$$

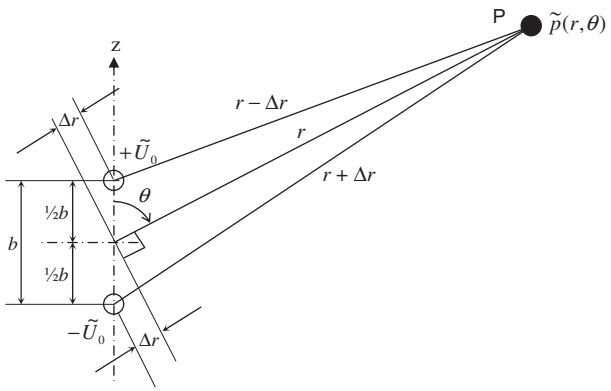

FIG. 4.21 Geometry of dipole point source.

Obviously, the separation distance b can never be zero as this would result in complete cancellation of the two monopole outputs. As we shall see, their combined output is directly proportional to b. From Fig. 4.21, we have the following relationship

$$\Delta r = \frac{1}{2} b \cos\theta. \tag{4.109}$$

We can now write the pressure field as the sum of the two monopole point sources from Eq. (4.71) as follows:

$$\begin{aligned} \tilde{p}_d(r,\theta) &= -\frac{jk\rho_0 c\tilde{U}_0}{4\pi}\left(\frac{e^{-jk(r-\Delta r)}}{r-\Delta r} - \frac{e^{-jk(r+\Delta r)}}{r+\Delta r}\right) \\ &= -\frac{jk\rho_0 c\tilde{U}_0 e^{-jkr}}{4\pi}\left(\frac{(r+\Delta r)e^{jk\Delta r} - (r-\Delta r)e^{-jk\Delta r}}{r^2-(\Delta r)^2}\right), \end{aligned} \tag{4.110}$$

where $\tilde{U}_0$ is the volume velocity of each source. Because $\Delta r < r$, we ignore the $(\Delta r)^2$ term in the denominator. Also, we can expand the exponents within the parentheses in Eq. (4.110) as follows:

$$e^{\pm jk\Delta r} = \cos k\Delta r \pm j\sin k\Delta r. \tag{4.111}$$

Substituting Eq. (4.111) into Eq. (4.110) we obtain

$$\tilde{p}_d(r,\theta) = -jk\rho_0 c\tilde{U}_0\left(2j\sin k\Delta r + 2\frac{\Delta r}{r}\cos k\Delta r\right)\frac{e^{-jkr}}{4\pi r}. \tag{4.112}$$

We can make further approximations based on the assumption that the path difference Δr is very small in comparison with the wavelength λ as follows:

$$\sin k\Delta r \approx k\Delta r, \qquad \cos k\Delta r \approx 1. \tag{4.113}$$

Substituting Eqs. (4.109) and (4.113) in Eq. (4.112) yields

$$\tilde{p}_d(r,\theta) = -j(kb\rho_0 c\tilde{U}_0)\left(\frac{1}{r}+jk\right)\frac{e^{-jkr}}{4\pi r}\cos\theta, \tag{4.114}$$

where $\tilde{U}_0 =$ strength in m^3/s of each point source and the first term in parentheses is a force known as the *dipole strength*.

The ratio of the complex sound pressure $\tilde{p}_d$ produced by the dipole point source to the complex sound pressure $\tilde{p}_m$ produced by a monopole point source is found by dividing Eq. (4.114) by Eq. (4.71). This division yields

$$\frac{\tilde{p}_d(r,\theta)}{\tilde{p}_m(r,\theta)} = -\frac{b}{r}(1+jkr)\cos\theta. \tag{4.115}$$

When the square of the distance r from the acoustic doublet is large compared with $\lambda^2/36$ ($k^2r^2 >> 1$), Eq. (4.114) reduces to

$$\tilde{p}_d(r,\theta) = \frac{\omega^2\rho_0\tilde{U}_0 b}{c}\cdot\frac{e^{-jkr}}{4\pi r}\cos\theta. \tag{4.116}$$

For this case the pressure varies with θ as shown in Fig. 4.22 and Fig. 4.23. It changes inversely with distance r in exactly the same manner as for the simple source.

Near the acoustic doublet, for $r^2 << \lambda^2/36$ (that is, $k^2r^2 << 1$), Eq. (4.114) reduces to

$$\tilde{p}_d = -\omega\rho_0\tilde{U}_0 b\,\frac{e^{j(\pi/2-kr)}}{4\pi r^2}\cos\theta. \tag{4.117}$$

For this case, the pressure also varies with $\cos\theta$ as shown in Fig. 4.23, but it changes inversely with the square of the distance r. We are still assuming that $r >> b$. We can also derive the particle velocity $\tilde{u}(r,\theta)$ from Eq. (4.114) using Eq. (2.4a) as follows:

$$\begin{aligned}\tilde{u}(r,\theta) &= \frac{1}{-jk\rho_0 c}\frac{\partial}{\partial r}\tilde{p}(r,\theta)\\ &= -\tilde{U}_0 b\left(\frac{2}{r^2}-k^2+j\frac{2k}{r}\right)\frac{e^{-jkr}}{4\pi r}\cos\theta.\end{aligned} \tag{4.118}$$

Now we can derive the free-field specific acoustic impedance by dividing the pressure from Eq. (4.114) by the particle velocity from Eq. (4.118) as follows:

$$\begin{aligned}z_s = \frac{\tilde{p}(r,\theta)}{\tilde{u}(r,\theta)} &= \frac{jkr\,(1+jkr)}{2-k^2r^2+2jkr}\rho_0 c\\ &= \frac{k^4r^4+j\,(k^3r^3+2kr)}{k^4r^4+4}\rho_0 c.\end{aligned} \tag{4.119}$$

In the near-field where $kr << 1$, the imaginary part of the impedance dominates and so the load is mass-like. This results from the fact that, at low frequencies in particular, we have a virtual acoustic

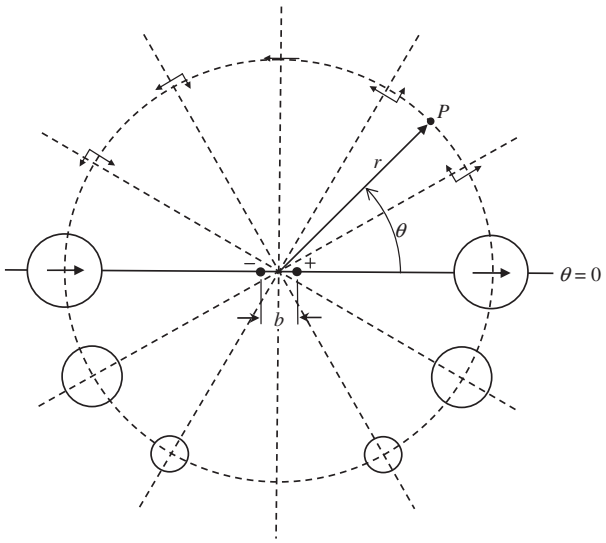

FIG. 4.22 Dipole point source.

This type of source consists of two monopole point sources vibrating 180° out of phase. They are located a distance b apart and are at an angle θ and a distance r with respect to the observation point P. The lower half of the graph shows by the area of the circles the magnitude of the sound pressure as a function of angle θ. The upper half of the graph shows the variation of the radial and azimuthal components of the particle velocity as a function of angle θ.

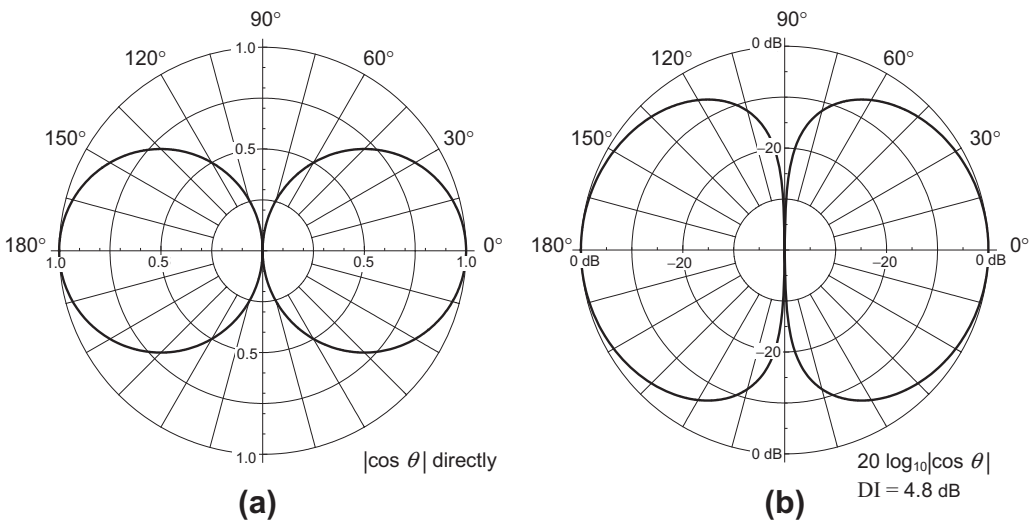

FIG. 4.23 Far-field directivity pattern for a dipole point sound source (a) on a linear scale, (b) on a logarithmic scale.

The directivity index (DI) is given at $\theta = 0°$.

short circuit between the two sources. Therefore, the dipole has to move a significant amount of air in order to radiate any sound. However, in the far field, the waves are spherically diverging and the impedance approaches the characteristic impedance of free space

$$z_s|_{kr\to\infty} = \rho_0 c. \tag{4.120}$$

Near-field and far-field. The difference between *near-field* and *far-field* behaviors of sources must always be borne in mind. When the directivity pattern of a loudspeaker or some other sound source is presented in a technical publication, it is always understood that the data were taken at a distance r sufficiently large so that the sound pressure was decreasing linearly with distance along a radial line connecting with the source, as was the case for Eq. (4.116). This is the *far-field* case. For this to be true, two conditions usually have to be met. First, the extent b of the radiating array must be small compared with r, and r^2 must be large compared with $\lambda^2/36$. In acoustics the size factor indicated is usually taken to be larger than 3 to 10.

One more item is of interest in connection with the acoustic doublet. The particle velocity is composed of two components: one radially directed, and the other perpendicular to that direction. At $\theta = 0$ and 180° the particle velocity is directed radially entirely (see Fig. 4.22). At $\theta = 90°$ and 270° the particle velocity is entirely perpendicular to the radial line. In between, the radial component varies as the $\cos\theta$ and the perpendicular component as the $\sin\theta$.

An interesting fact is that at $\theta = 90°$ and 270° a doublet sound source appears to propagate a transversely polarized sound wave. To demonstrate this, take two unbaffled small loudspeakers into an anechoic chamber. Unbaffled loudspeakers (transducers) are equivalent to doublets because the pressure increases on one side of the diaphragm whenever it decreases on the other. Hold the two transducers about 0.5 m apart with *both* diaphragms facing the floor (not facing each other). Let one transducer radiate a low-frequency sound and the other act as a microphone connected to the input of an audio amplifier. As we see from Fig. 4.22, no sound pressure will be produced at the diaphragm of the microphone, but there will be transverse particle velocity. A particle velocity is always the result of a pressure gradient in the direction of the velocity. Therefore, the diaphragm of the microphone will be caused to move when the two transducers are held as described above. When one of the transducers is rotated through 90° about the axis joining the units, the diaphragm of the microphone will not move because the pressure gradient will be in the plane of the diaphragm. Hence, the sound wave appears to be plane polarized.

You have now learned the elementary principles governing the directional characteristics of sound sources. We shall be able to use these principles in understanding the measured or calculated behavior of some of the more complicated sound sources found in acoustics.

4.15 RADIATION FROM AN OSCILLATING SPHERE

We saw that the monopole point source is effectively a pulsating sphere with an infinitesimally small radius. Similarly, the dipole point source can be considered as a rigid sphere with an infinitesimally small radius oscillating back and forth along its axis. This provides us with some useful insight into the operation of a loudspeaker without any baffle or enclosure whatsoever, but unlike the more accurate circular piston in free space (see Sec. 13.10), it yields simple closed-form solutions for the pressure field and radiation impedance. As in the case of the pulsating sphere, the impedance can be represented

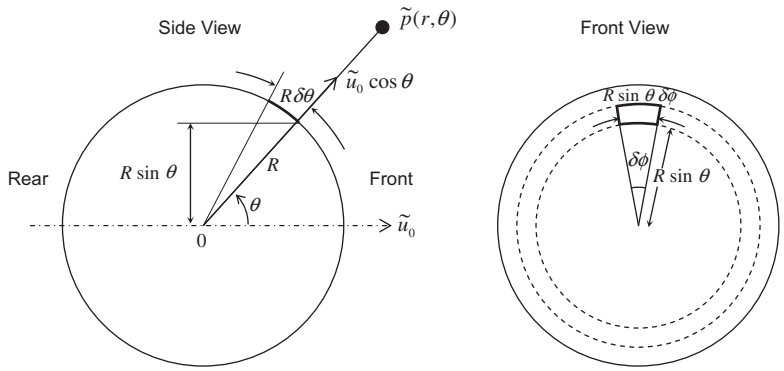

FIG. 4.24 Geometry of oscillating sphere.

by a simple equivalent circuit. We shall now consider a sphere of radius R that oscillates back and forth along a dipole axis with velocity $\tilde{u}_0$ as shown in Fig. 4.24 so that the normal surface velocity in the radial direction is $\tilde{u}_0 \cos\theta$. A spherical coordinate system is used where r is the distance from the origin at the centre of the sphere and θ is the angle subtended with the dipole axis. The area of each surface element is

$$\delta S = R^2 \sin\theta\, \delta\theta\delta\phi. \tag{4.121}$$

Near-field pressure. The volume velocity produced by each element is

$$\begin{aligned} \delta\tilde{U}_0 &= \tilde{u}_0 \cos\theta\, \delta S \\ &= \tilde{u}_0 \cos\theta(R^2 \sin\theta\, \delta\theta\delta\phi). \end{aligned} \tag{4.122}$$

If we now integrate this over the surface of the sphere, we obtain the volume velocity:

$$\tilde{U}_0 = 2R^2\tilde{u}_0 \int_0^{2\pi} \int_0^{\pi/2} \cos\theta \sin\theta\, d\theta\, d\phi = S\,\tilde{u}_0, \tag{4.123}$$

where S is the *effective* surface area of the sphere (including both front and rear surfaces) given by

$$S = 2\pi R^2. \tag{4.124}$$

We see from Eq. (4.114) that the dipole source produces a pressure field that is proportional to $\cos\theta$ as follows:

$$\tilde{p}(r,\theta) = -jk\rho_0 c\tilde{A}_0 \left(\frac{1}{r} + jk\right) \frac{e^{-jkr}}{4\pi r} \cos\theta, \tag{4.125}$$

where the term $\tilde{U}_0 b$ has been replaced with the unknown coefficient $\tilde{A}_0 = \tilde{U}_0 b$. Likewise, from Eq. (4.118) we have the particle velocity

$$\tilde{u}(r,\theta) = -\tilde{A}_0\left(\frac{2}{r^2} - k^2 + j\frac{2k}{r}\right)\frac{e^{-jkr}}{4\pi r}\cos\theta. \tag{4.126}$$

Let us now impose a boundary condition at the surface of the sphere whereby the particle velocity normal to the surface is equal to the angle-dependent surface velocity $\tilde{u}_0\cos\theta$. Hence at $r = R$ we have

$$\begin{aligned}\tilde{u}(R,\theta) &= -\tilde{A}_0\left(\frac{2}{R^2} - k^2 + j\frac{2k}{R}\right)\frac{e^{-jkR}}{4\pi R}\cos\theta \\ &= -\tilde{u}_0 e^{-jkR}\cos\theta.\end{aligned} \tag{4.127}$$

Solving this for $\tilde{A}_0$ yields

$$\tilde{A}_0 = \frac{4\pi R^3\tilde{u}_0}{2 - k^2R^2 + 2jkR}. \tag{4.128}$$

If we now substitute this in Eq. (4.125), together with $\tilde{U}_0 = 2\pi R^2\tilde{u}_0$ from Eq. (4.123), we obtain the pressure

$$\tilde{p}(r,\theta) = -j\rho_0 c\frac{kR\tilde{U}_0}{2 - k^2R^2 + 2jkR}\left(\frac{1}{r} + jk\right)\frac{e^{-jkr}}{2\pi r}\cos\theta. \tag{4.129}$$

Far-field pressure. In the far field, where $r \to \infty$, Eq. (4.129) simplifies to

$$\tilde{p}(r,\theta)\big|_{r\to\infty} = -jk\rho_0 c\tilde{U}_0\frac{e^{-jkr}}{4\pi r}D(\theta), \tag{4.130}$$

where

$$D(\theta) = \frac{2jkR}{2 - k^2R^2 + 2jkR}\cos\theta. \tag{4.131}$$

The directivity pattern $20\log_{10}(D(\theta)/D(0))$ is plotted in Fig. 4.25 along with that of a pulsating sphere, and the on-axis response $D(0)$ is plotted in Fig. 4.26. It can be seen that when $kR = \sqrt{2}$, the pressure is proportional to *acceleration*:

$$\tilde{p}(r,\theta)|_{r\to\infty,kR=\sqrt{2}} = -jk\rho_0 c\tilde{U}_0\frac{e^{-jkr}}{4\pi r}\cos\theta. \tag{4.132}$$

At this frequency, we have a resonant peak with a Q factor of $1/\sqrt{2}$. Above this frequency, the pressure is proportional to *velocity* as in the case of the pulsating sphere:

$$\tilde{p}(r,\theta)\Big|_{r\to\infty,kR>>1} = -\rho_0 c\frac{\tilde{U}_0}{R}\cdot\frac{e^{-jkr}}{2\pi r}\cos\theta, \tag{4.133}$$

but below it the pressure is proportional to the *time derivative* of the acceleration:

$$\tilde{p}(r,\theta)\Big|_{r\to\infty,kR<<1} = k^2R^2\rho_0 c\frac{\tilde{U}_0}{R}\cdot\frac{e^{-jkr}}{4\pi r}\cos\theta. \tag{4.134}$$

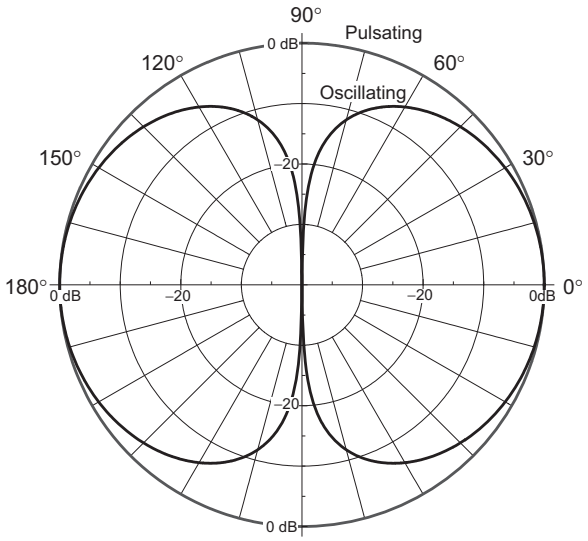

FIG. 4.25 Far-field directivity patterns 20 $\log_{10}(|D(\theta)|/|D(0)|)$ of the oscillating and pulsating spheres.

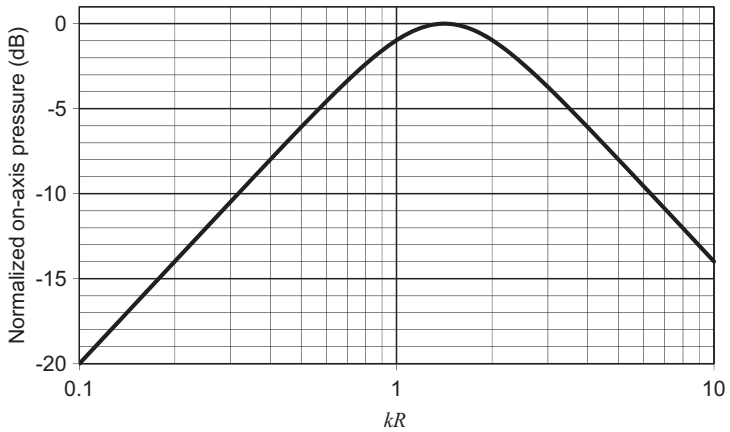

FIG. 4.26 Plot of 20 $\log_{10}(D(0))$ for an oscillating sphere of radius R with constant axial acceleration.

Frequency is plotted on a normalized scale, where $kR = 2\pi R/\lambda = 2\pi fR/c$.

When the sphere moves forwards, it compresses the air in front of it causing an increase in pressure above static pressure. Similarly, it creates a partial vacuum behind it causing a net decrease in pressure. Hence the radiated sound pressures in front of and behind it are in *opposite* phases. The anti-phase sound from the rear partially cancels the sound from the front at low frequencies. However, complete cancellation never occurs, due to the finite path length from the rear to the front of the sphere. Hence, the phase difference is

$$-(1+2\delta/\lambda)\,\pi \text{ radians}$$

where δ is the path length difference and λ is the wavelength. As the frequency decreases, the wavelength increases relative to the path difference and the phase difference asymptotically approaches $-\pi$. This results in a pressure response that falls at a rate of -6 dB per halving of frequency.

In Sec. 4.14 we derived the pressure field due to a *compact* dipole point source. However, from Eq. (4.112), we can write the equation for the on-axis pressure response of a dipole point source where the spacing Δz_0 between the two point sources is comparable to the wavelength λ of the sound being radiated:

$$\tilde{p}(r,0) = \rho_0 \omega \tilde{U}_0 \sin(\pi \Delta z_0/\lambda)\frac{e^{-jkr}}{2\pi r}, \tag{4.135}$$

from which it can be seen that the pressure magnitude versus frequency, with constant acceleration, is just a series of half sinusoids like a comb filter. Nulls occur when $\Delta z_0 = n\lambda$. and peaks occur when $\Delta z_0 = (n + ½)\lambda$. This is in stark contrast with the oscillating sphere which has a continuous monotonic pressure response with just a single peak and no nulls. This is because the resulting sound field is due to an infinite number of point sources all over the surface according to the Huygens–Fresnel principle, which will be discussed in greater detail in Sec. 12.1. Hence there are many path lengths between the rear and front and at no frequency do they all produce a cancellation. However, the peak at $kR = \sqrt{2}$ is due to an *average* path length difference of $\Delta z_0 = \pi R/\sqrt{2}$.

Radiation impedance. The total force $\tilde{F}$ acting upon the sphere is obtained by integrating the pressure from Eq. (4.129) over the surface as follows:

$$\begin{aligned}\tilde{F} &= -2R^2 \int_0^{2\pi}\int_0^{\pi/2} \tilde{p}(R,\theta)\sin\theta\, d\theta\, d\phi \\ &= \rho_0 c \tilde{U}_0 \frac{jkR(1+jkR)}{2-k^2R^2+2jkR} e^{-jkR}.\end{aligned} \tag{4.136}$$

The specific radiation impedance Z_s can be written as follows:

$$\begin{aligned}Z_s = R_s + jX_s &= \frac{\tilde{F}}{\tilde{U}_0 e^{-jkR}} \\ &= \frac{jkR(\,1+jkR)}{2-k^2R^2+2jkR}\rho_0 c \\ &= \frac{k^4R^4 + j(k^3R^3+2kR)}{k^4R^4+4}\rho_0 c.\end{aligned} \tag{4.137}$$

It turns out that this is the same as the impedance from Eq. (4.119) for a freely propagating wave due to a dipole point source at a distance R from the origin. The real and imaginary parts, R_s and X_s are plotted in Fig. 4.27. The main difference between Fig. 4.27 and the impedance of a pulsating sphere shown in Fig. 4.13 is that the real part falls even more rapidly at low frequencies due to the rear

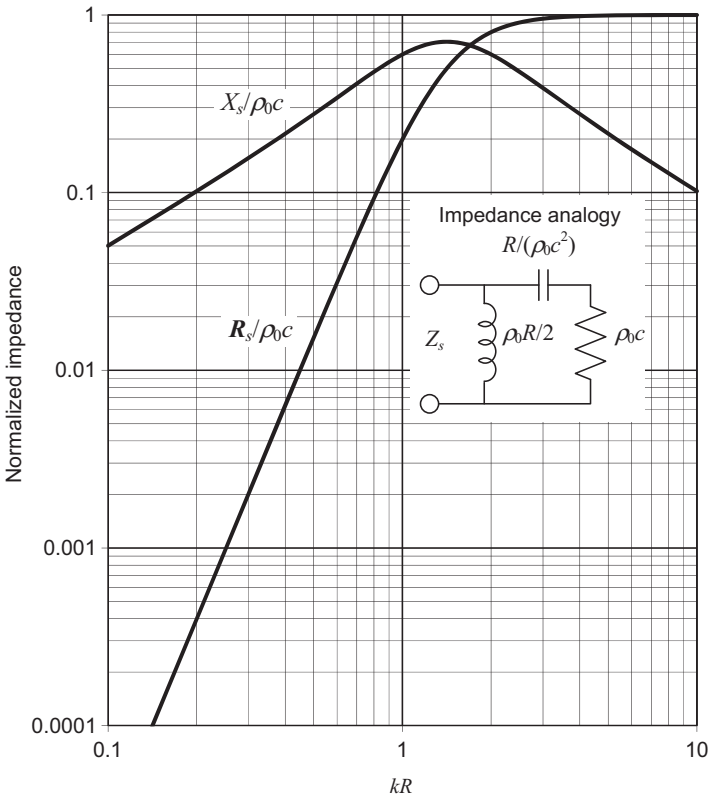

FIG. 4.27 Real and imaginary parts of the normalized specific radiation impedance $Z_s/\rho_0 c$ of the air load on an oscillating sphere of radius R in free space.

Frequency is plotted on a normalized scale, where $kR = 2\pi R/\lambda = 2\pi fR/c$.

wave cancellation. It is proportional to $(kR)^4$ as opposed to $(kR)^2$ in the case of the pulsating sphere. In both cases, the imaginary part is proportional to kR at low frequencies and $1/(kR)$ at high frequencies.

PART XII: DIRECTIVITY INDEX

4.16 DIRECTIVITY INDEX AND DIRECTIVITY FACTOR

Charts of the directivity patterns of sound sources are sufficient in many cases, such as when the source is located outdoors at a distance from reflecting surfaces. Indoors, it is necessary in addition to know something about the total power radiated in order to calculate the reinforcing effect of the reverberation in the room on the output of the sound source. A number is calculated at each frequency that tells

the degree of directivity without the necessity for showing the entire directivity pattern. This number is the directivity factor or, when expressed in decibels, the directivity index.

Directivity factor [Q(f)]. The directivity factor is the ratio of the intensity [6] on a designated axis of a sound radiator at a stated distance r to the intensity that would be produced at the same position by a point source if it were radiating the *same* total acoustic power as the radiator. Free space is assumed for the measurements. Usually, the designated axis is taken as the axis of maximum radiation, in which case $Q(f)$ always exceeds unity. In some cases, the directivity factor is desired for other axes where $Q(f)$ may assume any value equal to or greater than zero.

Directivity index [DI(f)]. The directivity index is 10 times the logarithm to the base 10 of the directivity factor:

$$\mathrm{DI}(f) = 10 \log_{10} Q(f). \tag{4.138}$$

Calculation of Q(f) and DI(f). The intensity I at a point removed a distance r from the acoustical center of a source of sound located in free space is determined by first measuring the effective sound pressure p_{rms} and letting $I = |p|_{rms}^2/\rho_0 c$. If the source is a point source so that I is not a function of V and is located in free space, the total acoustic power radiated is:

$$W_p = 4\pi r^2 I.$$

If the source is not a point source, the total acoustic power radiated is determined by summing the intensities over the surface of a sphere of radius r. That is, the total radiated power is

$$W = \frac{r^2}{\rho_0 c} \int_0^{2\pi} \int_0^{\pi} p_{rms}{}^2(\theta, \phi, r) \sin\theta \, d\theta \, d\phi, \tag{4.139}$$

where the coordinate of any point in space is given by the angles θ and ϕ and the radius r (see Fig. 4.28) and $p_{rms}{}^2(\theta,\phi,r)$ equals the mean-square sound pressure at the point designated by θ, ϕ, and r.

Usually an analytical expression for $p_{rms}{}^2(\theta,\phi)$ does not exist. In practice, therefore, data are taken at the centers of a number of areas, approximately equal in magnitude, on the surface of a sphere of

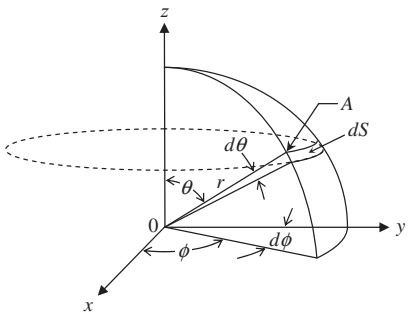

FIG. 4.28 Coordinate system defining the angle θ and ϕ and the length r of a line connecting a point A to the center of a sphere.

The area of the incremental surface $dS = r^2 \sin\theta \, d\theta \, d\phi$.

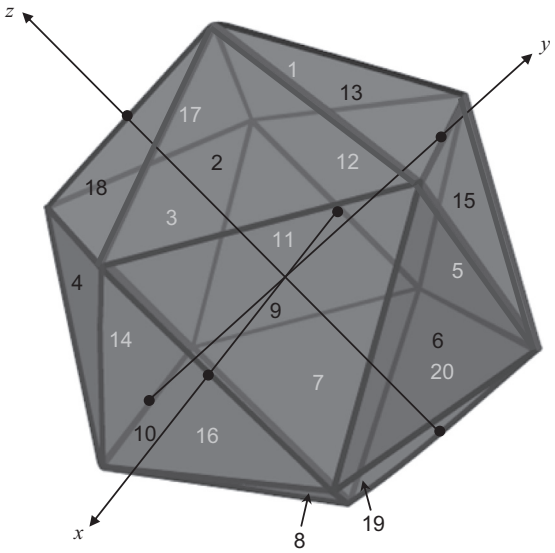

FIG. 4.29 Division of a spherical surface into 20 planar surfaces bound by identical equilateral triangles.

Black numbers denote surfaces on nearest side and white numbers denote ones on farthest side. Resulting polyhedron is a regular icosahedron, in which the twelve apexes are the corners of three intersecting golden rectangles (that is, having side ratios of $1{:}(1+\sqrt{5})/2$) that lie in the *xy*, *yz*, and *xz* planes with their centers at the origin. The coordinates of the midpoints of the sectors are given in Table 4.2.

radius r surrounding the source. As an example, we show in Fig. 4.29 a spherical surface divided into 20 equal parts of the same shape. The measured intensities on each of these parts may be called I_1, I_2, I_3 etc. The total power radiated W is found from

$$W = I_1 S_1 + I_2 S_2 + \cdots + I_{20} S_{20}, \tag{4.140}$$

where $S_1, S_2, \cdots, S_{20}$ are the areas of the 20 parts of the spherical surface. If, as in Fig. 4.29, the surface is divided into 20 equal parts, then $S_1 = S_2 = S_3 = \cdots = S_{20}$.

By definition, the directivity factor $Q(f)$ is

$$Q(f) = \frac{|p_{ax}|^2}{\rho_0 c}\frac{4\pi r^2}{W} = \frac{4\pi |p_{rms}(\theta_{ax}, \phi_{ax})|^2}{\int_0^{2\pi}\int_0^{\pi} |p_{rms}(\theta, \phi)|^2 \sin\theta \, d\theta \, d\phi}, \tag{4.141}$$

where $|p_{ax}|^2$ is the magnitude of the mean-square sound pressure on the designated axis of the sound source at a certain distance r (see Fig. 4.31, 0° axis, as an example).

For the special case where, for any particular value of θ, the sound pressure produced by the sound source is independent of the value of ϕ, that is to say, there is an axis of symmetry, Eq. (4.141) simplifies to

$$Q(f) = \frac{4\pi\, p_{rms}^2(0)}{2\pi \int_0^{\pi} p_{rms}^2(\theta)\, \sin\theta\, d\theta}. \tag{4.142}$$

where the designated axis is the axis of symmetry. The magnitude signs are left off for convenience. Many sources, such as loudspeakers, are fairly symmetrical about the principal axes so that Eq. (4.142) is valid. We notice that the integral in the denominator has the same form as that of Eq. (13.271) used for the Bouwkamp impedance theorem and thus represents the total radiated power. Also, for pistons of area S, where $R_{AR} = R_s/S$, the on-axis pressure $p(0)$ is given by Eqs. (13.101) and (13.235) so that

$$Q(f) = \frac{k^2 a^2 \rho_0 c |D(0)|^2}{\boldsymbol{R}_s}, \tag{4.143}$$

which is a useful result since $D(0)$ and $\boldsymbol{R}_s$ have relatively simple analytical solutions for pistons.

If no analytical solution is available, the only choice is to take measurements at a number of points with the angles θ_n in a horizontal plane around the source so that

$$Q(f) = \frac{(4\pi\, p_{rms}^2(0))(180^\circ/\pi)}{2\pi \sum_{n=1}^{180^\circ/\Delta\theta} p_{rms}^2(\theta_n)\, \sin\theta_n\, \Delta\theta}, \tag{4.144}$$

where

$\Delta\,\theta$ is separation in degrees of the successive points around the sound source at which measurement of $p_{rms}(\theta_n)$ was made (see Fig. 4.31 as an example).
$180^\circ/\Delta\theta$ is the number of measurements that were made in passing from a point directly in front of the source to one directly behind the source (0 to 180°). The sound source is assumed to be symmetrical so that the variation between 360° and 180° is the same as that between 0 and 180°.

If the source is mounted in an infinite baffle, measurement is possible only in a hemisphere. Hence, the value of n in Eq. (4.142) varies from 1 to $90^\circ/\Delta\theta$. If the source in an infinite baffle is nondirectional in the hemisphere, which is usually the case for $ka < 0.5$, then the directivity factor $Q = Q_h = 2$, that is, DI = 3 dB.

If the directivity pattern is not quite symmetrical, then the factor of 4 in the numerator of Eq. (4.142) becomes 8 and the value of n varies from 1 to $360^\circ/\Delta\theta$. This, in effect, averages the two sides of the directivity pattern.

For easy reference, the directivity indexes for (1) a piston in free space, (2) an oscillating sphere in free space, (3) a piston in an infinite plane baffle, (4) a hemispherical dome in an infinite baffle, and (5) a one-sided piston in free space are plotted as a function of ka in Fig. 4.30.

Detailed calculations are shown in Table 4.3 for a box-enclosed loudspeaker having the directivity pattern at a frequency of 3000 Hz shown in Fig. 4.31.

After a directivity factor has been calculated at each frequency, a plot of directivity index DI(f) in decibels is made with the aid of Eq. (4.138). For the loudspeaker with the directivity patterns of Fig. 4.31, the directivity index as a function of frequency is shown in Fig. 4.32.

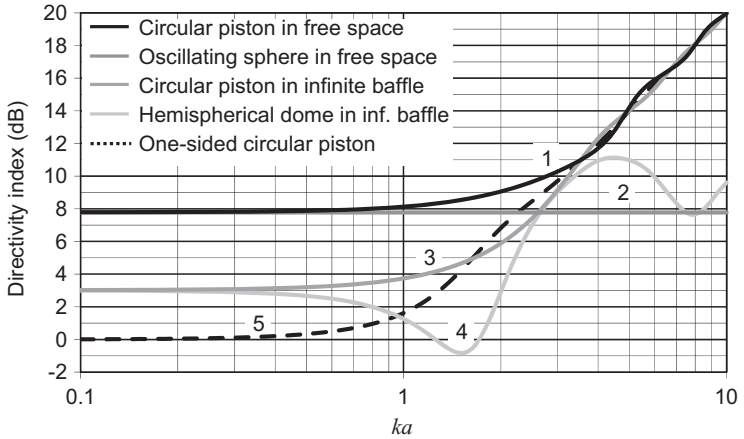

FIG. 4.30 Directivity indexes for the radiation from (1) a circular piston in free space without any baffle; (2) an oscillating sphere in free space; (3) a circular piston in an infinite plane baffle; (4) a hemispherical dome in an infinite baffle; and (5) a one-sided circular piston in free space.

Frequency is plotted on a normalized scale, where $ka = 2\pi a/\lambda = 2\pi fa/c$.

$$Q(f) = \frac{4\pi \times (180^\circ/\pi)}{2\pi \sum_1^{18} \left|\frac{p_{rms}(\theta_n)}{p_{rms}(0)}\right|^2 \sin\theta_n \times 10^\circ} = \frac{11.5}{1.48} = 7.7,$$

$$\mathrm{DI}(f) = 10 \log 7.7 = 8.9 \text{ dB}.$$

Table 4.2 Coordinates of mid-points of sectors

Sector numbers	Coordinate		
	x	***y***	***z***
1–8	$\pm\frac{1}{\sqrt{3}} = \pm 0.577$	$\pm\frac{1}{\sqrt{3}} = \pm 0.577$	$\pm\frac{1}{\sqrt{3}} = \pm 0.577$
9–12	$\pm\frac{2(\sqrt{5}+2)}{\sqrt{6(3\sqrt{5}+7)}} = \pm 0.934$	$\pm\frac{\sqrt{5}+1}{\sqrt{6(3\sqrt{5}+7)}} = \pm 0.357$	0
13–16	0	$\pm\frac{2(\sqrt{5}+2)}{\sqrt{6(3\sqrt{5}+7)}} = \pm 0.934$	$\pm\frac{\sqrt{5}+1}{\sqrt{6(3\sqrt{5}+7)}} = \pm 0.357$
17–20	$\pm\frac{\sqrt{5}+1}{\sqrt{6(3\sqrt{5}+7)}} = \pm 0.357$	0	$\pm\frac{2(\sqrt{5}+2)}{\sqrt{6(3\sqrt{5}+7)}} = \pm 0.934$

Table 4.3 Calculation of directivity index DI(f)[1]

θ_n (degrees)	sin θ_n	Directivity (dB)	$\left\|\frac{p(\theta_n)}{p_{ax}}\right\|^2$	$\left\|\frac{p(\theta_n)}{p_{ax}}\right\|^2 \sin\theta_n$
5	0.087	0.1	1.02	0.09
15	0.259	–0.4	0.92	0.24
25	0.423	–1.5	0.71	0.30
35	0.574	–3.2	0.47	0.27
45	0.707	–5.3	0.30	0.21
55	0.819	–7.4	0.18	0.15
65	0.906	–10.4	0.09	0.08
75	0.966	–14.5	0.04	0.03
85	0.996	–16.9	0.02	0.02
95	0.996	–15.7	0.03	0.03
105	0.966	–16.5	0.02	0.02
115	0.906	–23.1	0.00	0.00
125	0.819	–22.7	0.01	0.00
135	0.707	–18.0	0.02	0.01
145	0.574	–22.3	0.01	0.00
155	0.423	–26.6	0.00	0.00
165	0.259	–16.6	0.02	0.01
175	0.087	–12.9	0.05	0.00
				1.48

[1]*At* f = *3000 Hz for a type 8030A loudspeaker having the directivity patterns shown in Fig. 4.31. The quantity* $\Delta\theta = 10^\circ = \pi/18$ *rad.*

PART XIII: RADIATION IMPEDANCES

4.17 PULSATING SPHERE

In Part XI we derived the radiation impedance for a sphere with a uniformly pulsating surface. For the results, refer to Eq. (4.69) and Fig. 4.13.

It is seen from Fig. 4.13 that for $kR < 0.3$, that is, when the diameter is less than one-tenth the wavelength, the impedance load on the surface of the sphere is that of a mass reactance because the resistive component is negligible compared with the reactive component.

At all frequencies, the loading shown in Fig. 4.13 may be represented by the equivalent circuits of Fig. 4.33. The element sizes for the mechanical and acoustic admittances and impedances are given with the circuits.

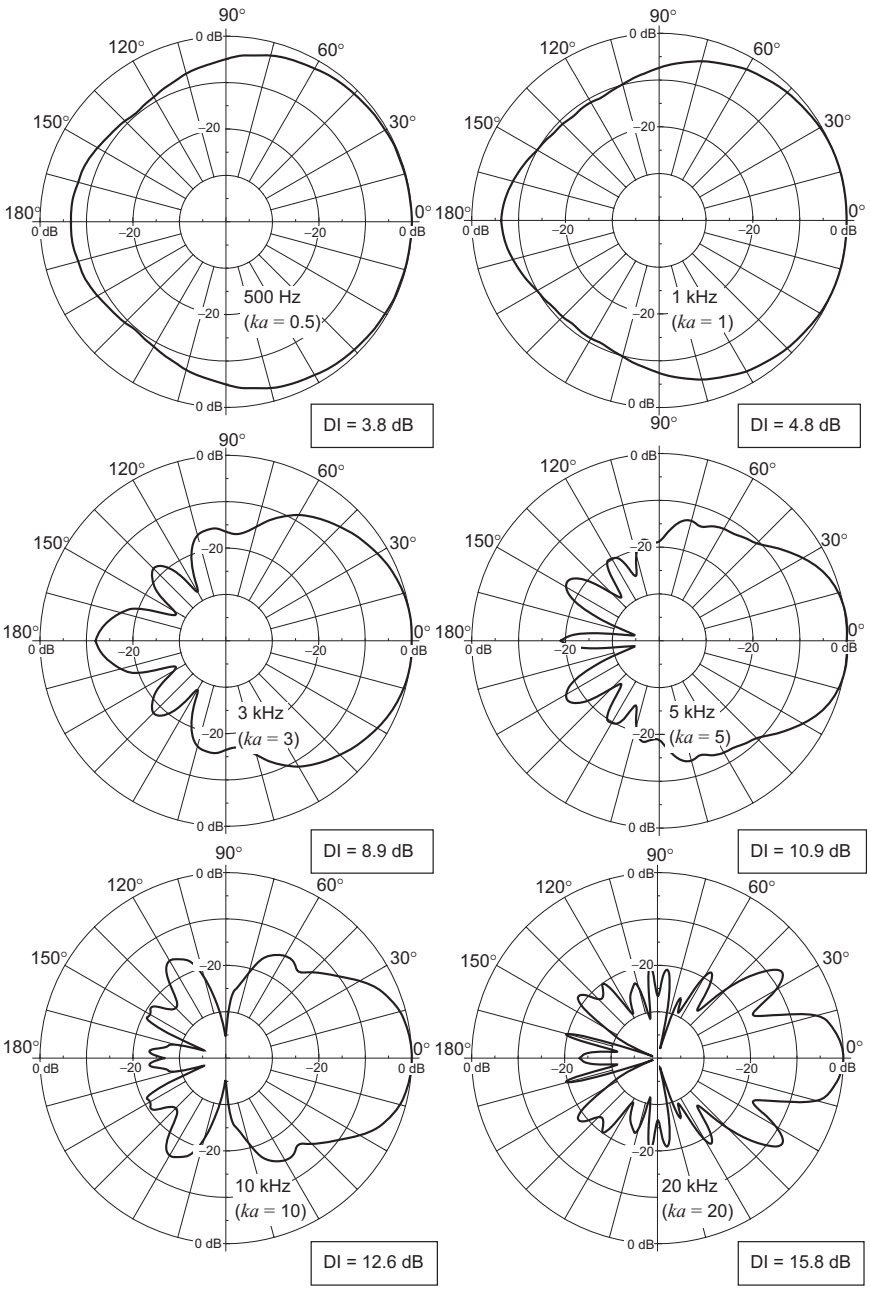

FIG. 4.31 Measured directivity patterns for a type 8030A 5-in direct-radiator loudspeaker in a 285- by 189- by 178-mm aluminum box.

The squares give the directivity index at $\theta = 0°$.

Courtesy of Genelec OY, Finland.

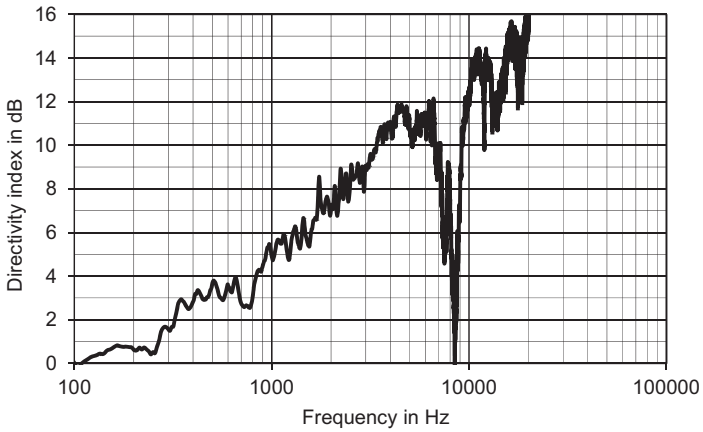

FIG. 4.32 Directivity indexes for O° axes of the directivity patterns of Fig. 4.31.

The data apply to a type 8030A 5-in direct-radiator loudspeaker in a 285- by 189- by 178-mm aluminum box.
Courtesy of Genelec OY, Finland.

4.18 OSCILLATING SPHERE

In Part XI we derived the radiation impedance for a rigid sphere that oscillates axially. For the results, refer to Eq. (4.137) and Fig. 4.27.

It is seen from Fig. 4.27 that for $kR < 1$, that is, when the diameter is less than one-third the wavelength, the impedance load on the surface of the sphere is that of a mass reactance because the resistive component is negligible compared with the reactive component.

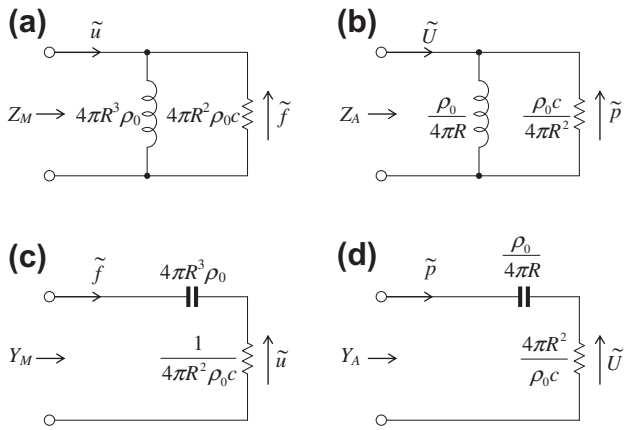

FIG. 4.33 Exact radiation impedances and admittances for all values of *kR* for a sphere with a surface that vibrates radially.

(a) Mechanical-impedance analogy; (b) acoustic-impedance analogy; (c) mechanical-admittance analogy; (d) acoustic-admittance analogy. The quantity R is the radius of the sphere.

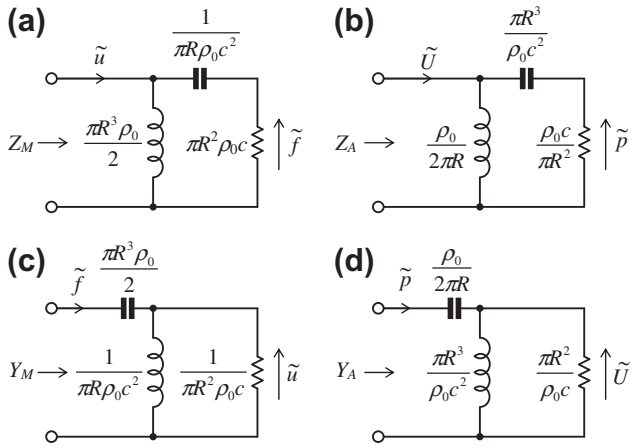

FIG. 4.34 Exact radiation impedances and admittances for all values of *kR* for a rigid sphere that oscillates axially.

(a) Mechanical-impedance analogy; (b) acoustic-impedance analogy; (c) mechanical-admittance analogy; (d) acoustic-admittance analogy. The quantity R is the radius of the sphere.

At all frequencies, the loading shown in Fig. 4.27 may be represented by the equivalent circuits of Fig. 4.34. The element sizes for the mechanical and acoustic admittances and impedances are given with the circuits.

4.19 PLANE CIRCULAR PISTON IN INFINITE BAFFLE

The specific impedance in $\mathrm{N\cdot s/m^3}$ of the air load upon one side of a plane piston mounted in an infinite baffle (see Fig. 13.3) and vibrating sinusoidally is given by Eqs. (13.116), (13.117), and (13.118). Plots of the real and imaginary parts of

$$\frac{Z_s}{\rho_0 c} = \frac{\boldsymbol{R}_s + jX_s}{\rho_0 c} \tag{4.145}$$

are shown in Fig. 4.35 as a function of ka. Similar graphs of the real and imaginary parts of the specific admittance

$$Y_s\rho_0 c = \rho_0 c(\boldsymbol{G}_s + jB_s) = \rho_0 c\left(\frac{\boldsymbol{R}_s}{\boldsymbol{R}_s^2 + X_X^s} - j\frac{X_s}{\boldsymbol{R}_s^2 + X_s^2}\right) \tag{4.146}$$

are shown in Fig. 4.36. The specific admittance is in $\mathrm{m^3\cdot N^{-1}\cdot s^{-1}}$ ($\mathrm{rayls^{-1}}$).

The data of Fig. 4.35 are used in dealing with impedance analogies and the data of Fig. 4.36 in dealing with admittance analogies.

We see from Fig. 4.35 that, for $ka < 0.5$, the reactance varies as the first power of frequency while the resistance varies as the second power of frequency. At high frequencies, for $ka > 5$, the reactance becomes small compared with the resistance, and the resistance approaches a constant value.

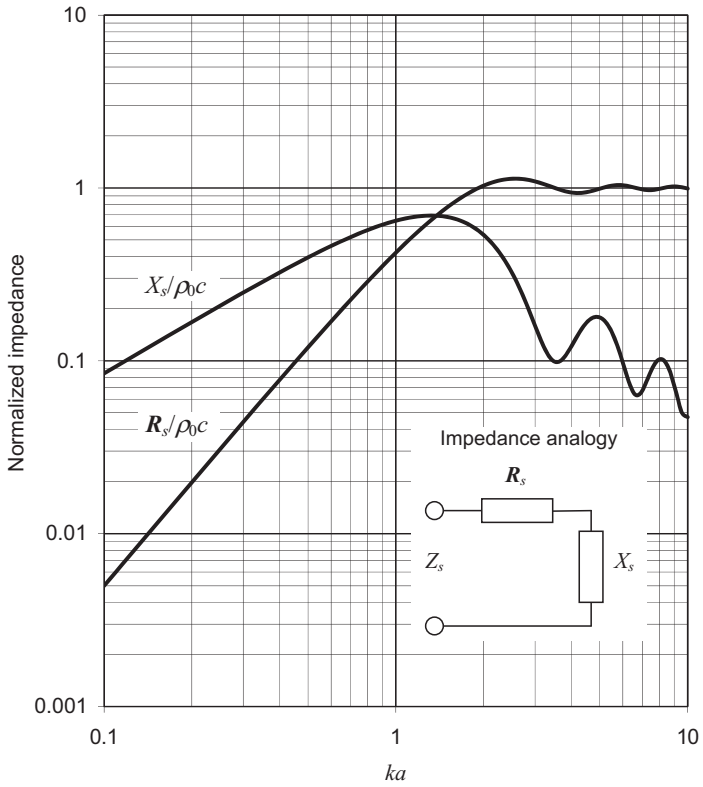

FIG. 4.35 Real and imaginary parts of the normalized specific radiation impedance $Z_s/\rho_0 c$ of the air load on one side of a plane circular piston of radius a in an infinite flat baffle.

Frequency is plotted on a normalized scale, where $ka = 2\pi a/\lambda = 2\pi fa/c$.

The admittance, on the other hand, is better behaved. The conductance is constant for $ka < 0.5$, and it is also constant for $ka > 5$ although its value is larger.

Approximate analogous circuits. The behavior just noted suggests that, except for the ripples in the curves for ka between 1 and 5, the impedance and the admittance for a piston in an infinite baffle can be approximated over the whole frequency range by the analogous circuits of Fig. 4.37. Those circuits give the mechanical and acoustic impedances and admittances, where

$$R_{M2} = \pi a^2 \rho_0 c \text{ N}\cdot \text{ s/m} \tag{4.147}$$

$$\begin{aligned} R_M &= R_{M2} + R_{M1} = 128a^2\rho_0 c/(9\pi) \\ &= 4.53a^2\rho_0 c \text{ N}\cdot\text{s/m} \end{aligned} \tag{4.148}$$

$$R_{M1} = 1.386a^2\rho_0 c \text{ N}\cdot\text{s/m} \tag{4.149}$$

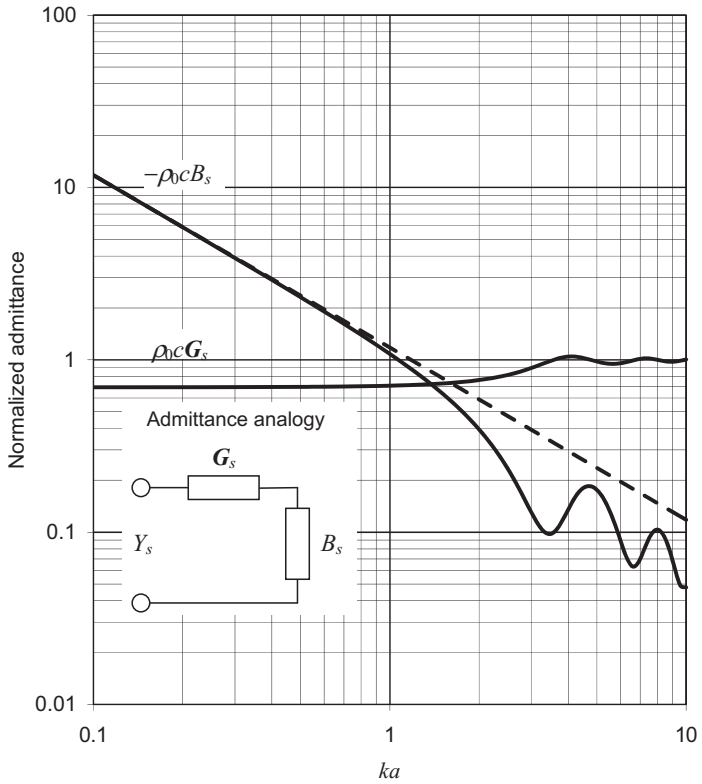

FIG. 4.36 Real and imaginary parts of the normalized specific radiation admittance $\rho_0 c Y_s$ of the air load on one side of a plane circular piston of radius a in an infinite flat baffle.

Frequency is plotted on a normalized scale, where $ka = 2\pi a/\lambda = 2\pi fa/c$.

$$C_{M1} = 1.89/(\pi a \rho_0 c^2) = 0.6/(a\rho_0 c^2)\ \text{m/N} \tag{4.150}$$

$$M_{M1} = 8a^3\rho_0/3 = 2.67a^3\rho_0\ \text{kg} \tag{4.151}$$

$$G_{M2} = 1/(\pi a^2 \rho_0 c) = 0.318/(a^2\rho_0 c)\ \text{m}\cdot\text{N}^{-1}\cdot\text{s}^{-1} \tag{4.152}$$

$$G_{M1} = 0.722/(a^2\rho_0 c)\ \text{m}\cdot\text{N}^{-1}\cdot\text{s}^{-1} \tag{4.153}$$

$$R_{A2} = \rho_0 c/(\pi a^2) = 0.318\rho_0 c/a^2\ \text{N}\cdot\text{s/m}^5 \tag{4.154}$$

$$\begin{aligned} R_A &= R_{A2} + R_{A1} = 128\rho_0 c/(9\pi^3 a^2) \\ &= 0.459\rho_0 c/a^2\ \text{N}\cdot\text{s/m}^5 \end{aligned} \tag{4.155}$$

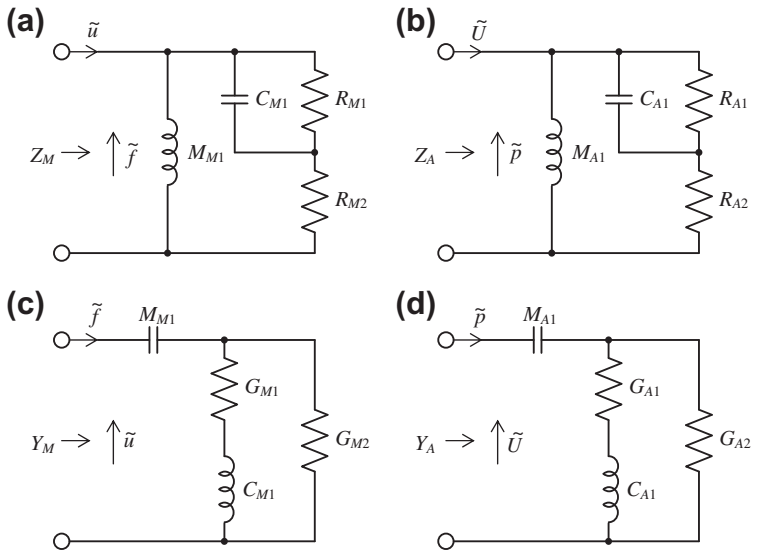

FIG. 4.37 Approximate radiation impedances and admittances for a piston in an infinite baffle or for a closed-back piston for all values of *ka*.

(*a*) Mechanical-impedance analogy; (*b*) acoustic-impedance analogy; (*c*) mechanical-admittance analogy; (*d*) acoustic-admittance analogy.

$$R_{A1} = 0.1404\rho_0 c/a^2 \text{ N}\cdot\text{s/m}^5 \tag{4.156}$$

$$C_{A1} = 1.89\pi a^3/(\rho_0 c^2) = 5.94a^3/(\rho_0 c^2) \text{ m}^5/\text{N} \tag{4.157}$$

$$M_{A1} = 8\rho_0/(3\pi^2 a) = 0.27\rho_0/a \text{ kg/m}^4 \tag{4.158}$$

$$G_{A2} = \pi a^2/(\rho_0 c) \text{ m}^5\cdot\text{N}^{-1}\cdot\text{s}^{-1} \tag{4.159}$$

$$G_{A1} = 7.12a^2/(\rho_0 c) \text{ m}^5\cdot\text{N}^{-1}\cdot\text{s}^{-1} \tag{4.160}$$

All constants are dimensionless and were chosen to give the best average fit to the functions of Fig. 4.35 and Fig. 4.36.

Low- and high-frequency approximations. At low and at high frequencies these circuits may be approximated by the simpler circuits given in the last column of Table 4.4.

It is apparent that when $ka < 0.5$, that is, when the circumference of the piston $2\pi a$ is less than one-half wavelength $\lambda/2$, the impedance load presented by the air on the vibrating piston is that of a mass shunted by a very large resistance. In other words $R^2 = (R_1 + R_2)^2$ is large compared with $\omega^2 M_1^2$. In fact, this loading mass may be imagined to be a layer of air equal in area to the area of the piston and equal in thickness to about 0.85 times the radius, because

Table 4.4 Radiation impedance and admittance for one side of a plane circular piston in an infinite baffle[1]

Impedance	Mechanical **f** = ***drop*** **u** = ***flow***	Specific **p** = ***drop*** **u** = ***flow***	Acoustic **p** = ***drop*** **U** = ***flow***	Analogous circuits
$ka < 0.5$: Series resistance, $\boldsymbol{R}$ Shunt resistance, R Mass, M_1 $ka > 5$: Resistance, R_2	$\boldsymbol{R}_M = \frac{\pi a^4 \rho_0 \omega^2}{2c}$ $R_M = \frac{128 a^2 \rho_0 c}{9\pi}$ $M_{M1} = \frac{8a^3\rho_0}{3}$ $R_{M2} = \pi a^2 \rho_0 c$	$\boldsymbol{R}_S = \frac{a^2 \rho_0 \omega^2}{2c}$ $R_S = \frac{128\rho_0 c}{9\pi^2}$ $M_{S1} = \frac{8a\rho_0}{3\pi}$ $R_{S2} = \rho_0 c$	$\boldsymbol{R}_A = \frac{\rho_0 \omega^2}{2\pi c}$ $R_A = \frac{128\rho_0 c}{9\pi^3 a^2}$ $M_{A1} = \frac{8\rho_0}{3\pi^2 a}$ $R_{A2} = \frac{\rho_0 c}{\pi a^2}$	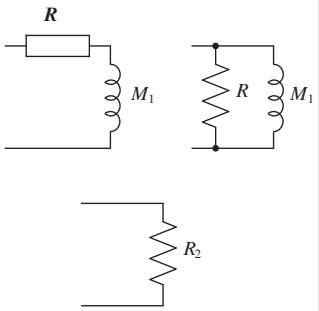
Admittance	**u** = ***drop*** **f** = ***flow***	**u** = ***drop*** **p** = ***flow***	**U** = ***drop*** **p** = ***flow***	
$ka < 0.5$: Series conductance, G Mass, M_1 $ka > 5$: Conductance, G_2	$G_M = \frac{9\pi}{128 a^2 \rho_0 c}$ $M_{M1} = \frac{8a^3\rho_0}{3}$ $G_{M2} = \frac{1}{\pi a^2 \rho_0 c}$	$G_S = \frac{9\pi^2}{128\rho_0 c}$ $M_{S1} = \frac{8a\rho_0}{3\pi}$ $G_{S2} = \frac{1}{\rho_0 c}$	$G_A = \frac{9\pi^3 a^2}{128\rho_0 c}$ $M_{A1} = \frac{8\rho_0}{3\pi^2 a}$ $G_{A2} = \frac{\pi a^2}{\rho_0 c}$	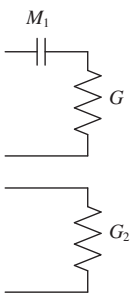

[1]*This table gives element sizes for analogous circuits in the region where* ka < 0.5 *and* ka > 5. *All constants are dimensionless. For the region between 0.5 and 5.0, the charts of Fig. 4.35 and Fig. 4.36 should be used.*

$$(\pi a^2)(0.85a)\rho_0 \approx 2.67 a^3 \rho_0 = M_{M1}$$

At high frequencies, $ka > 5$, the air load behaves exactly as though it were connected to one end of a tube of the same diameter as the piston, with the other end of the tube perfectly absorbing. As we saw in Eq. (2.89), the input mechanical resistance for such a tube is $\pi a^2 \rho_0 c$. Hence, intuitively one might expect that at high frequencies the vibrating rigid piston beams the sound outward in lines perpendicular to the face of the piston. This is actually the case for the immediate near-field close to the piston. At a distance, however, the far-field radiation spreads, as we learned earlier in this chapter.

4.20 PLANE CIRCULAR FREE DISK

A disk in free space without surrounding structure is a suitable model, at low frequencies, for a direct-radiator loudspeaker without a baffle of any sort. In other words, the loudspeaker radiates as a dipole. The radiation impedance is given by Eqs. (13.249), (13.250), and (13.251).

Graphs of the real and imaginary parts of the normalized specific impedance load *on one side of the diaphragm*, $Z_s/\rho_0 c$, as a function of ka for the free disk, are shown in Fig. 4.38. The data of Fig. 4.38 are used in dealing with impedance analogies. For admittance analogies, the complex admittance can be obtained by taking the reciprocal of the complex impedance.

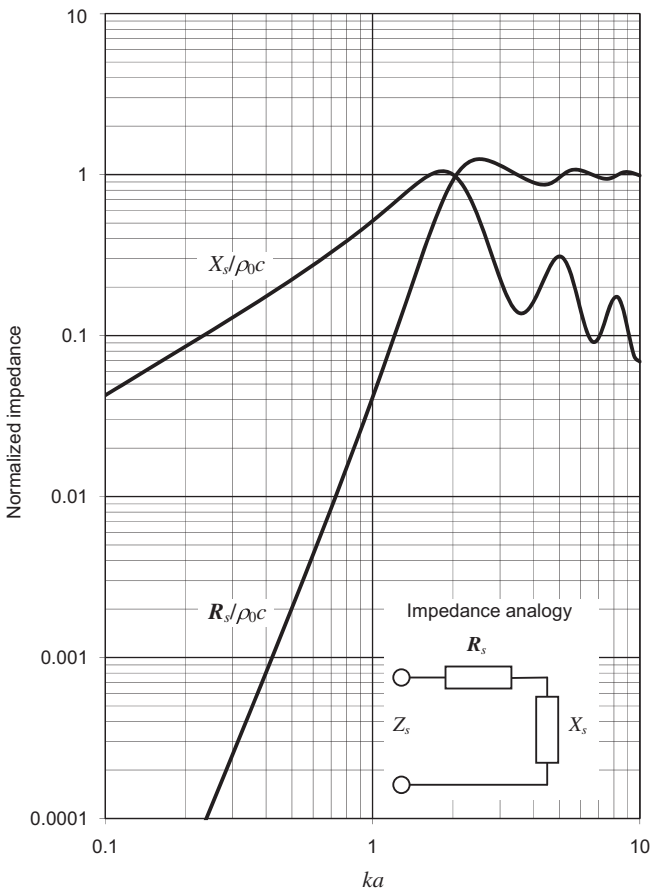

FIG. 4.38 Real and imaginary parts of the normalized specific radiation impedance $Z_s/\rho_0 c$ of the air load on one side of a plane circular piston of radius a in free space.

Frequency is plotted on a normalized scale, where $ka = 2\pi a/\lambda = 2\pi fa/c$.

A simple equivalent circuit, approximately valid for all frequencies like those shown in Fig. 4.37, cannot be drawn for this case. At very low frequencies, however, it is possible to represent the impedance by an equivalent circuit, which is similar to that for an oscillating sphere. In the frequency ranges where $ka < 0.5$ and $ka > 5$, analogous circuits of the type shown in Table 4.5 may be used.

4.21 PLANE CIRCULAR PISTON RADIATING FROM ONE SIDE ONLY IN FREE SPACE

The specific impedance ($N \cdot s/m^3$) of the air load on a plane piston in free space, which has one surface vibrating sinusoidally while the other remains stationary, is given by Eqs. (13.254) and (13.255) and plotted in Fig. 4.39.

Table 4.5 Radiation impedance and admittance for one side of a plane circular piston in free space[1]

Impedance	Mechanical ***f* = drop** ***u* = flow**	Specific ***p* = drop** ***u* = flow**	Acoustic ***p* = drop** ***U* = flow**	Analogous circuits
$ka < 0.5$: Series resistance, $\boldsymbol{R}$ Mass, M_1	$\boldsymbol{R}_M = \frac{8a^6\rho_0\omega^4}{27\pi c^3}$ $M_{M1} = \frac{4a^3\rho_0}{3}$	$\boldsymbol{R}_S = \frac{8a^4\rho_0\omega^4}{27\pi^2 c^3}$ $M_{S1} = \frac{4a\rho_0}{3\pi}$	$\boldsymbol{R}_A = \frac{8a^2\rho_0\omega^4}{27\pi^3 c^3}$ $M_{A1} = \frac{4\rho_0}{3\pi^2 a}$	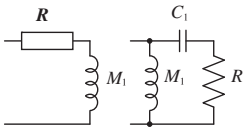
Compliance, C_1	$C_{M1} = \frac{1}{\sqrt{6}\pi a\rho_0 c^2}$	$C_{S1} = \frac{a}{\sqrt{6}\rho_0 c^2}$	$C_{S1} = \frac{\pi a^3}{\sqrt{6}\rho_0 c^2}$	
$ka > 5$: Resistance, R	$R_M = \pi a^2\rho_0 c$	$R_S = \rho_0 c$	$R_A = \frac{\rho_0 c}{\pi a^2}$	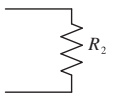
Admittance	***u* = drop** ***f* = flow**	***u* = drop** ***p* = flow**	***U* = drop** ***p* = flow**	
$ka < 0.5$: Series conductance, $\boldsymbol{G}$ Mass, M_1	$\boldsymbol{G}_M = \frac{\omega^2}{6\pi\rho_0 c^3}$ $M_{M1} = \frac{4a^3\rho_0}{3}$	$\boldsymbol{G}_S = \frac{a^2\omega^2}{6\rho_0 c^3}$ $M_{S1} = \frac{4a\rho_0}{3\pi}$	$\boldsymbol{G}_A = \frac{\pi a^4\omega^2}{6\rho_0 c^3}$ $M_{A1} = \frac{4\rho_0}{3\pi^2 a}$	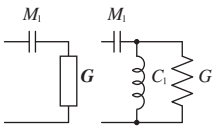
Compliance, C_1	$C_{M1} = \frac{1}{\sqrt{6}\pi a\rho_0 c^2}$	$C_{S1} = \frac{a}{\sqrt{6}\rho_0 c^2}$	$C_{A1} = \frac{\pi a^3}{\sqrt{6}\rho_0 c^2}$	
$ka > 5$: Conductance, G	$G_M = \frac{1}{\pi a^2\rho_0 c}$	$G_S = \frac{1}{\rho_0 c}$	$G_A = \frac{\pi a^2}{\rho_0 c}$	

[1] *This table gives element sizes for analogous circuits in the region where* ka < 0.5 *and* ka > 5. *All constants are dimensionless. For the region between 0.5 and 5.0, the chart of Fig. 4.38 should be used.*

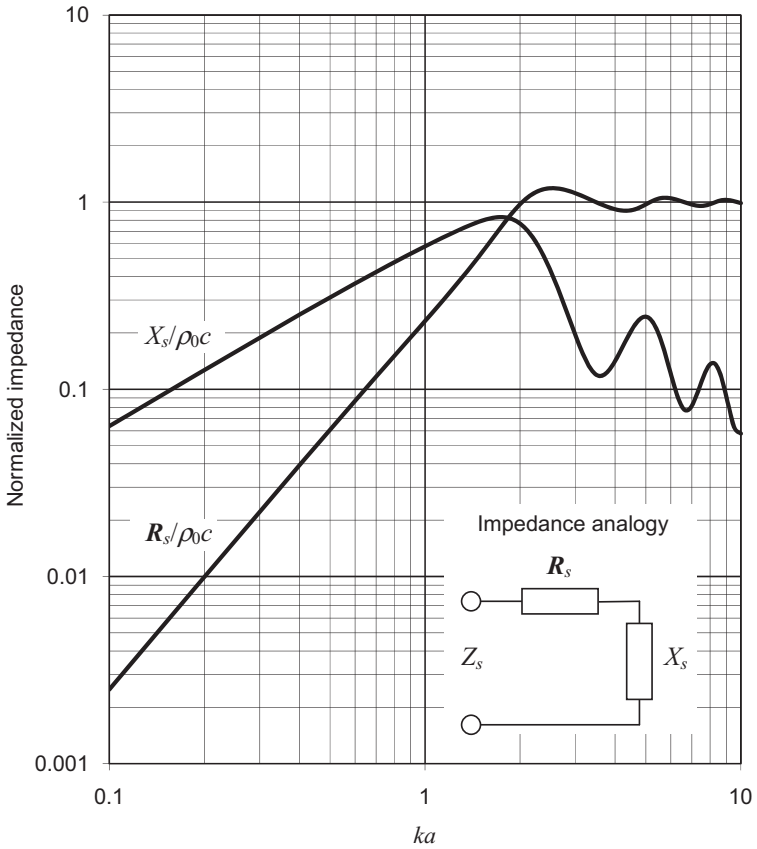

FIG. 4.39 Real and imaginary parts of the normalized specific radiation impedance $Z_s/\rho_0 c$ of the air load on one side of a plane circular piston of radius a radiating from one side only into free space.

Frequency is plotted on a normalized scale, where $ka = 2\pi a/\lambda = 2\pi fa/c$.

It is simply the mean of the impedances of a plane circular piston in an infinite baffle and the same in free space.

To a fair approximation, the radiation impedance for a one-sided piston in free space may be represented over the entire frequency range by the same analogous circuits used for the piston in an infinite baffle and shown in Fig. 4.37, where the elements now are:

$$R_{M2} = \pi a^2 \rho_0 c \ \text{N}\cdot\text{s/m} \tag{4.161}$$

$$\begin{aligned} R_M &= R_{M2} + R_{M1} = 16a^2\rho_0 c/\pi \\ &= 5.09a^2\rho_0 c \ \text{N}\cdot\text{s/m} \end{aligned} \tag{4.162}$$

$$R_{M1} = 1.95a^2\rho_0 c \ \text{N}\cdot\text{s/m} \tag{4.163}$$

$$C_{M1} = 1/(\pi a \rho_0 c^2) = 0.318/(a\rho_0 c^2)\ \text{m/N} \tag{4.164}$$

$$M_{M1} = 2a^3\rho_0\ \text{kg} \tag{4.165}$$

$$G_{M2} = 1/(\pi a^2 \rho_0 c) = 0.318/(a^2\rho_0 c)\ \text{m}\cdot\text{N}^{-1}\cdot\text{s}^{-1} \tag{4.166}$$

$$G_{M1} = 0.513/(a^2\rho_0 c)\ \text{m}\cdot\text{N}^{-1}\cdot\text{s}^{-1} \tag{4.167}$$

$$R_{A2} = \rho_0 c/(\pi a^2) = 0.318\rho_0 c/a^2\ \text{N}\cdot\text{s/m}^5 \tag{4.168}$$

$$\begin{aligned} R_A &= R_{A2} + R_{A1} = 16\rho_0 c/(\pi^3 a^2) \\ &= 0.516\rho_0 c/a^2\ \text{N}\cdot\text{s/m}^5 \end{aligned} \tag{4.169}$$

$$R_{A1} = 0.1977\rho_0 c/a^2\ \text{N}\cdot\text{s/m}^5 \tag{4.170}$$

$$C_{A1} = \pi a^3/(\rho_0 c^2) = 3.142a^3/(\rho_0 c^2)\ \text{m}^5/\text{N} \tag{4.171}$$

$$M_{A1} = 2\rho_0/(\pi^2 a) = 0.2026\rho_0/a\ \text{kg/m}^4 \tag{4.172}$$

$$G_{A2} = \pi a^2/(\rho_0 c)\ \text{m}^5\cdot\text{N}^{-1}\cdot\text{s}^{-1} \tag{4.173}$$

$$G_{A1} = 5.06a^2/(\rho_0 c)\ \text{m}^5\cdot\text{N}^{-1}\cdot\text{s}^{-1} \tag{4.174}$$

In the frequency ranges where $ka < 0.5$ and $ka > 5$, analogous circuits of the type shown in Table 4.6 may be used.

PART XIV: VISCOUS AND THERMAL LOSSES

4.22 SOUND IN LOSSY TUBES

In Sec. 2.4, we examined the propagation of one-dimensional waves in a loss-free tube. In order to be able to neglect viscous losses inside the tube, the radius of the tube must not be too small. Also, in order to be able to neglect transverse resonances in the tube, the radius must not be too large. Here we shall re-derive the one-dimensional wave equation using a slightly different procedure than before, taking into account the viscous and thermal losses that take place at the boundary wall, using what are known as the Navier–Stokes equations. In accordance with the continuum theory of gases, traditional models have assumed that the axial velocity at the wall of the tube is zero and that the

Table 4.6 Radiation impedance and admittance for a plane circular piston radiating from one side only in free space[1]

Impedance	Mechanical f = drop u = flow	Specific p = drop u = flow	Acoustic p = drop U = flow	Analogous circuits
$ka < 0.5$: Series resistance, $\boldsymbol{R}$ Shunt resistance, R Mass, M_1 $ka > 5$: Resistance, R_2	$\boldsymbol{R}_M = \frac{\pi a^4 \rho_0 \omega^2}{4c}$ $R_M = \frac{16a^2\rho_0 c}{\pi}$ $M_{M1} = 2a^3\rho_0$ $R_{S2} = \pi a^2 \rho_0 c$	$\boldsymbol{R}_S = \frac{a^2\rho_0\omega^2}{4c}$ $R_S = \frac{16\rho_0 c}{\pi^2}$ $M_{S1} = \frac{2a\rho_0}{\pi}$ $R_{S2} = \rho_0 c$	$\boldsymbol{R}_A = \frac{\rho_0\omega^2}{4\pi c}$ $R_A = \frac{16\rho_0 c}{\pi^3 a^2}$ $M_{A1} = \frac{2\rho_0}{\pi^2 a}$ $R_{S2} = \frac{\rho_0 c}{\pi a^2}$	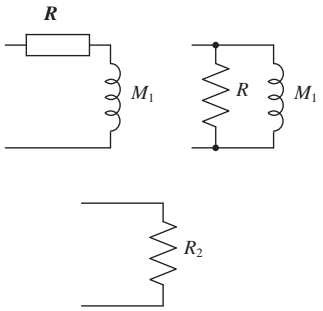
Admittance	$\boldsymbol{u}$ = drop $\boldsymbol{f}$ = flow	$\boldsymbol{u}$ = drop $\boldsymbol{p}$ = flow	$\boldsymbol{U}$ = drop $\boldsymbol{p}$ = flow	
$ka < 0.5$: Series conductance, G Mass, M_1 $ka > 5$: Conductance, G_2	$G_M = \frac{\pi}{16a^2\rho_0 c}$ $M_{M1} = 2a^3\rho_0$ $G_{M2} = \frac{1}{\pi a^2 \rho_0 c}$	$G_S = \frac{\pi^2}{16\rho_0 c}$ $M_{S1} = \frac{2a\rho_0}{\pi}$ $G_{S2} = \frac{1}{\rho_0 c}$	$G_A = \frac{\pi^3 a^2}{16\rho_0 c}$ $M_{A1} = \frac{2\rho_0}{\pi^2 a}$ $G_{A2} = \frac{\pi a^2}{\rho_0 c}$	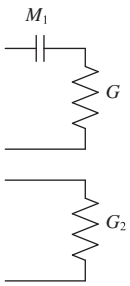

[1] *This table gives element sizes for analogous circuits in the region where* ka < 0.5 *and* ka > 5. *All constants are dimensionless. For the region between 0.5 and 5.0, the chart of Fig. 4.39 should be used.*

temperature there is ambient, due to the sheer number of collisions occurring between air molecules and the wall. However, as the diameter of the tube is reduced relative to the mean free path of the molecules, fewer collisions occur so that the axial velocity and temperature both increase at the wall. This is generally known as a slip boundary condition. Formulation is now available [7] that models this slip, thus allowing us to model tubes of much smaller diameter than was previously possible. The resulting wave-number is complex and from this new wave-number we shall derive two new parameters called the dynamic density and dynamic compressibility which replace the density and inverse bulk modulus respectively in the expressions for wave-number and characteristic impedance. These result from the average flow over the cross-section of the tube as if the losses were homogeneous throughout the bulk of the acoustic medium, even though they are actually localized near the tube wall. We will also define a viscous boundary thickness to define the region

within which most of the viscous losses occur. For those readers who are not interested in the full derivation but only wish to apply the results to practical uses, you may skip on to the results shown in Fig. 4.46 to Fig. 4.51.

Two-terminal electrical components generally obey Kirchhoff's law. In other words, the current flowing out of one terminal is equal to that flowing into the other. However, the exact model of a tube does not obey this law because, due to losses, the volume velocity flowing out of one end is less than that flowing into the other. Therefore, we must model it as a four-terminal device, or 2-port model. We shall develop a discrete-element 2-port model, which is a useful result as it allows us to apply electrical circuit theory. However, we shall see that under certain frequency or diameter ranges, we can make useful two-terminal approximations for an open or closed tube which form the basis of some of the acoustic components presented in Sec. 4.4.

4.23 WAVE EQUATION FOR AN INFINITE LOSSY TUBE

Assumptions. The circular tube of radius a shown in Fig. 4.40 has z as the axial ordinate and w as the radial ordinate. In the following discussion, it is assumed that the radial pressure distribution is uniform and that the pressure variations are purely axial. This has been shown to be valid provided that $a(\text{meters}) \leq 10^4/f^{3/2}$. [8] Also, it is assumed that the radial velocity is zero, but the axial velocity is allowed to vary radially due to laminar flow resulting from viscous losses. Thermal conduction through the tube wall is also taken into consideration, where the wall is at ambient temperature T_0. However, boundary slip is allowed for, whereby the axial particle velocity adjacent to the tube wall can be non-zero and the air temperature there can be non-ambient. Furthermore, the degree of slip is proportional to the gradient of the radial distribution of the velocity or temperature at the tube wall.

The momentum conservation equation. In accordance with the conservation of momentum law, we can write the linearized Navier–Stokes equation [10]

$$\left(\rho_0 \frac{\partial}{\partial t} - \mu \nabla^2\right) u(w) = -\frac{\partial p}{\partial z}, \tag{4.175}$$

where

$$\nabla^2 = \partial^2/(\partial w^2) + w^{-1}\partial/(\partial w)$$

and u is the axial velocity, p is the axial pressure, $\rho_0 = 1.18\ \text{kg/m}^3$ and $\mu = 18.6 \times 10^{-6}\ \text{N}\cdot\text{s/m}^2$ are the density and viscosity of air respectively, and z is the axial ordinate. Replacing the time derivative with $j\omega$ gives

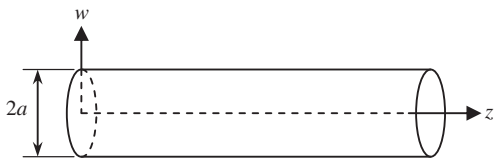

FIG. 4.40 Geometry of tube.

$$(\nabla^2 + k_V^2)\tilde{u}(w) = -\frac{k_V^2}{j\omega\rho_0}\frac{\partial\tilde{p}}{\partial z}, \tag{4.176}$$

where

$$k_V = \sqrt{-j\omega\rho_0/\mu}. \tag{4.177}$$

The gas law and thermal conduction (entropy). For an ideal gas we can write the following linearized equation of state [11]

$$\frac{\tilde{p}}{P_0} = \frac{\tilde{\delta}}{\rho_0} + \frac{\tilde{\tau}(w)}{T_0}, \tag{4.178}$$

where $\tilde{p}$, $\tilde{\delta}$ and $\tilde{\tau}$ are the small pressure, density and temperature fluctuations respectively. Fourier's law for thermal conduction gives

$$\kappa\nabla^2\tilde{\tau}(w) = j\omega T_0(\rho_0 C_V\tilde{p}/P_0 - C_P\tilde{\delta}), \tag{4.179}$$

where $\kappa = 25.4 \times 10^{-3}\ \mathrm{N\cdot s^{-1}\cdot K^{-1}}$ is the thermal conductivity, C_V is the specific heat capacity under constant volume, and C_P is the specific heat capacity under constant pressure. Eliminating $\tilde{\delta}$ from Eqs. (4.178) and (4.179) gives

$$\kappa\nabla^2\tilde{\tau}(w) = j\omega\rho_0 T_0\left((C_V - C_P)\frac{\tilde{p}}{P_0} + C_P\frac{\tilde{\tau}(w)}{T_0}\right). \tag{4.180}$$

We also note that $C_P - C_V = P_0/(\rho_0 T_0)$ so that

$$(\nabla^2 + P_r k_V^2)\tilde{\tau}(w) = \frac{P_r k_V^2}{\rho_0 C_P}\tilde{p}, \tag{4.181}$$

where the P_r is the (dimensionless) Prandtl number given by

$$P_r = \mu C_P/\kappa \tag{4.182}$$

which is the ratio of the viscous diffusion rate to the thermal diffusion rate.

Solution of the velocity and temperature radial equations. Equations (4.176) and (4.181) for the radial velocity and temperature distributions respectively are subject to the following slip boundary conditions:

$$\tilde{u}(a) = -aB_u\frac{\partial\tilde{u}(w)}{\partial w}\Big|_{w=a}, \tag{4.183}$$

$$\tilde{\tau}(a) = -aB_e\frac{\partial\tilde{\tau}(w)}{\partial w}\Big|_{w=a}, \tag{4.184}$$

where the boundary slip factors B_u and B_e are given by

$$B_u = (2\alpha_u^{-1} - 1)K_n, \tag{4.185}$$

$$B_e = (2\gamma/P_r(1+\gamma))(2\alpha_e^{-1} - 1)K_n. \tag{4.186}$$

We note that $\gamma = C_P/C_v$ is the specific heat ratio, α_u and α_e are the accommodation coefficients, both of which are assumed to have a value of 0.9, and K_n is the (dimensionless) Knudsen number given by

$$K_n = \lambda_m/a, \tag{4.187}$$

where $\lambda_m = 60$ nm is the molecular mean free path length between collisions. Substituting

$$\tilde{u}(w) = -\frac{1}{j\omega\rho_0}\frac{\partial\tilde{p}}{\partial z}(1 - F(k_V, w, B_u)), \tag{4.188}$$

$$\tilde{\tau}(w) = \frac{\tilde{p}}{\rho_0 C_P}(1 - F(k_T, w, B_e)) \tag{4.189}$$

in Eqs. (4.176) and (4.181) respectively leads to a new pair of equations:

$$(\nabla^2 + k_V^2)F(k_V, w, B_u) = 0, \tag{4.190}$$

$$(\nabla^2 + k_T^2)F(k_T, w, B_e) = 0, \tag{4.191}$$

where

$$k_T = \sqrt{P_r}k_V. \tag{4.192}$$

Eqs. (4.190) and (4.191) are subject to the boundary conditions

$$F(k_V, a, B_u) + aB_u\frac{\partial}{\partial w}F(k_V, w, B_u)\big|_{w=a} = 1, \tag{4.193}$$

$$F(k_T, a, B_e) + aB_e\frac{\partial}{\partial w}F(k_T, w, B_e)\big|_{w=a} = 1 \tag{4.194}$$

Solutions to Eqs. (4.190) and (4.191) are given by

$$F(k_V, w, B_u) = AJ_0(k_V w), \tag{4.195}$$

$$F(k_T, w, B_e) = BJ_0(k_T w). \tag{4.196}$$

The unknown coefficients can be found by substituting Eqs. (4.195) and (4.196) in the boundary conditions of Eqs. (4.193) and (4.194) respectively to give

$$A = (J_0(k_V a) - B_u k_V a J_1(k_V a))^{-1}$$

and

$$B = (J_0(k_T a) - B_e k_T a J_1(k_T a))^{-1}.$$

The average values across the tube cross-section are defined by

$$\langle F(k_V, a, B_u)\rangle = \frac{1}{\pi a^2}\int_0^{2\pi}\int_0^{a} F(k_V, w, B_u) w dw d\phi$$
$$= \frac{Q(k_V a)}{1 - 0.5 B_u k_V^2 a^2 Q(k_V a)}, \tag{4.197}$$

where

$$Q(x) = 2J_1(x)/(xJ_0(x)) \tag{4.198}$$

and similarly

$$\langle F(k_T, a, B_e)\rangle = \frac{Q(k_T a)}{1 - 0.5 B_e k_T^2 a^2 Q(k_T a)}. \tag{4.199}$$

In Fig. 4.41, the axial velocity along the radius of a narrow tube is plotted at a frequency of 100 Hz using Eq. (4.188), where the radius of the tube is 1 μm. Also, the axial velocity along the radius of a wide tube is plotted in Fig. 4.42 at a frequency of 10 kHz, where the radius is 1 mm

The effective boundary layer thickness δ_{visc} can be calculated using the formula

$$\delta_{visc} = \sqrt{\frac{\mu}{\rho_0 \omega}} \tag{4.200}$$

In Fig. 4.41, the effective boundary layer thickness of 155 μm is much greater than the radius of the tube, so the normalized velocity never reaches the theoretical maximum value of unity even at the center ($w = 0$). At the wall, the boundary slip condition is clearly visible as the velocity does not reach zero. By contrast, the effective boundary layer thickness in Fig. 4.42 of 15.5 μm is only 1.55% of the radius, which explains why the normalized velocity is unity over most of the radius and only falls

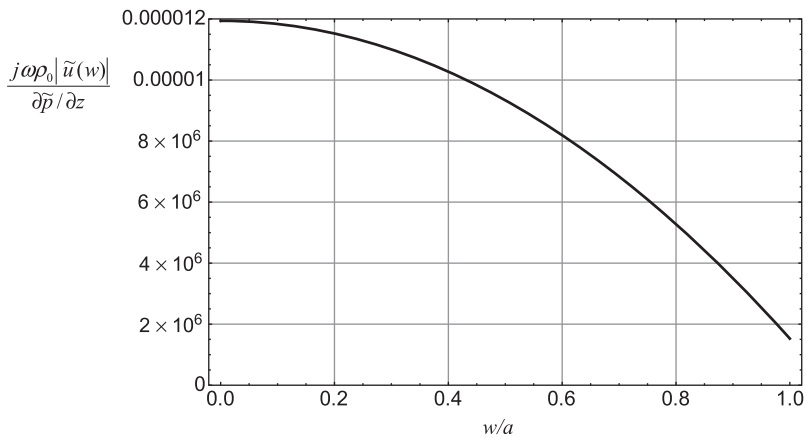

FIG. 4.41 Variation of normalized velocity along radius of ultra-narrow tube of radius 1 μm at a frequency of 100 Hz.

The effective boundary layer thickness is 155 μm.

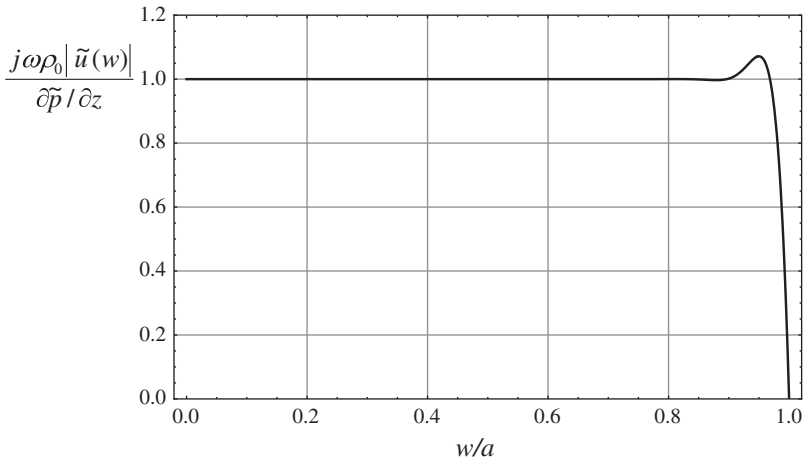

FIG. 4.42 Variation of normalized velocity along radius of medium-sized tube of radius 1 mm at a frequency of 10 kHz.

The effective boundary layer thickness is 15.5 μm.

rapidly close to the wall ($w = a$), albeit after a small peak. At the wall, the velocity is virtually zero, so there is no appreciable slip

Mass conservation and Helmholtz wave equation. Finally, we use the following mass conservation equation or equation of continuity [12]

$$j\omega\langle\tilde{\delta}\rangle + \rho_0\frac{\partial}{\partial z}\langle\tilde{u}\rangle = 0. \tag{4.201}$$

For the average velocity, we can write from Eq. (4.188)

$$\langle\tilde{u}\rangle = -\frac{1}{j\omega\rho_0}\frac{\partial\tilde{p}}{\partial z}(1 - \langle F(k_V, a, B_u)\rangle). \tag{4.202}$$

Differentiating Eq. (4.202) with respect to z and inserting it in Eq. (4.201) yields

$$\langle\tilde{\delta}\rangle = -\frac{1}{\omega^2}(1 - \langle F(k_V, a, B_u)\rangle)\frac{\partial^2\tilde{p}}{\partial z^2}. \tag{4.203}$$

Also, from the gas law of Eq. (4.178)

$$\frac{\tilde{p}}{P_0} = \frac{\langle\tilde{\delta}\rangle}{\rho_0} + \frac{\langle\tilde{\tau}\rangle}{T_0}, \tag{4.204}$$

where the average temperature is derived from Eq. (4.189) as follows

$$\langle\tilde{\tau}\rangle = \frac{\tilde{p}}{\rho_0 C_P}(1 - \langle F(k_T, a, B_e)\rangle). \tag{4.205}$$

Substituting Eq. (4.205) in Eq. (4.204) while noting that

$$C_P - C_v = P_0/(\rho_0 T_0) \text{ and } \gamma = C_P/C_v$$

so that

$$C_P = \frac{\gamma P_0}{(\gamma - 1)\rho_0 T_0} \tag{4.206}$$

gives

$$\langle \tilde{\delta} \rangle = \frac{\rho_0}{\gamma P_0}(1 + (\gamma - 1)\langle F(k_T, a, B_e)\rangle)\tilde{p}. \tag{4.207}$$

Equating Eqs. (4.203) and (4.207) then leads to the following Helmholtz wave equation:

$$\frac{\partial^2 \tilde{p}}{\partial z^2} + k^2 \tilde{p} = 0, \tag{4.208}$$

where

$$k^2 = \frac{(1 + (\gamma - 1)\langle F(k_T, a, B_e)\rangle)\omega^2 \rho_0}{(1 - \langle F(k_V, a, B_u)\rangle)\gamma P_0} \tag{4.209}$$

or, using Eqs. (4.197) and (4.199),

$$k^2 = \frac{\left(1 + (\gamma - 1)\dfrac{Q(k_T a)}{1 - 0.5 B_e k_T^2 a^2 Q(k_T a)}\right)\omega^2 \rho_0}{\left(1 - \dfrac{Q(k_V a)}{1 - 0.5 B_u k_V^2 a^2 Q(k_V a)}\right)\gamma P_0}. \tag{4.210}$$

Dynamic density. In order to simplify the expressions for the wave-number k and characteristic impedance Z_0, we can use the following shorthand known as the dynamic density where $\langle \tilde{u} \rangle$ is given by Eq. (4.202) so that

$$\begin{aligned} \rho &= -\frac{1}{j\omega\langle \tilde{u} \rangle}\frac{\partial \tilde{p}}{\partial z} = \frac{\rho_0}{1 - \langle F(k_V, a, B_u)\rangle} \\ &= \rho_0 \left(1 - \frac{Q(k_V a)}{1 - 0.5 B_u k_V^2 a^2 Q(k_V a)}\right)^{-1}. \end{aligned} \tag{4.211}$$

Dynamic compressibility. Also, the dynamic compressibility is defined by

$$C = \frac{\langle \tilde{\delta} \rangle}{\rho_0 \tilde{p}}. \tag{4.212}$$

From the ideal gas law of Eq. (4.207) we obtain

$$\frac{\langle \tilde{\delta} \rangle}{\rho_0 \tilde{p}} = \frac{1}{\gamma P_0}(1 + (\gamma - 1)\langle F(k_T, a, B_e)\rangle), \tag{4.213}$$

which is inserted in Eq. (4.212) to give

$$C = \frac{1}{\gamma P_0}\left(1 + \frac{(\gamma - 1)Q(k_T a)}{1 - 0.5B_e k_T^2 a^2 Q(k_T a)}\right). \tag{4.214}$$

Wave-number and characteristic impedance. Using the expressions for the dynamic density ρ and dynamic compressibility C from Eqs. (4.211) and (4.214) respectively, the wave-number of Eq. (4.210) simply becomes

$$k = \omega\sqrt{\rho C} \tag{4.215}$$

By comparing this with the wave-number for a loss-free plane wave [from Eqs. (2.19) and (2.45)]

$$k = \omega\sqrt{\frac{\rho_0}{\gamma P_0}} \tag{4.216}$$

we see that when there are no viscous or thermal losses $\rho = \rho_0$ and $C = 1/(\gamma P_0)$. Hence the compressibility is the inverse bulk modulus of the medium. Similarly, from Eq. (2.89), we see that the characteristic specific impedance of an infinite tube is

$$Z_s = \sqrt{\rho/C}. \tag{4.217}$$

A 2-port network for a finite tube [9]. We have already introduced 2-port networks for transducers using z-parameters in Sec. 3.10. Here we shall apply the theory to a tube with viscous and thermal losses. A general equivalent circuit for passive 2-port networks is shown in Fig. 4.43. Due to the reciprocity of the tube, or in other words, the fact that it does not matter at which end there is a transmitter or receiver, we obtain $z_{22} = z_{11}$ and $z_{21} = z_{12}$.

From Eq. (3.64) we write

$$\begin{bmatrix} \tilde{p}_{in} \\ \tilde{p}_{out} \end{bmatrix} = \begin{bmatrix} z_{11} & z_{12} \\ z_{21} & z_{22} \end{bmatrix} \cdot \begin{bmatrix} \tilde{u}_{in} \\ -\tilde{u}_{out} \end{bmatrix}. \tag{4.218}$$

The equations for the tube with losses take on the same form as those without losses which we have already derived in Chapter 2. From Eqs. (2.58) and (2.59) for the pressure and velocity in a finite tube, the following z-parameters are obtained:

$$z_{11} = z_{22} = \frac{\tilde{p}(l)}{-\tilde{u}(l)}\Big|_{Z_T = \infty} = -jZ_s \cot kl, \tag{4.219}$$

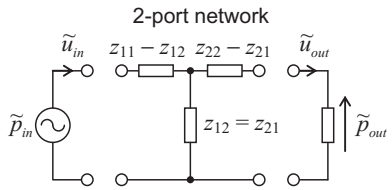

FIG. 4.43 Equivalent electrical circuit for a general passive 2-port network.

$$z_{12} = z_{21} = \frac{\tilde{p}(0)}{-\tilde{u}(l)}\Big|_{Z_T=\infty} = -jZ_s \operatorname{cosec} kl, \tag{4.220}$$

where we have replaced $\rho_0 c$ with Z_s for a tube with viscous and thermal losses. This is equivalent to using a piston to apply a velocity $\tilde{u}(l)$ at $z = l$ while the other end (at $z = 0$) is blocked (hence $z_T = \infty$) and using a probe microphone to measure the pressure at $z = l$ and $z = 0$. The pressures $\tilde{p}(l)$ and $\tilde{p}(0)$ are then divided by $\tilde{u}(l)$ in order to determine z_{11} and z_{12} respectively. The wave-number k and characteristic impedance Z_s with losses are given by Eqs. (4.215) and (4.217) respectively. Using the relationships of Eqs. (3.74) to (3.77), we can write the following equations for the transmission parameters

$$\begin{bmatrix} \tilde{p}_{in} \\ \tilde{u}_{in} \end{bmatrix} = \begin{bmatrix} a_{11} & a_{12} \\ a_{21} & a_{22} \end{bmatrix} \cdot \begin{bmatrix} \tilde{p}_{out} \\ \tilde{u}_{out} \end{bmatrix}, \tag{4.221}$$

where

$$a_{11} = \frac{\tilde{p}(l)}{\tilde{p}(0)}\Big|_{Z_T=\infty} = \cos kl, \tag{4.222}$$

$$a_{12} = \frac{\tilde{p}(l)}{-\tilde{u}(0)}\Big|_{Z_T=0} = jZ_s \sin kl, \tag{4.223}$$

$$a_{21} = \frac{-\tilde{u}(l)}{\tilde{p}(0)}\Big|_{Z_T=\infty} = \frac{j \sin kl}{Z_s}, \tag{4.224}$$

$$a_{22} = \frac{-\tilde{u}(l)}{-\tilde{u}(0)}\Big|_{Z_T=0} = \cos kl. \tag{4.225}$$

If the tube is blocked at the far end, the impedance Z_{in} at the entrance is simply

$$Z_{in} = \frac{\tilde{p}_{in}}{\tilde{u}_{in}}\Big|_{\tilde{u}_{out}=0} = z_{11} = -jZ_s \cot kl. \tag{4.226}$$

If the far end is open, then

$$Z_{in} = \frac{\tilde{p}_{in}}{\tilde{u}_{in}}\Big|_{\tilde{p}_{out}=0} = z_{11} + \left(\frac{1}{z_{11}} + \frac{1}{z_{12}}\right)^{-1} = jZ_s \tan kl. \tag{4.227}$$

A 2-port network for a short finite tube. When the wavelength is about six times greater than the length l of the tube or greater, we can take just the first two terms of the equivalent series forms for the cotangent and cosecant so that Eqs. (4.219) and (4.220) reduce to

$$z_{11} = z_{22} \approx -jZ_s\left(\frac{\boldsymbol{1}}{kl} - \frac{kl}{3}\right) = \frac{1}{j\omega \boldsymbol{C}_s} + \frac{j\omega \boldsymbol{M}_s}{3}, \tag{4.228}$$

$$z_{12} = z_{21} \approx -jZ_s\left(\frac{\boldsymbol{1}}{kl} + \frac{kl}{6}\right) = \frac{1}{j\omega \boldsymbol{C}_s} - \frac{j\omega \boldsymbol{M}_s}{6}. \tag{4.229}$$

where $\boldsymbol{C}_s = Cl$ is a lossy specific compliance and $\boldsymbol{M}_s = \rho l$ is a lossy specific mass. The bold typeface indicates that these are not pure reactances, but also contain resistive components due to losses. The compliance $\boldsymbol{C}_s$ contains thermal losses and $\boldsymbol{M}_s$ contains viscous losses. The dynamic compressibility C and dynamic density ρ are given by Eqs. (4.214) and (4.211) respectively. The compliance and mass are shown in Fig. 4.44 as an equivalent electrical circuit. It is valid so long as the radius a is greater than the molecular mean free path length λ_m. When one end of the tube is open and the radiation load is negligible, the corresponding pair of terminals is effectively shorted and, at low frequencies, the two upper mass elements $\frac{1}{2}\boldsymbol{M}_s$ dominate so that the total mass is $\boldsymbol{M}_s$.

When one end is closed, the corresponding pair of terminals is open circuited and, at low frequencies, the compliance element $\boldsymbol{C}_s$ dominates. The mass is now due to one upper element and the negative middle element which gives

$$\frac{1}{2}\boldsymbol{M}_s - \frac{1}{6}\boldsymbol{M}_s = \frac{1}{3}\boldsymbol{M}_s.$$

The fact that the mass of a blocked tube is one third of that of an open tube can be verified by expanding the tangent function of Eq. (4.227), as we did in Sec. 4.2.

A 2-port network for a short finite tube using approximate discrete elements. Let us now shorten the equivalent series forms of the Bessel functions in the function $Q(x)$ of Eq. (4.198) to just their first two terms:

$$Q(x) = \frac{2J_1(x)}{xJ_0(x)} \approx \frac{8 - x^2}{8 - 2x^2} \tag{4.230}$$

We now apply this to the dynamic density from Eq. (4.211) to obtain

$$\rho = -\rho_0 \frac{8 - (2 + 4B_u)k_V^2 a^2 + 0.5B_u k_V^4 a^4}{(1 + 4B_u)k_V^2 a^2 + 0.5B_u k_V^4 a^4}. \tag{4.231}$$

For small values of $k_V a$, this simplifies to

$$\rho = \frac{-8\rho_0}{(1 + 4B_u)k_V^2 a^2}, \tag{4.232}$$

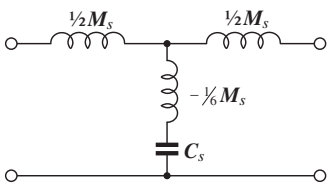

FIG. 4.44 A 2-port network for a short tube of radius *a*, length *l*, which is valid for $a > \lambda_m$, the molecular mean free path.

which after substituting k_V from Eq. (4.177) yields

$$\rho = \frac{8\mu}{j\omega(1+4B_u)a^2}. \tag{4.233}$$

We also apply Eq. (4.230) to the dynamic compressibility from Eq. (4.214) to obtain

$$C = \frac{1}{\gamma P_0}\left(\frac{8\gamma - (1+\gamma+4B_e)k_T^2a^2 + 0.5B_ek_T^4a^4}{8-(2+4B_e)k_T^2a^2+0.5B_ek_T^4a^4}\right). \tag{4.234}$$

For small values of k_Ta, this simplifies to

$$C = 1/P_0, \tag{4.235}$$

By substituting Eqs. (4.233) and (4.235) into Eqs. (4.215) and (4.217), we obtain the asymptotic wavenumber and characteristic impedance for a short narrow tube

$$k\big|_{a\to 0} = \frac{2(1-j)}{a}\sqrt{\frac{\mu\omega}{(1+4B_u)P_0}}, \tag{4.236}$$

$$Z_s\big|_{a\to 0} = \frac{2(1-j)}{a}\sqrt{\frac{\mu P_0}{(1+4B_u)\omega}}. \tag{4.237}$$

In order to separate out the reactive and resistive elements of Fig. 4.44, we have to include the second-order terms of Eqs. (4.215) and (4.217). However, the approximation is not optimum because the singularity of the polynomial approximation of $Q(x)$ in Eq. (4.230) does not match that of the Bessel function expression. Hence we will modify Eq. (4.230) in order to align the singularities

$$Q(x) = \frac{2J_1(x)}{xJ_0(x)} \approx \frac{\alpha^2-(1-\alpha^2/8)x^2}{\alpha^2-x^2}, \tag{4.238}$$

where $\alpha = 2.4048$ is the first zero of $J_0(x)$. In other words $J_0(\alpha) = 0$. The numerator part of this approximation has been determined in order to lead to the same asymptotic expressions for ρ, C, k, and Z_s as Eq. (4.230). We now apply this to the dynamic density from Eq. (4.211) to obtain

$$\rho = \rho_0\frac{8-\left(\frac{8}{\alpha^2}+4B_u\right)k_V^2a^2+\frac{8-\alpha^2}{2\alpha^2}B_uk_V^4a^4}{-(1+4B_u)k_V^2a^2+\frac{8-\alpha^2}{2\alpha^2}B_uk_V^4a^4}. \tag{4.239}$$

Ignoring the fourth-order terms and substituting k_V from Eq. (4.177) yields

$$\rho = \frac{8\mu}{j\omega(1+4B_u)a^2} + \frac{(8/\alpha^2)+4B_u}{1+4B_u}\rho_0. \tag{4.240}$$

The impedance due to the complex mass $\boldsymbol{M}_s$ is then given by

$$Z_V = j\omega \boldsymbol{M}s = j\omega\rho l = \frac{8\mu l}{(1+4B_u)a^2} + j\omega\rho_0 l\frac{(8/\alpha^2)+4B_u}{1+4B_u}. \tag{4.241}$$

We see that the first term represents the resistance due to viscous flow losses while the second term represents the mass reactance. We also apply Eq. (4.238) to the dynamic compressibility from Eq. (4.214) to obtain

$$C = \frac{1}{\gamma P_0}\cdot\frac{8\gamma - \left(1+\left(\frac{8}{\alpha^2}-1\right)\gamma + 4B_e\right)k_T^2a^2 + \frac{8-\alpha^2}{2\alpha^2}B_e k_T^4 a^4}{8 - \left(\frac{8}{\alpha^2}+4B_e\right)k_T^2a^2 + \frac{8-\alpha^2}{2\alpha^2}B_e k_T^4 a^4}. \tag{4.242}$$

Ignoring the fourth-order terms and substituting k_T from Eqs. (4.177), (4.182), (4.192), and (4.206) yields

$$C = \frac{1}{\gamma P_0}\cdot\frac{\gamma + j\omega\frac{\left(1+\left((8/\alpha^2)-1\right)\gamma+4B_e\right)\gamma P_0 a^2}{8(\gamma-1)\kappa T_0}}{1+j\omega\frac{\left((8/\alpha^2)+4B_e\right)\gamma P_0 a^2}{8(\gamma-1)\kappa T_0}}. \tag{4.243}$$

We will use the approximation that

$$1+((8/\alpha^2)-1)\gamma \approx 8/\alpha^2.$$

The impedance due to the complex compliance $\boldsymbol{C}_s$ is then given by

$$\begin{aligned} Z_T &= \frac{1}{j\omega \boldsymbol{C}_s} = \frac{1}{j\omega Cl} = \frac{1+j\omega R_T C_T}{j\omega(C_0+C_T+j\omega R_T C_0 C_T)} \\ &= \frac{1}{j\omega C_0 + \dfrac{1}{R_T + \dfrac{1}{j\omega C_T}}}, \end{aligned} \tag{4.244}$$

where

$$C_0 = \frac{l}{\gamma P_0}, \tag{4.245}$$

$$C_T = (\gamma-1)C_0, \tag{4.246}$$

$$\begin{aligned} R_T &= \frac{\left((8/\alpha^2)+4B_e\right)\gamma P_0 a^2}{8(\gamma-1)\kappa T_0 C_T}, \\ &\approx \frac{(1+3B_e)\gamma P_0 a^2}{6(\gamma-1)\kappa T_0 C_T}. \end{aligned} \tag{4.247}$$

Similarly, we can separate Z_V from Eq. (4.241) into its constituent elements:

$$Z_V = R_V + j\omega M_0, \tag{4.248}$$

where

$$R_V = \frac{8\mu l}{(1 + 4B_u)a^2}, \tag{4.249}$$

$$M_0 = \frac{(8/\alpha^2) + 4B_u}{1 + 4B_u}\rho_0 l \approx \frac{1 + 3B_u}{1 + 4B_u}\cdot\frac{4}{3}\rho_0 l. \tag{4.250}$$

These elements are shown on the equivalent electrical circuit of Fig. 4.45 and are known as *lumped elements* as opposed to the *distributed* ones of Eqs. (4.219) and (4.220) because the mass, compliance, and resistance elements have been separated out into discrete elements whereas in reality they are evenly distributed over the length of the tube. However, the distributed parameter model may be considered as an infinite number of lumped parameter sections coupled together, where each one is infinitesimally short. At low frequencies, the impedance due to C_T is larger than R_T, so that the total compliance is effectively $C_0 + C_T = 1/P_0$. The low-frequency pressure fluctuations are isothermal due to heat transfer to and from the wall of the tube. At higher frequencies, R_T represents energy loss due to the time taken for the heat to flow back and forth. At even higher frequencies, R_T is greater than the impedance due to C_T, so very little heat is transferred, making the pressure fluctuations adiabatic in nature. The total compliance is then effectively $C_0 = 1/(\gamma P_0)$. Hence the compliance at low frequencies is greater than that at high frequencies by a factor of γ (that is, around 40% greater).

Regimes for an open-ended tube. The real and imaginary impedances at the entrance of the tube with the far end open, that is, with one pair of terminals of the 2-port network shorted, are shown in Fig. 4.46 and Fig. 4.47 respectively. In each case, four different curves are plotted. For the *exact* curves (black), Eq. (4.227) is used together with the exact wave-number and characteristic impedance of Eqs. (4.215) and (4.217) respectively. These are valid for $a > \lambda_m$. Real and imaginary approximate curves are also shown for the three following regimes:

For the *very narrow* radius or asymptotic curves (dark grey) Eq. (4.227) is also used but with the asymptotic wave-number and characteristic impedance of Eqs. (4.236) and (4.237) respectively.

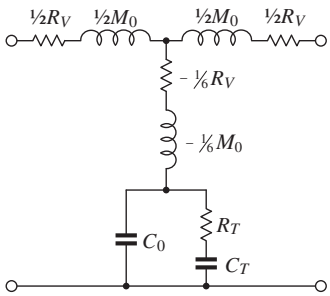

FIG. 4.45 A 2-port network for a short narrow tube of radius *a* length *l*, which is valid for $a > \lambda_m$, the molecular mean free path.

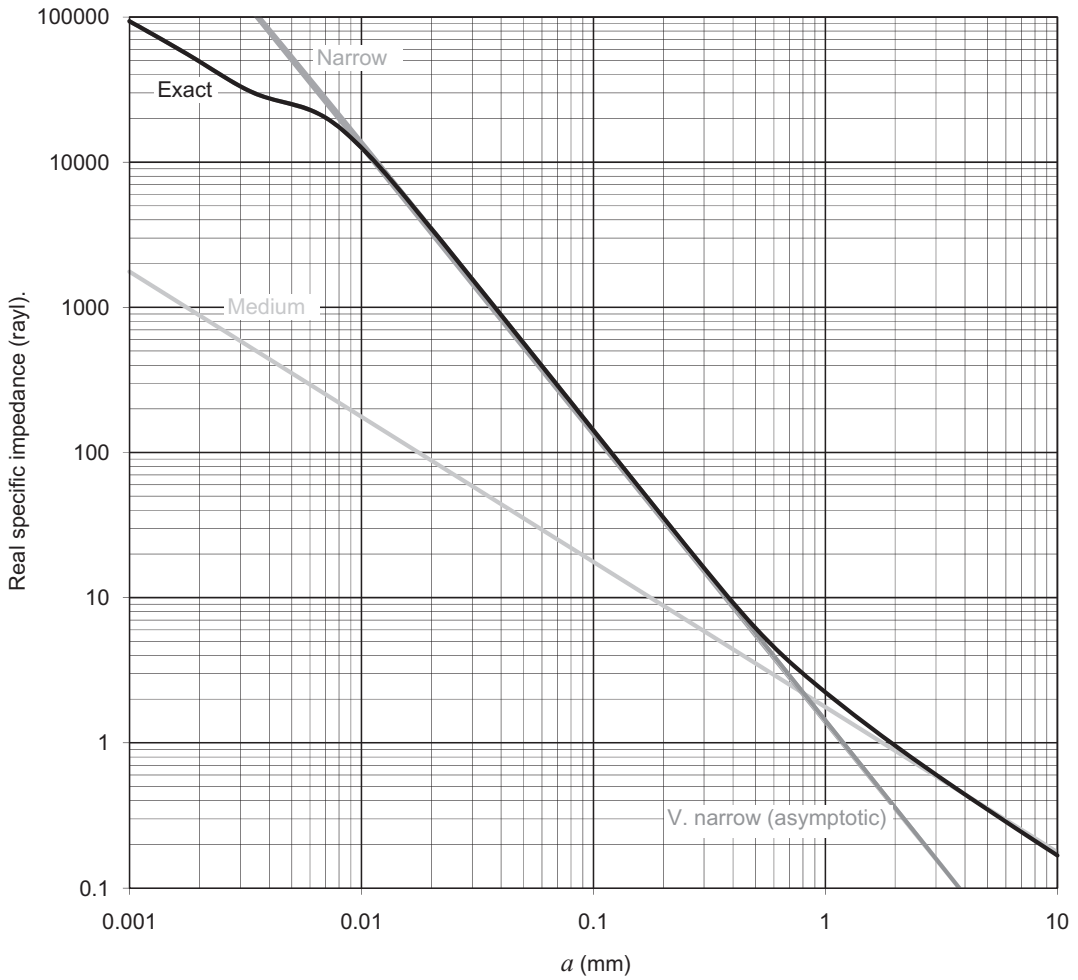

FIG. 4.46 Real impedance at the entrance of an open-ended tube at a frequency of 100 Hz plotted against its radius *a* where the length *l* of the tube is 10 mm.

The exact solution is given by Eq. (4.227) together with Eqs. (4.215) and (4.217), the very narrow solution by Eq. (4.227) together with Eqs. (4.236) and (4.237). For narrow and medium tubes, $Z_{in} = R_V + j\omega M_0$ where R_V and M_0 are given by Eqs. (4.249) and (4.250) for narrow tubes and Eqs. (4.251) and (4.252) for medium tubes.

The real curve is valid for $\lambda_m < a < 0.00008l\sqrt{f}$ and the imaginary curve for $\lambda_m < a < 0.0005\sqrt{l}$. Unfortunately, the discrete element equivalent circuit of Fig. 4.45 cannot be used in this range.

At low frequencies, we can ignore the compliance elements of Fig. 4.45 for an open tube. Hence the input impedance reduces to $Z_{in} = R_V + j\omega M_0$ where R_V and M_0 are given by Eqs. (4.249) and (4.250) respectively and these are used for the *narrow* radius curves (medium grey), commonly

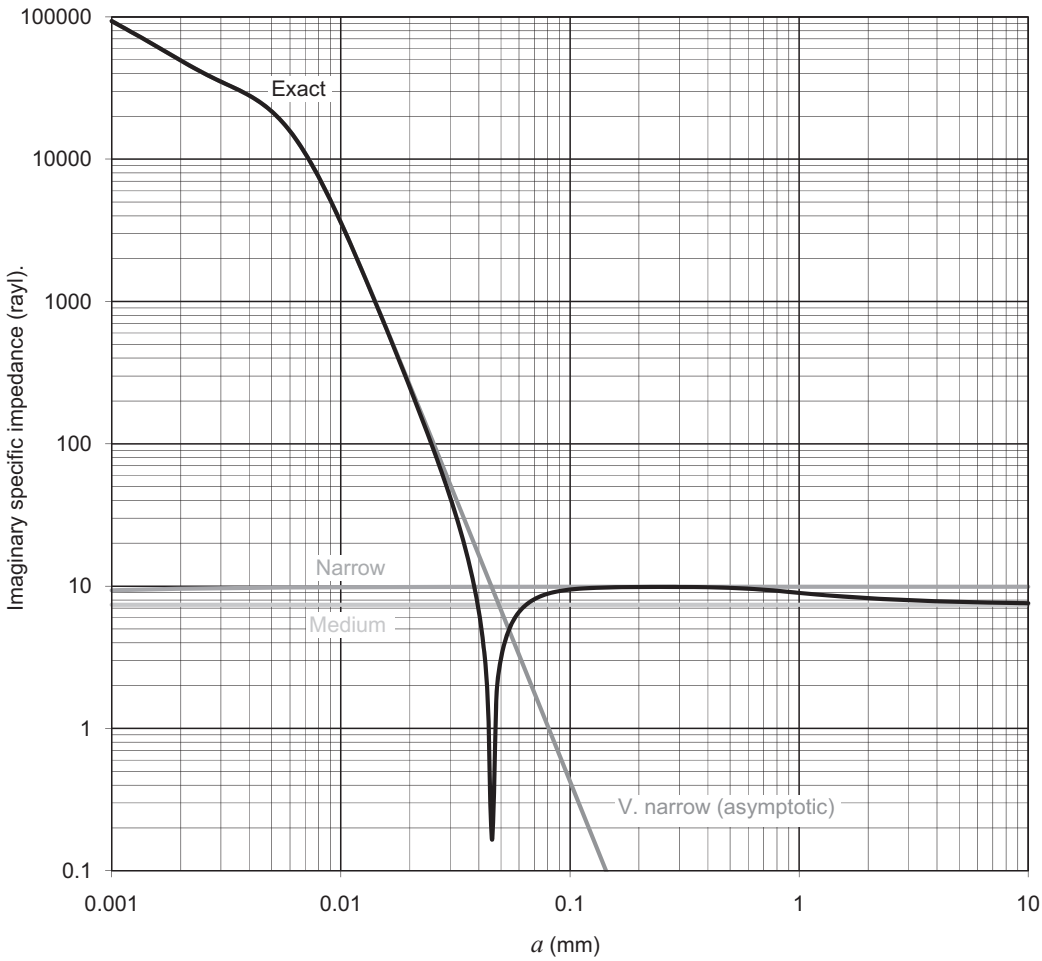

FIG. 4.47 Imaginary impedance at the entrance of an open-ended tube at a frequency of 100 Hz plotted against its radius *a* where the length *l* of the tube is 10 mm.

The exact solution is given by Eq. (4.227) together with Eqs. (4.215) and (4.217), the very narrow solution by Eq. (4.227) together with Eqs. (4.236) and (4.237). For narrow and medium tubes, $Z_{in} = R_V + j\omega M_0$ where R_V and M_0 are given by Eqs. (4.249) and (4.250) for narrow tubes and Eqs. (4.251) and (4.252) for medium tubes.

known as the *Poisseulle flow*. The real curve is valid for $0.00008l\sqrt{f} < a < 0.002/\sqrt{f}$ and the imaginary curve for $0.0005\sqrt{l} < a < 0.002/\sqrt{f}$.

For *medium* radius tubes, that is for $a > 0.01/\sqrt{f}$,we again ignore the compliance elements of Fig. 4.45 and use the expression $Z_{in} = R_V + j\omega M_0$, but this time apply the expressions developed by Ingard for R_V and M_0 as follows:

$$R_V = \frac{l}{a}\sqrt{2\omega\rho_0\mu} \tag{4.251}$$

$$M_0 = \rho_0 l \tag{4.252}$$

The fact that the resistance in Eq. (4.251) varies with frequency does not really matter much in practice. In a resonant system, such as where the acoustic mass of the tube is combined with the acoustic compliance of a cavity, the resistance only dominates over a small range of frequencies either side of the resonant frequency, especially as the resistance of a medium tube is relatively small and so the Q value is likely to be high. Hence we can simply use the value of the resistance at the resonant frequency for all frequency values.

Let us now examine the elements R_V and M_0 of Fig. 4.45. Using Eqs. (4.249) and (4.250) but with zero slip ($B_u = 0$), the frequency at which their impedances are equal is given by

$$\omega_V = \frac{R_V}{M_0} = \frac{6\mu}{a^2\rho_0} \text{ or } a = \sqrt{\frac{6\mu}{\omega_V \rho_0}} \tag{4.253}$$

It turns out that an effective viscous boundary layer thickness δ_V can be defined by

$$\delta_V = \sqrt{\frac{\mu}{\omega\rho_0}} \tag{4.254}$$

In other words, at $\omega = \omega_V$, we have $a = \sqrt{6}\delta_V$ so that the radius is about two and a half times greater than the effective boundary layer thickness when the mass reactance and resistance are equal. Above this frequency, the mass reactance of the air in the tube dominates and below it the viscous resistance dominates. If we insert the values $\mu = 1.86 \times 10^{-5}$ N·s/m^2 and $\rho_0 = 1.18$ kg/m^3 into Eq. (4.253) we also obtain $a = 0.004/\sqrt{f}$, which is the demarcation between narrow and medium radius tubes above. Hence, in a narrow tube the frequency-invariant resistance dominates, and in a medium diameter one the mass reactance dominates and the resistance is proportional to the square root of frequency. This can be clearly seen from Fig. 4.46 and Fig. 4.47 where the mass reactance and resistance are both approximately 10 rayl at $a = 0.4$ mm.

Ultra-narrow tube. At high frequencies in narrow tubes we encounter a fourth regime which is distinct from those already discussed (very narrow, narrow and medium) and where the lumped parameter model of Fig. 4.45 no longer applies. In that respect it is similar to the very narrow or asymptotic regime. Let us now examine some properties of the tangent function in Eq. (4.227) for the impedance of an open tube. The argument kl and Z_s can be expressed in terms of lumped parameters using the wave-number from Eq. (4.215), together with $j\omega\rho l = j\omega \boldsymbol{M}_s = Z_V$ and $j\omega Cl = j\omega \boldsymbol{C}_s = 1/Z_T$ so that

$$Z_{in} = j\sqrt{Z_V Z_T} \tan \sqrt{-Z_V/Z_T}. \tag{4.255}$$

We can see that for small arguments of the tangent function, where $\tan kl \approx kl$, the impedance of the blocked tube is just $Z_{in} = Z_V$. Using similar arguments with Eq. (4.226), where $\cot kl \approx 1/(kl,)$, we find that the impedance of a blocked tube is $Z_{in} = Z_T$. From Eq. (4.248), $Z_V = R_V + j\omega M_0$. From Eq. (4.244) we will use the approximation $Z_T = 1/(j\omega C_0)$. Putting these into Eq. (4.255) we obtain

$$Z_{in} = j\sqrt{Z_V Z_T} \tan \sqrt{-(R_V + j\omega M_0) j\omega C_0}. \tag{4.256}$$

If $\omega << \omega_V$, then this simplifies to

$$Z_{in}\Big|_{\omega << \omega_V} = j\sqrt{Z_V Z_T} \tan \sqrt{-j\omega R_V C_0} = j\sqrt{Z_V Z_T} \tan \left((1-j)\sqrt{\omega R_V C_0/2} \right). \tag{4.257}$$

From Eq. (48) of Appendix II, one property of the tangent function is that $\tan(x - jy) \approx -j$ for virtually any value of x provided that y is greater than or equal to about 2. Hence we can define a transition frequency ω_T by

$$\omega_T = \frac{8}{R_V C_0} = \frac{\gamma P_0 a^2}{\mu l^2}. \tag{4.258}$$

Below the transition frequency, the tube regimes are those for an open-ended tube above. Above it, the impedance is given by

$$Z_{in}\Big|_{\omega << \omega_V} = \sqrt{Z_V Z_T} = Z_s. \tag{4.259}$$

where the asymptotic expression for Z_s is given by Eq. (4.237). In this regime, the impedance is proportional to the inverse square root of frequency and the real and imaginary parts are equal, as can be seen in Fig. 4.48 and Fig. 4.49 where the transition frequency according to Eq. (4.258) is 1.45 kHz. Above this frequency, the dashed curves for Z_s from Eq. (4.237) match very closely with the black curves for the exact expression of Eq. (4.227). At low frequencies, the dark grey curves representing the lumped parameter model of Fig. 4.45 with one pair of terminals shorted appear to be a good approximation for the black exact curves. Although there is up to 25% error in the imaginary lumped impedance at low frequencies, it is less than 10% of the total impedance, which is mainly resistive and so the impedance modulus is fairly accurate.

Interestingly, above the transition frequency of 1.45 kHz, the real and imaginary impedances of the closed tube shown in Fig. 4.50 and Fig. 4.51 respectively are virtually identical to those of the open tube shown in Fig. 4.48 and Fig. 4.49 respectively. This is not so surprising considering that if the tangent function in Eq. (4.227) converges towards $-j$, then the cotangent function in Eq. (4.226) must

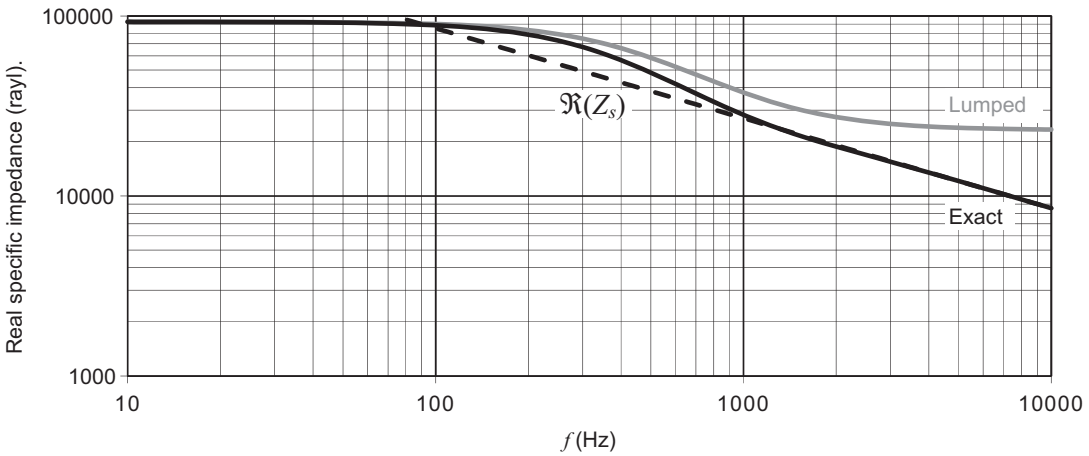

FIG. 4.48 Real impedance at the entrance of an open-ended tube plotted against frequency *f*.

The radius *a* of the tube is 1.1 μm and the length *l* is 1 mm. The exact solution is given by Eq. (4.227) and the characteristic impedance Z_s by Eq. (4.217). The lumped parameter model is as shown in Fig. 4.45, where the pair of terminals at the far end is short-circuited.

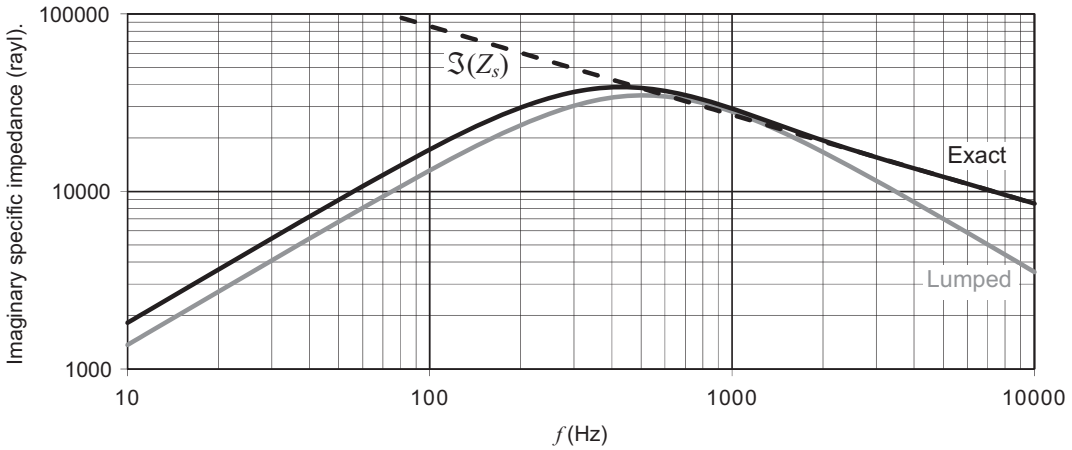

FIG. 4.49 Imaginary impedance at the entrance of an open-ended tube plotted against frequency *f*.

The radius *a* of the tube is 1.1 μm and the length *l* is 1 mm. The exact solution is given by Eq. (4.227) and the characteristic impedance Z_s by Eq. (4.217). The lumped parameter model is as shown in Fig. 4.45, where the pair of terminals at the far end is short-circuited.

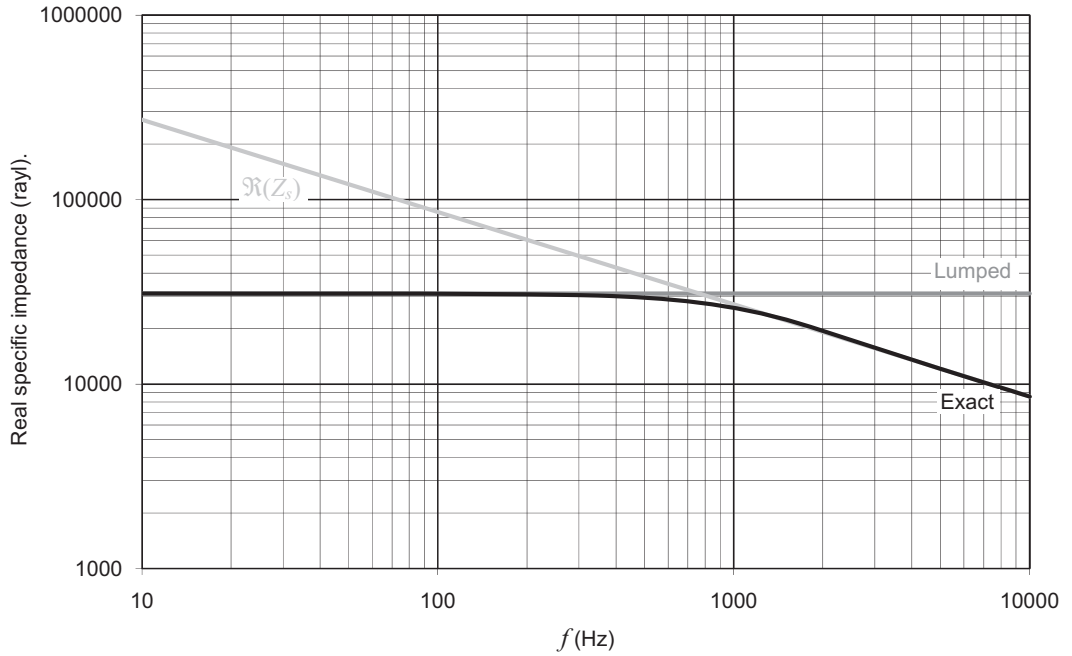

FIG. 4.50 Real impedance at the entrance of a closed tube plotted against frequency *f*.

The radius *a* of the tube is 1.1 μm and the length *l* is 1 mm. The exact solution is given by Eq. (4.227) and the characteristic impedance Z_s by Eq. (4.217). The lumped parameter model is as shown in Fig. 4.45, where the pair of terminals at the far end is open-circuit.

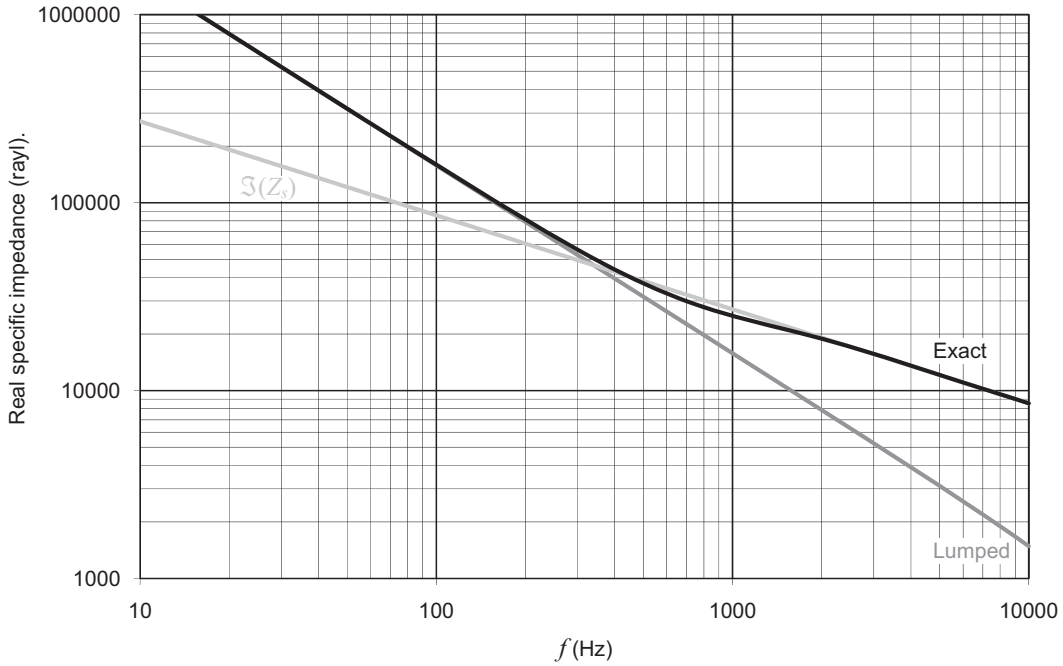

FIG. 4.51 Imaginary impedance at the entrance of a closed tube plotted against frequency *f*.

The radius *a* of the tube is 1.1 μm and the length *l* is 1 mm. The exact solution is given by Eq. (4.227) and the characteristic impedance Z_s by Eq. (4.217). The lumped parameter model is as shown in Fig. 4.45, where the pair of terminals at the far end is open-circuit.

converge towards j. Together with the fact that the input impedance is the characteristic impedance Z_s, this suggests that the tube under this regime behaves as an infinitely long one in which no sound is transmitted to the far end or reflected back from it due to full internal absorption. This can be confirmed if we take a look at the 2-port model of Fig. 4.43. The z-parameters are described by Eqs. (4.219) and (4.220), which under this regime reduce to

$$z_{11}\big|_{\omega>\omega_T} = z_{22}\big|_{\omega>\omega_T} \approx Z_s, \tag{4.260}$$

$$z_{12}\big|_{\omega>\omega_T} = z_{21}\big|_{\omega>\omega_T} \approx 0, \tag{4.261}$$

because $\text{cotan}(x - jy) \to j$ and $\text{cosec}(x - jy) \to 0$ for $y > 2$ for any x. As stated above, the existence of this regime is conditional that $\omega_T << \omega_V$ where ω_V and ω_T are given by Eqs. (4.253) and (4.258) respectively. Hence

$$\frac{8}{R_V C_0} << \frac{R_V}{M_0}. \tag{4.262}$$

Now let us define a Q value by

$$Q = \frac{1}{R_V}\sqrt{\frac{M_0}{C_0}} << \frac{1}{\sqrt{8}}. \tag{4.263}$$

In practice, the regime only exists for highly damped tubes where $Q < 0.05$ or $l > (6 \times 10^7)a^2$. According to Eq. (4.258), it describes the asymptotic curves in Fig. 4.46 and Fig. 4.47 for $a < 3$ μm and hence can be regarded as an "ultra-narrow" tube regime.

Notes

[1] Crandall IB. Vibrating Systems and Sound. New York: D. Van Nostrand Company, Inc; 1926.
[2] Ingard U. Scattering and Absorption by Acoustic Resonators, doctoral dissertation, Massachusetts Institute of Technology, 1950. J Acoust Soc Am 1953;25:1044–5.
[3] Olson HF. Elements of Acoustical Engineering. 2nd ed. New York: D. Van Nostrand Company, Inc; 1947. 109–111.
[4] L. Fincham and P. Brown, Line Arrays with Controllable Directional Characteristics - Theory and Practice, in the 125th AES Convention, 2008, paper no. 7535.
[5] Walker PJ. New Developments in Electrostatic Loudspeakers. J Audio Eng Soc 1980;28(11):795–9.
[6] See the definition for intensity in Section 1.10. The intensity equals the sound pressure squared, divided by $\rho_0 c$ for a plane wave in free space or for a spherical wave.
[7] Kozlov VF, Fedorov AV. Acoustic Properties of Rarefied Gases Inside Pores of Simple Geometries. J Acoust Soc Am 2005;117(6):3402–12.
[8] Stinson MR. The Propagation of Plane Sound Waves in Narrow and Wide Circular Tubes, and Generalization to Uniform Tubes of Arbitrary Cross-sectional Shape. J Acoust Soc Am 1991;89(2):550–8.
[9] Veijola T. A Two-Port Model for Wave Propagation Along a Long Circular Microchannel. Microfluidics and Nanofluidics 2007;3(3):359–68.
[10] P. M. Morse and K. U. Ingard, Theoretical Acoustics (McGraw-Hill, New York, 1968), p. 279, Eq. (6.4.17).
[11] P. M. Morse and K. U. Ingard, Theoretical Acoustics (McGraw-Hill, New York, 1968), p. 231, Eq. (6.1.5).
[12] P. M. Morse and K. U. Ingard, Theoretical Acoustics (McGraw-Hill, New York, 1968), p. 8, Eq. (6.1.11).